Chemical and Biological Oceanographic Conditions on the Scotian Shelf and in the Eastern Gulf of Maine during 2025

Benoit Casault, Catherine L. Johnson, Emmanuel Devred, Stephanie Clay, Lindsay Beazley

Fisheries and Oceans Canada
Maritimes Region
Bedford Institute of Oceanography
P.O. Box 1006
Dartmouth, NS
B2Y 4A2

2026

Canadian Technical Report of Fisheries and Aquatic Sciences 3810

Fisheries and Oceans Canada Pêches et Océans Canada

Canada

Canadian Technical Report of Fisheries and Aquatic Sciences

Technical reports contain scientific and technical information that contributes to existing knowledge but which is not normally appropriate for primary literature. Technical reports are directed primarily toward a worldwide audience and have an international distribution. No restriction is placed on subject matter and the series reflects the broad interests and policies of Fisheries and Oceans Canada, namely, fisheries and aquatic sciences.

Technical reports may be cited as full publications. The correct citation appears above the abstract of each report. Each report is abstracted in the data base *Aquatic Sciences and Fisheries Abstracts*.

Technical reports are produced regionally but are numbered nationally. Requests for individual reports will be filled by the issuing establishment listed on the front cover and title page.

Numbers 1-456 in this series were issued as Technical Reports of the Fisheries Research Board of Canada. Numbers 457-714 were issued as Department of the Environment, Fisheries and Marine Service, Research and Development Directorate Technical Reports. Numbers 715-924 were issued as Department of Fisheries and Environment, Fisheries and Marine Service Technical Reports. The current series name was changed with report number 925.

Rapport technique canadien des sciences halieutiques et aquatiques

Les rapports techniques contiennent des renseignements scientifiques et techniques qui constituent une contribution aux connaissances actuelles, mais qui ne sont pas normalement appropriés pour la publication dans un journal scientifique. Les rapports techniques sont destinés essentiellement à un public international et ils sont distribués à cet échelon. II n'y a aucune restriction quant au sujet; de fait, la série reflète la vaste gamme des intérêts et des politiques de Pêches et Océans Canada, c'est-à-dire les sciences halieutiques et aquatiques.

Les rapports techniques peuvent être cités comme des publications à part entière. Le titre exact figure au-dessus du résumé de chaque rapport. Les rapports techniques sont résumés dans la base de données *Résumés des sciences aquatiques et halieutiques.*

Les rapports techniques sont produits à l'échelon régional, mais numérotés à l'échelon national. Les demandes de rapports seront satisfaites par l'établissement auteur dont le nom figure sur la couverture et la page du titre.

Les numéros 1 à 456 de cette série ont été publiés à titre de Rapports techniques de l'Office des recherches sur les pêcheries du Canada. Les numéros 457 à 714 sont parus à titre de Rapports techniques de la Direction générale de la recherche et du développement, Service des pêches et de la mer, ministère de l'Environnement. Les numéros 715 à 924 ont été publiés à titre de Rapports techniques du Service des pêches et de la mer, ministère des Pêches et de l'Environnement. Le nom actuel de la série a été établi lors de la parution du numéro 925.

Canadian Technical Report of
Fisheries and Aquatic Sciences 3810

2026

CHEMICAL AND BIOLOGICAL OCEANOGRAPHIC CONDITIONS ON THE SCOTIAN SHELF AND IN THE EASTERN GULF OF MAINE DURING 2025

by

Benoit Casault, Catherine L. Johnson, Emmanuel Devred, Stephanie Clay, Lindsay Beazley

Fisheries and Oceans Canada
Maritimes Region
Bedford Institute of Oceanography
P.O. Box 1006
Dartmouth, NS
B2Y 4A2

Cat. No. Fs97-6/3810E-PDF ISBN 978-1-100-00477-8 ISSN 1488-5379
https://doi.org/10.60825/8eyc-0d16

Correct citation for this publication:

Casault, B., Johnson, C.L., Devred, E., Clay, S., Beazley, L. 2026. Chemical and Biological Oceanographic Conditions on the Scotian Shelf and in the Eastern Gulf of Maine during 2025. Can. Tech. Rep. Fish. Aquat. Sci. 3810: vi + 63 p. https://doi.org/10.60825/8eyc-0d16

CONTENTS

ABSTRACT

Casault, B., Johnson, C.L., Devred, E., Clay, S., Beazley, L. 2026. Chemical and Biological Oceanographic Conditions on the Scotian Shelf and in the Eastern Gulf of Maine during 2025. Can. Tech. Rep. Fish. Aquat. Sci. 3810: vi + 63 p. https://doi.org/10.60825/8eyc-0d16

Amid continued surface warming and recent cooling of mid-depth and bottom waters in the Maritimes Region, biogeochemical conditions in the region in 2025 indicated mainly below-normal inventories of surface nitrate while subsurface nitrate inventories reached normal levels across the region. For the Prince 5 station in Bay of Fundy, this ended a decade of below-normal nitrate conditions. Bottom dissolved oxygen saturation remained near- to above-normal levels for a third consecutive year, with a record-high anomaly observed at Cabot Strait. *In situ* chlorophyll-*a* inventories were near to slightly above normal in eastern sections but below normal in western areas, partly influenced by *in situ* sampling having occurred either near or after the peak of the phytoplankton bloom. Satellite-derived surface chlorophyll-*a* revealed widespread negative anomalies, including record lows at Halifax-2, the western Scotian Shelf, and on Georges Bank. The timing of the spring bloom was slightly earlier in the eastern (Cabot Strait and eastern Scotian Shelf) part of the region but normal elsewhere. The fall bloom was generally delayed and weak in intensity, with Georges Bank showing record-low intensity. Copepod and non-copepod abundances were near to above normal across the region. *Calanus finmarchicus* abundance remained near- to slightly above-normal levels for a third consecutive year. *Pseudocalanus* spp. abundance was mainly above normal in 2025, reaching record highs at Halifax-2 and on the Halifax section. Mesozooplankton biomass remained slightly below normal, consistent with the long-term trend observed since 2011. Copepod indicator species (i.e. Arctic *Calanus*, and warm-water shelf and offshore species) exhibited mixed anomalies across the region.

RÉSUMÉ

Casault, B., Johnson, C.L., Devred, E., Clay, S., Beazley, L. 2026. Chemical and Biological Oceanographic Conditions on the Scotian Shelf and in the Eastern Gulf of Maine during 2025. Can. Tech. Rep. Fish. Aquat. Sci. 3810: vi + 63 p. https://doi.org/10.60825/8eyc-0d16

Dans un contexte de réchauffement continu des eaux de surface et d'un récent refroidissement des eaux intermédiaires et profondes dans la région des Maritimes, les conditions biogéochimiques dans la région en 2025 ont révélé des inventaires de nitrate en surface principalement inférieurs à la normale, tandis que les inventaires de nitrate en profondeur ont atteint des niveaux normaux dans toute la région. Pour la station Prince 5, située dans la baie de Fundy, ces conditions ont mis fin à une décennie d'inventaires en nitrate inférieurs à la normale. L'oxygène dissous près du fond est demeuré à des niveaux de saturation près ou supérieurs à la normale pour une troisième année consécutive, dont une anomalie positive record observée dans le détroit de Cabot. Les inventaires *in situ* de chlorophylle-*a* étaient près ou légèrement supérieurs à la normale dans les secteurs est de la région, mais inférieurs à la normale dans les zones ouest, en partie en raison d'un échantillonnage *in situ* effectué près ou après le pic printanier de floraison du phytoplancton. Les données satellitaires de chlorophylle-*a* en surface ont révélé des anomalies négatives généralisées, notamment des niveaux minimums records à la station Halifax-2, dans la partie ouest du plateau néo-écossais, et sur le banc Georges. La floraison printanière du phytoplancton était légèrement plus hâtive que la normale dans la partie est de la région (détroit de Cabot et est du plateau néo-écossais), mais normale ailleurs. La floraison automnale a été généralement tardive et de faible intensité, le banc Georges affichant une intensité minimale record. L'abondance des copépodes et des non-copépodes était près ou supérieure à la normale dans l'ensemble de la région. L'abondance de *Calanus finmarchicus* est demeurée près ou légèrement supérieure à la normale pour une troisième année consécutive. L'abondance de *Pseudocalanus* spp. était principalement supérieure à la normale en 2025, atteignant des sommets records à la station Halifax-2 et sur la section d'Halifax. La biomasse du mésozooplancton est demeurée près ou légèrement inférieure à la normale, conformément à la tendance à long terme observée depuis 2011. Les espèces indicatrices de copépodes (i.e., *Calanus* arctiques, et les copépodes d'eau chaude côtiers et extracôtiers) ont présenté des anomalies variables dans la région.

1. INTRODUCTION

The Atlantic Zone Monitoring Program (AZMP) was implemented in 1998 to enhance Fisheries and Oceans Canada's (DFO's) capacity to describe, understand, and forecast the state of the marine ecosystem (Therriault et al. 1998). The AZMP derives its information on the marine environment and ecosystem from data collected at a network of sampling locations (high-frequency sampling stations, cross-shelf sections, and ecosystem trawl surveys) in four DFO regions (Québec, Gulf, Maritimes, and Newfoundland and Labrador), sampled at a frequency of twice-monthly to once-annually. The sampling design provides fundamental information on the variability in physical, chemical, and biological properties of the Northwest Atlantic continental shelf and slope on seasonal and inter-annual scales. Cross-shelf sections and ecosystem trawl surveys provide information on broad-scale environmental variability (Harrison et al. 2005) but their seasonal coverage is limited. High-frequency sampling stations complement the broad-scale sampling by providing detailed information on seasonal changes in ocean properties. *In situ* sampling is also complemented by remote sensing of ocean colour measurements, providing additional information on the distribution of phytoplankton in the surface layer on a broad spatio-temporal scale.

The Scotian Shelf (SS) is located in a transition zone influenced by subpolar waters, mainly flowing into the region from the Gulf of St. Lawrence (GSL) and the Newfoundland Shelf and slope, and by warmer offshore waters of Gulf Stream origin. The deep-water properties of the SS exhibit significant shifts in temperature and nutrients that can be influenced by sustained periods of weak and strong large-scale atmospheric forcing represented by the winter North Atlantic Oscillation index (Petrie 2007). These shifts result in changes in the relative contribution of the cold, low-nutrient Labrador slope water and the warmer, nutrient-rich Atlantic slope water to the deep slope water that flows onto the shelf. Temperature and salinity on the SS are also influenced by heat transfer between the atmosphere and ocean, local mixing, precipitation, and, to some extent, runoff from land. Physical changes in the pelagic environment influence both plankton community composition and annual biological production cycles, with implications for energy transfer to higher trophic levels.

The objective of this report is to describe the nutrient, oxygen, and plankton conditions across the SS and in the eastern Gulf of Maine (GoM) in 2025 in the context of variability in shelf conditions observed since the beginning of the AZMP program. It complements assessments of the Maritimes Region's physical environment (Layton et al. 2026) and of the state of the Canadian Northwest Atlantic shelf system as a whole (Galbraith et al. 2026). A set of simple chemical and biological metrics is used to represent important processes related to plankton production cycles and composition. These include surface and subsurface nutrient inventories, which represent the availability of nutrients required for phytoplankton production, and bottom oxygen saturation which is an indicator of oxygen availability for demersal fish species and other benthic organisms. Phytoplankton metrics, including biomass and spring and fall bloom dynamics, are represented by *in situ* chlorophyll-*a* (chl-*a*) inventories in the upper water column and near-surface chlorophyll-*a* concentrations measured by satellite remote sensing. Zooplankton metrics include biomass and copepod and non-copepod abundance, representing the overall quantity of zooplankton present, and abundances of taxa or groups that represent dominant species (*Calanus finmarchicus*, *Pseudocalanus* spp.) or biogeographic associations (Arctic copepods, warm-water offshore copepods, and warm-water shelf copepods). Copepod relative abundance patterns are used to assess community variability at the high-frequency sampling stations.

2. METHODS

Sample collection and processing conform to established standard protocols to the best extent possible (Mitchell et al. 2002). Non-standard measurements or derived variables are described below.

2.1 Surveys and Sampling

AZMP sampling in the Maritimes Region consists of high-frequency sampling at two fixed stations (Halifax-2 and Prince 5), seasonal sampling during dedicated oceanographic cross-shelf surveys conducted in spring and fall, and through participation in the ecosystem trawl surveys conducted in winter and summer. In 2025, sampling was conducted on the spring and fall cross-shelf surveys and on the winter and summer ecosystem trawl surveys (collectively referred to as 'broad-scale' surveys herein), and on day trips to the two high-frequency sampling stations (Table 1, Figures 1-3). A total of 504 hydrographic station occupations were completed, with 250 plankton net tows (Table 1).

2.1.1 High-frequency Sampling Stations

The standard sampling suite for the Halifax-2 (HL2) and Prince 5 (P5) high-frequency sampling stations (Figure 1) includes the following:

- Conductivity, temperature, depth (CTD) profiles with dissolved oxygen, pH (HL2), fluorescence, photosynthetically active radiation (PAR), and turbidity measurements.
- Niskin water bottle samples at standard depths (see Gear Deployment) for nutrients, salinity and oxygen (for CTD data validation), chlorophyll-*a* analyses, and microscopic phytoplankton enumeration. Accessory phytoplankton pigments are also measured near the surface but are not reported in this document.
- Vertical ring net tows (202-µm mesh net) for zooplankton biomass (wet and dry weights), species and/or group abundance, and community composition.
- Secchi depth measurement for light attenuation when possible.

The HL2 and P5 stations were occupied 22 and 10 times, respectively, in 2025 (Table 1). However, at HL2, zooplankton net samples were not collected on three occupations (March 1st, March 18th, and April 27th) due to vessel equipment or logistics issues, and sampling was not possible during the month of December due to vessel issues. At P5, the station was not occupied in January, February and December due to vessel availability issues.

2.1.2 Cross-shelf Sections

During the regular spring and fall seasonal surveys, samples are collected on the four core sections (Cabot Strait [CSL]; Louisbourg [LL]; Halifax [HL]; Browns Bank [BBL]; Figure 1) and at several ancillary sections/stations (red markers in Figure 2). The standard sampling suite for the cross-shelf section stations is the same as for the high-frequency sampling stations listed above, except for integrated samples for phytoplankton enumeration and Secchi depth measurements, which are only collected at station HL2 when occupied as part of the HL section. Also, observations from the ancillary sections are not reported in this document due to inconsistent sampling over time.

In addition to the standard suite of analyses performed on water samples, parameters including particulate organic carbon, phytoplankton pigment composition, partial pressure of carbon dioxide (pCO_2), total alkalinity (TA), total inorganic carbon (TIC), and methane are measured at various depths. These parameters are not reported in this document; however, some of them (e.g., pCO_2, TA, pH, dissolved inorganic carbon, and calcite and aragonite saturation state) are included in a separate technical report (Galbraith et al. 2026).

In 2025, the spring survey took place from March 29th to April 18th, and the fall survey took place from September 28th to October 21st (Table 1 and Figure 2). A description of activities conducted during the 2025 spring and fall surveys is presented in Beazley et al. (2025) and Beazley et al. (2026), respectively.

2.1.3 Ecosystem Trawl Surveys

Ecosystem trawl surveys in the Maritimes Region are led by DFO's Population Ecology Science Division with AZMP staff participation. The sampling suite for the ecosystem trawl survey stations includes the measurements listed above for the high-frequency sampling stations, but the standard set of water bottle sampling depths is reduced to four or five depths depending on overall station depth, and vertical ring net tows (202-µm mesh) are only collected at a subset of stations (Table 1 and Figure 3).

In 2025, the winter survey on the western SS, Georges Bank (GB), and in the Bay of Fundy (BoF) took place from March 1st to March 30th, and the summer survey on the SS, in the eastern GoM, and in the BoF took place from June 30th to August 5th (Table 1 and Figure 3).

2.2 Gear Deployment

2.2.1 Conductivity, Temperature, Depth, and Water Sampling

Standard depths for water samples include:

- High-frequency sampling stations:
    1. HL2[1]: 1 m, 5 m, 10 m, 20 m, 30 m, 40 m, 50 m, 75 m, 100 m, 140 m
    2. P5: 1 m, 10 m, 25 m, 50 m, 95 m
- Cross-shelf sections: near-surface, 10 m, 20 m, 30 m, 40 m, 50 m, 60 m, 80 m, 100 m, 250 m, 500 m, 1000 m, 1500 m, 2000 m, to near-bottom (defined as ca. 5 m from bottom; depths sampled are limited by bottom depth)
- Ecosystem trawl surveys: 5 m, 25 m, 50 m, 100 m (in water near or deeper than 150 m), and near-bottom (defined as ca. 1-2 m from bottom) when possible.

[1] Sampling depths at HL2 when occupied during seasonal surveys include near-surface, 10 m, 20 m, 30 m, 40 m, 50 m, 60 m, 80 m, 100 m, and near-bottom.

2.2.2 Net Tows

Ring nets of a standard 202-µm mesh are towed vertically from near-bottom to surface at a speed of approximately 1 $m \cdot s^{-1}$. In deep offshore waters, the maximum tow depth is 1000 m. Samples are preserved in a 4% solution of buffered formaldehyde and analyzed according to the protocol outlined in Mitchell et al. (2002).

2.3 Derived Metrics

2.3.1 Vertically Integrated Variables

Integrated chlorophyll-*a* and nutrient inventories are calculated over various depth intervals (i.e., 0–100 m for chlorophyll-*a* concentration, and 0–50 m and 50–150 m for nutrients) using trapezoidal numerical integration. When the maximum depth at a given station is shallower than the lower depth limits noted above, the inventories are calculated by setting the lower integration limit to the maximum depth at that station (e.g., 95 m for P5). Data at the surface (0 m) is taken as the closest near-surface sampled value. Data at the lower depth is taken as:

1. the interpolated value when sampling occurs below the lower integration limit; or
2. the closest deep-water sampled value when sampling is shallower than the lower integration limit.

2.3.2 Phytoplankton Taxonomic Groups

Phytoplankton abundance and taxonomic composition at the high-frequency sampling stations are normally estimated from pooled aliquots of water collected in the upper 100 m (140 m for HL2) of the water column using the Utermöhl technique (Utermöhl 1931) as described in Mitchell et al. (2002). However, analysis of phytoplankton abundance and taxonomy was not performed in 2025 due to the unavailability of a trained phytoplankton taxonomist.

2.3.3 Oxygen Saturation

Dissolved oxygen saturation ($\%O_{2\,sat}$) was calculated as the oxygen concentration measured by the CTD ($O_{2\,mL/L}$), divided by the saturation oxygen concentration ($O_{2\,sat(T,S)}$) at the corresponding *in situ* temperature and salinity:

$$\%O_{2\,sat} = 100 \cdot \frac{O_{2\,mL/L} \cdot 44.6596}{O_{2\,sat(T,S)}}$$

where $O_{2\,sat(T,S)}$ is estimated from the equation of Garcia and Gordon (1992) and expressed in units of $\mu mol \cdot L^{-1}$.

2.4 Remote Sensing of Ocean Color

Data products from the Ocean Color Climate Change Initiative (OC-CCI; accessed on August 24, 2026) of the European Space Agency (ESA) were used to assemble time series of near-surface chlorophyll-*a* concentrations for different sub-regions of the Maritimes Region (HL2, P5, Cabot Strait [CS], Eastern Scotian Shelf [ESS], Central Scotian Shelf [CSS], Western Scotian Shelf [WSS], Lurcher Shoal [LS], Georges Bank [GB]; Figure 4). The OC-CCI product, for which the time series extends from September 1997 to present, offers improved spatial and temporal coverage due to the merging of data from multiple satellite optical sensors. Daily 4 km-resolution remote sensing reflectance (Rrs, sr^{-1}) data were downloaded from ESA's Ocean Color website (accessed on August 24, 2026). Chlorophyll-*a* concentrations were derived from Rrs data using the POLY4 band-ratio algorithm (Clay et al. 2019), which is based on the regionalisation of O'Reilly et al.'s (1998) algorithm. The OCxSPMcor algorithm was used to compute chlorophyll-*a* in the Bay of Fundy for the P5 station, as this algorithm accounts for high concentrations of suspended particulate matter that may interfere with the chlorophyll-*a* signal in that region (Wilson et al. 2024). Coefficients of the POLY4 and OCxSPMcor algorithms were tuned using regional *in situ* chlorophyll-*a* concentrations derived from high-performance liquid chromatography (HPLC) or from Turner Designs fluorometer measurements. The resulting daily chlorophyll-*a* data were downloaded through the R Shiny app *PhytoFit* (accessed on August 24, 2026; Clay et al. 2021) for the purpose of visualizing the annual cycle, calculating weekly, monthly, seasonal, and annual means and anomalies, and for estimating the descriptive parameters of the spring and fall phytoplankton blooms. Four metrics were computed to describe the timing and intensity characteristics of the spring and fall blooms (for all regions except P5, which has a more complex phenology that is not suited to these metrics): day of year of the maximum chlorophyll-*a* concentration during the bloom (i.e. peak of the Gaussian curve fitted to the daily data), day of year of the fall bloom initiation, and the spring and fall weighted average chlorophyll-*a* concentrations with weights proportional to the percentage of valid pixels (i.e., a proxy for cloud coverage) for a given sub-region. Spring and fall season periods in this context are defined by the phenology of the climatology and are unique to each region of interest (Bélanger et al. in preparation[2]).

2.5 Annual Anomaly Scorecards

Scorecards of key indices, based on normalized, seasonally-adjusted annual anomalies, represent changes in physical, chemical, and biological observations in a compact format. Annual estimates of phytoplankton abundance, water column inventories of nutrients and chlorophyll-*a*, zooplankton biomass, and the mean abundance of key zooplankton species or groups, at the high-frequency sampling stations and/or as an overall average along each of the four standard sections, are based on general linear models of the form:

$$Density = \alpha + \beta_{YEAR} + \delta_{MONTH} + \varepsilon$$

for the high-frequency sampling stations, and

$$Density = \alpha + \beta_{YEAR} + \delta_{STATION} + \gamma_{SEASON} + \varepsilon$$

for the sections.

Density is in units of concentration, abundance, or biomass per unit area or volume (e.g., individuals·m^{-2}, $mg_{chl\text{-}a}$·m^{-3}, etc.), α is the intercept and ε is the error. For the high-frequency sampling stations, β and δ are categorical effects for year and month, respectively. For the sections, β, δ *and* γ take into account the effect of year, station and season, respectively.

[2] Bélanger, D., Clay, S., Blais, M., and Devred, E. Ocean colour derived metrics for reporting on Northwest Atlantic phytoplankton phenology and interannual variability. Can. Tech. Rep. Hydrogr. Ocean. Sci. In preparation.

In addition to annual estimates, seasonal estimates of zooplankton indices (i.e., zooplankton biomass and *C. finmarchicus* abundance) for the individual sections were also calculated using a general linear model. In this case, a reduced model including the year and station effects was fitted to the seasonal data subsets.

Density in terms of surface chlorophyll-*a* concentration and *in situ* chlorophyll-*a* inventory was log-transformed [$log_{10}(n)$] to normalize the skewed distribution of these observations. For zooplankton and phytoplankton abundance, one is added to the log-transformed *Density* term [$log_{10}(n+1)$] to include observations for which the value equals zero. Integrated inventories of nutrients and zooplankton biomass were not log-transformed. An estimate of the least-squares means based on Type III Sums of Squares (Lenth et al. 2026) is used as the measure of the overall year effect.

For the ecosystem trawl surveys, seasonal mean indices were calculated as the arithmetic mean of the zooplankton biomass or the log-transformed *C. finmarchicus* abundance data collected within each season/year and each Northwest Atlantic Fisheries Organization (NAFO) area. The reporting of the zooplankton indices based on the NAFO areas for the ecosystem trawl surveys conforms with similar reporting for the physical indices (e.g., Galbraith et al. 2026) and with most fisheries stock assessment reports.

Annual anomalies are calculated as the deviation of an individual year from the mean of the annual estimates over the period 1999–2025. For the bottom oxygen data analysis, a pseudo-climatology is constructed by averaging the data over the period 2014-2025 due to data quality issues before 2014. The annual anomalies are expressed either in absolute units or as normalized quantities (i.e., by dividing by the standard deviation [sd] of the annual estimates over the same period). For the purpose of data interpretation, normalized anomalies are considered near normal when within ±0.5 sd, slightly above/below normal when between ±0.5 sd and ±1 sd, and above/below normal otherwise (i.e., larger/smaller than ±1 sd).

A standard set of indices representing anomalies of nutrient availability, dissolved oxygen saturation, phytoplankton biomass, and the abundance of dominant zooplankton species and groups (*C. finmarchicus*, *Pseudocalanus* spp., total copepods, and total non-copepods) is produced in each of the AZMP regions, including the Maritimes Region. To visualize Northwest Atlantic shelf-scale patterns of variability, zonal scorecards including observations from all AZMP regions is presented in a separate technical report (Galbraith et al. 2026).

3. OBSERVATIONS

3.1 Nutrients

The primary dissolved inorganic nutrients (i.e., nitrate, silicate, and phosphate) measured by the AZMP strongly co-vary in space and time (Petrie et al. 1999). For this reason, and because the availability of nitrogen is most often associated with phytoplankton growth limitation in coastal and shelf waters of the Maritimes Region (DFO 2000), this report focuses mainly on variability patterns for nitrate, with information on silicate and phosphate concentrations presented to help interpret phytoplankton taxonomic group succession at HL2 and P5 when phytoplankton abundance and taxonomic classification data are available.

3.1.1 High-frequency Sampling Stations

At HL2, the highest surface nitrate concentrations are typically observed in the winter when the water column is well mixed and primary production is low (Figure 5). Surface nitrate declines with the onset of the spring phytoplankton bloom, and the lowest surface nitrate concentrations are observed in spring through early fall. Deep-water nitrate concentrations are lowest from late fall until early spring, and increase from May to August, perhaps reflecting sinking and decomposition of the spring phytoplankton bloom (Petrie and Yeats 2000).

In 2025, the nitrate inventory in the upper 0–50 m layer at HL2 remained generally near normal, fluctuating between slightly above and slightly below normal for most of the year (Figure 6). In late July, the nitracline was above 50 m depth (Figure 5) which resulted in the above-normal nitrate inventory within the 0–50 m layer (Figure 6). Lower-than-normal inventories observed in September, early October, and early November (Figure 6) were associated with nitrate depleted conditions in the 0-50 m layer (Figure 5). Overall, the surface nitrate annual inventory at HL2 was slightly lower than normal in 2025, similar to 2024 (Figure 7).

The nitrate inventory in the 50–150 m layer at HL2 was generally near normal throughout most of 2025, varying between slightly below and slightly above normal levels (Figure 6). The most notable deviations occurred on March 29 and April 18, when inventories were below and above normal, respectively, and associated with below- and above-normal nitrate concentrations at depth (Figure 5). Overall, the annual subsurface nitrate inventory at HL2 was normal in 2025, in contrast with the previous two years when below-normal inventories were observed (Figure 7).

The surface and subsurface annual silicate inventories were near normal to slightly below normal in 2025 (Figure 7). The annual inventory of surface phosphate reached a record-low value (-1.59 sd) in 2025, while the subsurface phosphate inventory was slightly below normal, continuing the general pattern of near- or below-normal conditions observed during the previous decade (Figure 7).

The nitrate dynamics at P5 differ considerably from those at HL2 due to the high nutrient input from the outflow of the nearby Saint John River, combined with the strong tidal mixing which produces a more vertically uniform nitrate distribution, with lower nitrate accumulation in the deep water and a higher overall surface inventory. The highest nitrate concentrations throughout the water column are typically observed in the winter and late fall (Figure 5), when the water column is well mixed and phytoplankton growth is minimal due to light limitation. Nitrate concentrations start to decline in the upper water column when the spring phytoplankton bloom starts in April or May, and the lowest surface nitrate concentrations and corresponding inventory are typically observed from May to September (Figures 5 and 6).

At P5 in 2025, both the surface and subsurface nitrate inventories were slightly above normal in spring, slightly below normal in fall, and otherwise near normal (Figures 6), with near-normal mean annual levels (Figure 7). For both surface and subsurface inventories, the near-normal conditions observed in 2025 end a decade of mainly below-normal conditions (Figure 7).

The surface and subsurface silicate inventories in 2025 were slightly above and normal, respectively, continuing the return to near- or above-normal conditions observed during the last four years (Figure 7). The annual surface and subsurface inventories for phosphate at P5 in 2025 were slightly below and below normal, respectively, continuing the general pattern of near- to below-normal annual inventories observed during the previous 12 years (Figure 7).

3.1.2 Broad-scale Surveys

In 2025, nitrate concentrations in the upper 50 m of the water column were low at all stations along the CSL, LL and HL sections during both the spring (Figure 8a) and fall (Figure 8b) surveys. This indicates depleted surface nitrate conditions that typically follow the spring phytoplankton bloom, and sampling prior to fall replenishment of the surface layer. One exception was the BBL section where nitrate concentrations in the range of 3-5 mmol·m^{-3} were observed during spring in the top 50 m of the shelf stations (i.e., BBL1-4), which translated into positive anomalies at those stations (Figure 8a). Higher-than-normal nitrate concentrations in the surface layer were also observed during spring at HL1-2 and LL8-9 (Figure 8a) but near-surface concentrations were otherwise predominantly near or below normal for each section in both seasons.

The 50-150 m subsurface layer is characterized by a strong increase in nitrate concentrations with depth in both spring and fall (Figures 8a and 8b). A contrasting seasonal anomaly pattern was observed for the shelf stations (i.e., LL1-5, HL1-5, and BBL1-4), where nitrate concentrations were predominantly higher than normal during spring and mainly near or below normal during fall (Figures 8a and 8b). A similar contrasting pattern was also observed for CSL (i.e., CSL3-6).

The highest nitrate concentrations during spring and fall were observed in the deep (i.e., >150 m) water of each core section, particularly in central Cabot Strait, in Emerald Basin (HL3), and at the offshore stations of LL, HL, and BBL (Figures 8a and 8b). However, deep nitrate concentrations were notably below normal during spring in the slope areas of the LL, HL, and BBL sections (Figures 8a).

Overall, the annual inventory of surface nitrate, silicate, and phosphate were mainly slightly below or below normal for most sections in 2025 (Figure 7). The surface phosphate inventory reached a record-low (-2.09 sd) for HL in 2025 (Figure 7). On the other hand, the annual inventory of subsurface nitrate and silicate were mainly near normal in 2025, and mainly slightly below normal for phosphate (Figure 7). Surface and subsurface phosphate inventories have remained mainly near or below normal for all sections since 2015 and 2013, respectively (Figure 7).

Nitrate concentration profiles collected during the 2025 summer ecosystem trawl survey were used to estimate bottom nitrate fields using Barnes interpolation (Kelley and Richards 2025) with parameters tuned for the SS (following Layton et al. 2026). As expected, the highest bottom nitrate concentrations in 2025 were observed in the deep waters along the Laurentian Channel in area 4V, in the deep basins (Emerald and LaHave Basins) of the central SS in areas 4W and 4X, in the Northeast Channel, and in the deep basins (Georges, Crowell, and Jordan Basins) in the eastern GoM in area 4X (Figure 9; refer to Figure 1 for location of major banks and basins). Bottom nutrient anomalies were characterized by spatial variability (Figure 9). Positive anomalies were detected along the Laurentian Channel, on Banquereau, Canso, Sable Island, LaHave and Browns Banks, in the Northeast Channel, and in some basins in the GoM (Georges and Crowell Basins) (Figure 9). On the other hand, negative anomalies were observed in areas along the shelf break from western Cabot Strait, eastern Misaine Bank, the eastern, central and western slope areas, Lurcher Shoals, eastern GoM and the BoF (Figure 9). Overall, bottom nitrate concentrations in summer 2025 were slightly above normal for areas 4V and 4X, and slightly below normal for area 4W (Figure B1).

3.2 Dissolved Oxygen

Dissolved oxygen is a key indicator of marine ecosystem health. Oxygen depletion, or “deoxygenation”, has been documented at both global (e.g., Gilbert 2010) and local scales (e.g., Brennan et al. 2016). Oxygen deficiency is generally defined as concentrations below 6 mg/L (Bhuiyan et al. 2024). Further depletion can lead to hypoxic conditions (i.e., below ~2 mg/L), which are detrimental to most marine organisms (Vaquer-Sunyer and Duarte 2008). The solubility of oxygen in seawater is governed by temperature and salinity (Garcia and Gordon 1992). Under temperature and salinity conditions characteristic of the SS, the oxygen deficiency threshold of 6 mg/L corresponds to oxygen saturation levels of approximately 60% in winter to

75% in late summer. These values are therefore used as reference points for assessing the oxygen saturation levels reported here.

3.2.1 High-frequency Sampling Stations

In 2025, the bottom oxygen saturation at HL2 was mainly above normal in winter and fall, and otherwise near or slightly above normal for the rest of the year (Figure 10). Overall, oxygen saturation levels at HL2 were mainly within ca. 60 to 85% throughout the year resulting in a slightly positive anomaly for 2025 (Figure 10). At P5, bottom oxygen saturation levels are generally higher than at HL2 and remain mostly uniform throughout the year due in part to year-round intense vertical mixing. Bottom oxygen saturation at P5 in 2025 was normal throughout the year with saturation levels ranging between ca. 85 to 100% (Figure 10).

3.2.2 Broad-scale Surveys

Bottom oxygen saturation was relatively uniform on each section during both the spring and fall 2025 missions (Figure 11). Saturation levels near or below 60 % were observed in both seasons at HL3 (Emerald Basin) and in Cabot Strait (Figure 11). Although saturation levels for CSL were lower than those observed on the other sections during both seasons, the annual saturation anomaly level for CSL was a record-high (+2.31 sd) in 2025 (Figure 11). Otherwise, bottom oxygen saturation anomalies were normal for LL and HL and slightly above normal for BBL (Figure 11). Bottom oxygen saturation anomalies have been mainly near or above normal on the LL, HL and BBL sections and above the 60% oxygen deficiency threshold during the last three years (Figure 11).

Bottom oxygen saturation levels during the 2025 summer ecosystem trawl survey were estimated using the same method used for bottom nitrate concentrations (see section 3.1.2). The highest saturation levels were observed over most of the shallow areas of the SS and in the BoF (Figure 12). Oxygen saturation levels near or below 60% were mainly confined to deeper waters along the Laurentian Channel in area 4V, in Emerald Basin in area 4W, in LaHave Basin in area 4X east, and in Georges and Crowell Basins in area 4X west) (Figure 12; refer to Figure 1 for location of major banks and basins). Near- or above-normal saturation levels were observed over a large portion of the area, particularly along the outer Laurentian Channel and the SS slope, in the central SS and in the BoF (Figure 12). On the other hand, negative anomalies were observed in the eastern SS (south of Cape Breton Island, Banquereau, and north of Sable Island), in the western SS (LaHave and Browns Bank extended area), and in the eastern GoM (Figure 12). Overall, bottom oxygen saturation levels in summer 2025 were on average slightly above to above normal for areas 4W and 4V, respectively, and near normal for area 4X (Figure B2).

3.3 Phytoplankton

Although phytoplankton temporal and spatial variability is high in coastal and shelf waters, a recurrent annual pattern is observed across the SS, including a pronounced spring diatom-dominated phytoplankton bloom and a smaller secondary fall bloom (e.g., HL2, Figure 13). Blooms develop as phytoplankton growth outpaces losses due to grazing, sinking and other processes (Behrenfeld and Boss 2014). Spring bloom initiation is thought to be regulated by the light environment and temperature, starting with the onset of water column stratification in late winter and early spring (Sverdrup 1953). Bloom magnitude is thought to be regulated largely by nutrient supply, while bloom duration is regulated by both nutrient supply and, to a lesser extent, by loss processes such as aggregation-sinking, grazing by zooplankton (Johnson et al. 2012), and lysis (Mojica et al. 2016). Phytoplankton biomass is assessed in terms of two complementary indices: i) the integrated chlorophyll-*a* inventory derived from *in situ* measurements, and ii) the surface chlorophyll-*a* concentration derived from remote sensing observations. The abundance of the main phytoplankton functional groups (i.e., diatoms, dinoflagellates, ciliates, and flagellates) is not available for 2025; however, their annual anomalies are presented for prior years for consistency with previous reporting.

3.3.1 High-frequency Observations

The *in situ* chlorophyll-*a* concentration profiles at HL2 in 2025 indicated that the spring phytoplankton bloom observed in late March and early April was characterized by a slightly earlier-than-normal timing, a shorter-than-normal duration, and a higher-than-normal intensity as indicated by the integrated chlorophyll-*a* inventory (Figure 13). Similarly, observations of surface chlorophyll-*a* concentrations from remote sensing indicated a slightly earlier-than-normal timing (ca. 7 days) of the peak of the spring bloom occurring on March 30, with a normal intensity as expressed by the surface chlorophyll-*a* concentration averaged over the spring season (Figure 14 panel C). Following the spring phytoplankton bloom, the *in situ* chlorophyll-*a* inventory remained near or slightly below normal throughout the summer, before reaching near- to above-normal levels from mid-September until November (Figure 13). Both *in situ* (Figure 13) and remote sensing (Figure 14 panel B) observations indicated fall bloom conditions in November. Subsurface chlorophyll-*a* accumulation in the 20-40 m layer, albeit at relatively low concentrations, persisted from mid-June until the end of October (Figure 13).

Except for the peak period of the spring phytoplankton bloom, surface chlorophyll-*a* measured by remote sensing remained mainly near or slightly below normal throughout the year (Figure 14 panel B). Remote sensing observations suggested a delayed onset of the fall bloom with a lower-than-normal intensity (Figure 12 panel C). Both PAR-based and Secchi-based euphotic depth estimates at HL2 were near or slightly deeper than normal throughout most of the year in 2025, with the exception of shallower-than-normal depths observed in late March and in early August (Figure A1). Shallower euphotic depth estimates in March and August coincided with the peak of the spring bloom and the subsurface summer chlorophyll-*a* accumulation, respectively (Figure 13). Overall, at HL2 in 2025, both the annual estimates of the *in situ* chlorophyll-*a* inventory and the mean annual surface chlorophyll-*a* measured by remote sensing were below normal, the latter representing a time series record low (-1.85 sd) (Figure 15).

The chlorophyll-*a* dynamics at P5 differ considerably from those at HL2. The spring phytoplankton bloom typically occurs in June, followed by a secondary late-summer bloom occurring in late August to mid-September (Figure 13). The relatively high nitrate content in the surface layer (0-50 m) during summer (Figure 6) also sustains elevated chlorophyll-*a* inventories throughout this period. In 2025, the *in situ* chlorophyll-*a* concentration profiles at P5 indicated that the spring phytoplankton bloom peaked earlier than normal in May and had a shorter-than-normal duration (Figure 13). The intensity of the spring bloom, as indicated by the integrated chlorophyll-*a* inventory in May, was normal (Figure 13). Although chlorophyll-*a* accumulation near the surface was observed in July, the secondary summer bloom peaked later than normal, in September. Surface chlorophyll-*a* concentrations were then above normal, but the overall bloom intensity, as represented by the chlorophyll-*a* inventory, was near normal for that time of year (Figure 13)

Apart from the early-March sampling event, the *in situ* chlorophyll-*a* inventory at P5 in 2025 remained near to slightly below normal conditions for the rest of the year (Figure 13), such that its annual estimate for 2025 was near normal and contrasting with the previous two years when slightly above-normal inventories were observed (Figure 15). Surface chlorophyll-*a* concentrations measured by remote sensing were predominantly near or slightly below normal in 2025, except for the peak observed in early July (Figure 16, panel B), concurring with the *in situ* observations (Figure 13). The mean annual surface chlorophyll-*a* measured by remote sensing was slightly below normal in 2025, continuing the pattern mainly observed since 2017 (Figure 15). Both the PAR-based and Secchi-based estimates of the euphotic depth at P5 were mainly near normal in 2025, except for September (PAR-based) and November (Secchi-based), for which the estimates were deeper than normal (Figure A1).

3.3.2 Broad-scale Observations

The annual integrated *in situ* chlorophyll-*a* inventory in 2025 was above normal for HL, below normal for BBL, and near or slightly above normal for LL and CSL, respectively (Figure 17). Peak chlorophyll-*a* concentrations during the spring phytoplankton bloom are an important driver of the annual *in situ* chlorophyll-*a* inventory. Consequently, annual anomalies in this inventory are sensitive to the timing of the *in situ* sampling relative to the timing of the bloom. Nevertheless, the time series of the *in situ* chlorophyll-*a* inventory annual anomalies indicate considerable temporal variability within each section, as well as important spatial variability within specific years (Figure 17).

Annual averages of surface chlorophyll-*a* concentrations measured by satellite remote sensing ranged from near normal for LS, to slightly below normal for CS, to below normal elsewhere in 2025 (Figure 17). A record-low mean annual chlorophyll-*a* concentration was observed for WSS (-1.25 sd) and GB (-2.39 sd) in 2025 (Figure 17). Contradictory patterns between the *in situ* integrated chlorophyll-*a* inventory and the surface chlorophyll-*a* concentrations from remote sensing are not unusual (e.g., years 2005 and 2006; Figure 17). These two indices are complementary and present inherent differences in the vertical extent of the signal they capture (i.e., surface vs. water column integrated), the temporal resolution of the observations (i.e., daily vs. semi-annual), and the spatial extent they represent (i.e., averaging over sub-regions vs. section means).

Observations of surface chlorophyll-*a* concentrations from satellite remote sensing indicated an earlier-than-normal timing of the peak of the spring bloom for ESS, slightly earlier than normal for CS, and near normal elsewhere (Figure 18). The observed anomalies of the timing of the spring bloom translate to peak timing occurring around March 29 for ESS and CSS, April 6 for CS, and April 10 for WSS (Figure 18). This partially supports the above statement linking the anomalies of the *in situ* chlorophyll-*a* inventory on the core sections to the timing of sampling relative to the timing of the spring bloom, where negative anomalies for BBL (-1.18 sd; sampled on March 30-31) and LL (-0.19 sd; sampled on April 11-12) resulted from sampling prior and after the peak of the spring bloom, respectively, whereas positive anomalies for HL (+1.02 sd; sampled on April 4-6) and CSL (+0.54 sd; sampled on April 13) resulted from sampling within seven days of the peak of the spring bloom (refer to Figure 1 and Figure 4 for the association between the core sections and their respective remote sensing sub-regions).

The timing of the fall bloom initiation in 2025 was later than normal for WSS, slightly later than normal for LS and CS, and near normal elsewhere (Figure 18). Since 2022, the fall bloom initiation has been near or later than normal in the region (Figure 18).

The intensity of the spring and fall blooms is expressed as the weighted-average surface chlorophyll-*a* concentration in each season. The intensity of the spring and fall blooms was spatially variable and generally lacked coherent patterns throughout the respective time series. In 2025, the spring bloom intensity was below-normal for GB, slightly below normal for ESS, slightly above normal for CS and LS, and near normal for CSS and WSS (Figure 18). On the other hand, the intensity of the fall bloom was near (ESS and LS) to slightly below normal (CS) to below normal (CSS, WSS and GB) in 2025 (Figure 18). For GB, this represented a time series record-low (-1.41 sd) fall bloom intensity (Figure 18).

The weekly time series of surface chlorophyll-*a* concentrations indicated that the spring bloom in 2025 was slightly shorter than normal for ESS and CSS (Figure 19a). For GB, the variability in the surface chlorophyll-*a* concentrations during winter and early spring was such that spring bloom conditions were hardly discernable (Figure 19b). Surface chlorophyll-*a* concentrations in 2025 were predominantly slightly below normal during winter (i.e., prior to spring bloom) for most sub-regions, although missing data (i.e., cloud cover) may have partially obscured trends. They were also mainly below or slightly below normal from late spring (i.e., following the spring bloom) until early fall for all sub-regions (Figure 19a and Figure 19b). In late fall (November and December), surface chlorophyll-*a* concentrations were mainly near normal in most sub-regions, except for CS where data were unavailable (Figure 19a and Figure 19b).

3.4 Zooplankton

Zooplankton are a diverse group of small animals that feed primarily on phytoplankton and hence, are a critical link between primary producers and larger organisms. AZMP sampling focuses on the mesozooplankton, those zooplankton in the size range ca. 0.2 to 20 mm in length. Copepods are the most abundant zooplankton organisms in the Northwest Atlantic, while the less abundant non-copepods consist mostly of larval stages of benthic invertebrates, carnivorous groups that feed on other zooplankton, and small-particle feeders. The copepod *C. finmarchicus* is large, energy-rich, and broadly distributed throughout the region and represents an important prey for planktivorous consumers such as herring, mackerel, North Atlantic right whales, and other pelagic species. *Pseudocalanus* spp. are smaller and less energy-rich than *Calanus* spp., but they are also important prey for small fish due to their high abundance and wide spatial distribution. Zooplankton is primarily assessed here in terms of the abundance of copepods, non-copepods, *C. finmarchicus* and *Pseudocalanus* spp., and the biomass of the mesozooplankton of size class 0.2 to 10 mm.

3.4.1 High-frequency Sampling Stations

At HL2, the total abundance of zooplankton is, on average, lowest in January and February, and increases to maximum values in April, similar to the spring phytoplankton bloom peak timing, before declining to low levels again in the fall (Figure 20). In 2025, the total zooplankton abundance anomalies were variable through the year (Figure 20). Abundances were above normal in late spring (late May), early summer (late June), and during fall (late September to early November) and otherwise near or slightly below normal (Figure 20). The zooplankton community at HL2 was dominated by copepods, similar to climatological conditions. Copepods represented approximately 85 to 90% or more of the total zooplankton abundance throughout most of the year, except during peaks of appendicularians from late March to mid-April (*Fritillaria borealis*) and in mid-September (*Oikopleura* spp.) (Figure 20). Overall, at HL2, the annual mean abundances of copepods and non-copepods in 2025 were slightly above and above normal, respectively (Figure 21).

Because copepods typically dominate the local zooplankton community at both stations, their seasonal abundance pattern closely follows that of total zooplankton abundance. Total copepod abundances at HL2 in 2025 were above normal in late spring (late May), early summer (late June), and during fall (late September to early November) and otherwise near or slightly below normal (Figure 22). The abundance of the large copepod *C. finmarchicus* at HL2 in 2025 was above normal in January, February and early July (Figure 23). Otherwise, *C. finmarchicus* abundance remained near, slightly above or slightly below normal throughout the rest of the year (Figure 23), and its annual average abundance was near normal in 2025 (Figure 21 and Figure 24). The above-normal abundance of *C. finmarchicus* observed in January coincided with a higher-than-normal relative abundance of stages CIII and CIV, accounting for around 65% of the total *C. finmarchicus* abundance at that time (Figure 23). The first generation of *C. finmarchicus*, characterized by a higher abundance of early stages in spring, developed at the normal time from early April until late May (Figure 23).The dominance of stage CV occurred earlier than normal, in early July, and remained until the last sampling in November (Figure 23).

Among the eleven most abundant copepod taxa at HL2, only the small copepods *Oithona similis*, *Pseudocalanus* spp. and *Microcalanus* sp. had slightly-above or above-normal abundances in 2025 (Figure 24). *Pseudocalanus* spp. reached record-high abundance (+1.18 sd) in 2025 (similar to levels observed in 2021, Figure 21 and Figure 24) due in part to higher-than-normal relative abundances observed during the summer (Figure 22). On the other hand, *Metridia lucens* and *Temora longicornis* were relatively less abundant than normal during summer, along with *Centropages* spp. during fall (Figure 22) and their annual average abundance was lower than normal along with *O. atlantica* and *M. longa* (Figure 24).

At P5, the total abundance of zooplankton is typically lowest from January through May and increases to maximum values between July and October, lagging the increase in phytoplankton by about a month, before declining to low levels again in the late fall (Figure 20). In 2025, zooplankton abundance was near or below normal except in September and October when it was above and slightly above normal, respectively (Figure 20). The relative abundance of cirripede nauplii (included in “Others”) was above normal, particularly in May and October (Figure 20). Overall, at P5, the annual mean abundances of copepods and non-copepods in 2025 were normal and slightly above normal, respectively (Figure 21).

Similar to total zooplankton, the total copepod abundance at P5 in 2025 was near or below normal except in September and October when it was slightly above normal (Figure 25). The abundance of *C. finmarchicus* was near or slightly below normal throughout the year in 2025 (Figure 23), and its annual average abundance was near normal (Figure 21 and Figure 24). Peaks in the relative abundance of stage CI, normally associated with the development of successive generations, were observed in April, June, August, and October, and coincided with occupations with a low overall abundance of *C. finmarchicus* (e.g., ~150 individuals$\cdot m^{-2}$ in October) (Figure 23).

Annual average abundance of the nine most abundant copepod taxa was slightly above or above normal for *Pseudocalanus* spp., *Microcalanus* sp., and *Eurytemora* spp., while all other taxa had near- or below-normal abundances (Figure 24). A record-high anomaly was recorded for *Microcalanus* sp. (+1.69 sd) in 2025 due in part to its higher-than-normal relative abundance observed in spring and fall (Figure 25). Above-normal relative abundances were also observed for *Acartia* spp. and *Paracalanus* sp. in July and October, respectively (Figure 25). On the other hand, below-normal *C. finmarchicus* relative abundance was observed from July until November (Figure 23 and Figure 25).

Zooplankton biomass typically peaks around April-May at HL2 and between July and October at P5 (Figure 26). There is a strong similarity in the annual variability pattern of dry and wet biomass at both the HL2 and P5 stations (Figure 26). The dry biomass estimates are a close representation of the mesozooplankton size class (i.e., 0.2 mm to 10 mm) while the wet biomass estimates represents both mesozooplankton and macrozooplankton (i.e., larger than 10 mm), including gelatinous plankton. Wet biomass is not reported for samples containing large amounts of algae or jelly plankton. In 2025, the mesozooplankton dry biomass at HL2 was above normal in late March and early July, below normal in mid June, and otherwise near or slightly above/below normal (Figure 26). The spring peak of zooplankton biomass was observed earlier than normal in late March (Figure 26). Also, the high dry biomass observed at HL2 in early July coincided with the above-normal abundance of *C. finmarchicus*, dominated by stage CV, at that time (Figure 23). At P5, the mesozooplankton dry biomass was above normal in late March and July, below normal in August, slightly above normal in October, but otherwise mainly near or slightly below normal (Figure 26). Overall, the annual mean mesozooplankton dry biomass in 2025 was normal at both HL2 and P5 (Figure 21). For P5, this marks five consecutive years with near or above normal biomass while near to below normal at HL2 since 2021 (Figure 21).

3.4.2 Broad-scale Surveys

The abundance of *C. finmarchicus* (Figure 27) and mesozooplankton dry biomass (Figure 28) during the winter ecosystem trawl survey in area 5Ze were respectively slightly below normal and near normal in 2025. Those averages were based on a total of eight samples collected on Georges Bank (Figure 27 and Figure 28), which reflects the reduced spatial coverage of the newly updated winter survey design in the Georges Bank area. The abundance of *C. finmarchicus* during the 2025 summer ecosystem trawl survey was near normal in all three NAFO areas (i.e., 4V, 4W, and 4X) (Figure 27). For area 4W, this continues a pattern observed since 2021 (Figure 27). Mesozooplankton biomass during summer was slightly below normal in area 4X but near normal in 4V and 4W (Figure 28). Aside from years without sampling, summer biomass observations have indicated near- or below-normal levels in areas 4W since 2021, and since 2017 in areas 4V and 4X (Figure 28).

The abundance of *C. finmarchicus* on the core sections in 2025 was near to slightly below normal during the spring survey, and near to slightly above normal during the fall survey (Figure 29). Abundances were particularly high at the shelf break stations of BBL and HL during spring (Figure 29). Overall, the estimated annual abundance of *C. finmarchicus* was near normal for BBL, HL and CSL, and slightly above normal for LL (Figure 21). Mesozooplankton dry biomass was near to slightly below normal during the spring survey, and mainly near to slightly below normal during the fall survey, except slightly above normal for HL (Figure 30). High biomasses were evident during spring at LL5 and at the shelf break stations of BBL, HL and LL, and during fall in Emerald Basin (HL3) and on CSL (Figure 30). Overall, the annual estimates of mesozooplankton biomass for 2025 were normal for HL and LL and slightly below normal for BBL and CSL (Figure 21). For the central (HL) and easternmost (LL and CSL) sections, mesozooplankton biomass has remained mainly near or below normal since 2015 while BBL has shown more variability during that period (Figure 21).

The annual abundance of *Pseudocalanus* spp. in 2025 reached a record-high anomaly (+1.63 sd) for the HL section and was near (CSL) to slightly above (LL) to above (BBL) normal elsewhere (Figure 21). For HL, the abundance of *Pseudocalanus* spp. was near or above normal during both the spring and fall surveys (not shown). Total copepod abundance followed a pattern similar to *Pseudocalanus* spp. with normal abundance for CSL, slightly above normal abundance for BBL and LL, and above normal abundance for HL (Figure 21).

The non-copepod abundance anomalies for the core sections were normal (BBL and CSL) to above normal (HL and LL) in 2025 (Figure 21). Appendicularians and polychaetes reached record-high (+1.79 sd) and record-low (-1.53 sd) abundance anomalies in 2025, respectively (Figure 31). The abundances of ostracods, bivalves, echinoderms and amphipods were slightly below to below normal, while euphausiids and gastropods were at normal levels (Figure 31). The abundances of chaetognaths and cirripedes were above and slightly above normal, respectively (Figure 31). Ostracods have shown mainly lower-than-normal abundances since

2017, while other non-copepod groups have shown considerable inter-annual variability during recent years with no clear trends in their abundances (Figure 31).

3.4.3 Indicator Species

The abundance of Arctic *Calanus* species (*C. hyperboreus* and *C. glacialis*) in 2025 was slightly below to near normal for CSL, LL and HL, and slightly above to above normal for HL2, BBL and P5, following a longitudinal pattern (Figure 32). For CSL, the abundance of Arctic *Calanus* species has been mainly near or below normal since 2019 (Figure 32). The abundance of warm-water offshore species (*Clausocalanus* spp., *Mecynocera clausi*, and *Pleuromamma borealis*) reached a record-low (-1.14 sd) at P5 in 2025 (Figure 32). Their abundance anomalies were variable ranging from below normal for CSL, to near (HL2 and LL) or slightly above (BBL) normal, and above normal (HL) (Figure 32). For CSL, this is again consistent with the general pattern of near- or below-normal abundances observed in the last nine years. The abundance of warm-water shelf copepod species (the summer-fall copepods *Paracalanus* sp. and *Centropages typicus*) in 2025 was slightly above to above normal for BBL and HL, respectively, and otherwise near or slightly below normal elsewhere (Figure 32). Considerable spatial and temporal variability in the abundance of warm-water offshore and shelf species has been observed across the region in recent years (Figure 32).

4. DISCUSSION

In the Maritimes Region, the Scotian Shelf (SS) pelagic environment is characterized by a strong annual temperature and stratification cycle, and spatial variability in the form of longitudinal and cross-shelf gradients. While the temperature annual cycle and its perturbations are mostly driven by atmospheric forcing, spatial gradients are driven by the varying contributions of the three dominant source waters originating from the Gulf of St. Lawrence (GSL), the Labrador Current (LC), and the Gulf Stream (GS). Conditions at the tail of the Grand Banks (TGB), particularly sea surface height anomalies, are relevant in this context as they may help predict impending downstream shelf conditions with up to a year of lead time and with positive anomalies translating into reduced contribution of the LC to the shelf (Gonçalves Neto et al. 2021). Brickman et al. (2018) further suggested that the interaction between the LC and the GS at the TGB leads to the creation of anomalous warm/salty (or cold/fresh) eddies that travel east-to-west along the shelf break, directly influencing the spatial variability of temperature and salinity on the shelf. In addition, the complex bathymetry of the SS, with its shallow banks, deep basins, and trenches, contributes to local circulation patterns (Hannah et al. 2001), which, combined with the temporal and spatial hydrographic patterns, have direct and indirect influences on the distribution and dynamics of plankton and nutrients in the region.

Ocean temperatures on the SS and in the eastern Gulf of Maine (GoM) have shown strong inter-decadal variability since the 1950s, with recent years (2010 and onward) being generally warmer than the long-term average. In 2025, although surface conditions continued to be warmer than normal across the region, mid-depth and bottom temperatures were near or cooler than normal, particularly in Emerald and Georges Basins, and in NAFO zone 4W (Figures 59 and 60 in Layton et al. 2026). The composite anomalies (i.e., the sum of normalized anomalies) for both mid-depth and bottom temperature indices for 2025 were the lowest since 2010 (Figure 60 in Layton et al. 2026). Similar cooling of bottom waters has also been observed recently (e.g., 2024) in the GoM and was attributed to an influx of LC water entering the GoM through the Northeast Channel (Record et al. 2024). While the mean annual stratification on the SS remained above normal in 2025 (Figure 45 in Layton et al. 2026), it was spatially variable, with positive stratification anomalies observed mainly in the western part of the SS (Figure 44 in Layton et al. 2026). Stratification in 2025 remained consistent with the general increasing trend (Figure 45 in Layton et al. 2026). The contrasting pattern of continued surface warming and bottom cooling conditions likely reflects the influence of air-sea heat exchange on surface waters and changes in source water contribution in the region resulting from changes in shelf circulation. Positive shelf break transport anomalies for the Halifax section (Figure 50 and Figure 51 in Layton et al. 2026), which are usually associated with negative deep temperature anomalies, provide evidence for the role of circulation in driving temperature changes on the shelf. Surface and deep water hydrographic changes, combined with increased stratification, may be linked to changes observed in the nutrients and lower trophic level conditions presented in this report.

The nutrient environment on the SS is influenced by water inputs from upstream, including the outflow from the GSL through Cabot Strait, intrusions of slope water, and GS meanders (Pepin et al. 2013). The main advective source of nitrate and silicate for the SS is the GSL outflow during winter, while the contribution of on-shelf transport during summer can be almost as strong in some areas (Petrie and Yeats 2000). Surface nutrients display strong seasonality linked to phytoplankton production, with surface nutrient depletion typically associated with high production during spring and summer, followed by surface nutrient replenishment during late fall and winter when phytoplankton production is low and vertical mixing is high. On the other hand, deep nutrients, especially nitrate, provide a better representation of the nutrient pool available for new primary production. Deep nitrate concentrations are dependent not only on changes in shelf circulation but also on changes in the export of surface particulate nitrogen and its remineralization at depth, and on vertical flux toward the surface via mixing and/or upwelling. Nutrient-poor subsurface conditions on the SS have been reported over the period 2010-2020 despite evidence of a GS-dominated slope water source, possibly due to a shift to less dense, lower nutrient GS waters supplying the Scotian slope (Lehmann et al. 2023).

Subsurface nitrate levels were near normal across the region in 2025, which represented a slight increase over the previous two years. However, during the summer, strong negative bottom nitrate anomalies were observed along the shelf break in area 4W (i.e., portions of the central and eastern SS). These anomalies coincided with cold bottom-temperature anomalies (Figure 41 in Layton et al. 2026) and positive anomalies for bottom oxygen saturation. Summer bottom temperatures in area 4W were the coldest since 2008 (Figure 42 in Layton et al. 2026). The cool temperature, low nitrate and higher oxygen conditions are consistent with an increased influence of LC waters along the Scotian Slope, as reported in recent years (Hebert et al. 2024; Cyr et al. 2024). On-shelf transport appears to have facilitated the propagation of these anomalies toward the coast, with HL2 indicating cooler and fresher deep water throughout most of the year (Figure 18 in Layton et al. 2026), as well as above-normal oxygen saturation and relatively low nitrate in the bottom layer. Nevertheless, additional analyses are needed for a better understanding of the processes linking subsurface nutrient availability to changes in shelf circulation. Despite a temporary increase in subsurface nitrate and silicate levels in 2021 and 2022, the relatively low subsurface nutrient availability that has been observed since 2016, coupled with the increase in stratification observed on the SS, could drive lower primary productivity, with potential impacts on the community composition and productivity of the broader shelf ecosystem.

In ocean regions where annual-scale environmental variability is a dominant frequency, plankton life history, behaviour, and physiology provide adaptations that focus reproductive effort at favorable times of the year and minimize exposure to risk at unfavorable times of the year. However, unpredictable perturbations in the annual range of environmental seasonality and in seasonal timing can disrupt these adaptations (Greenan et al. 2008, Mackas et al. 2012).

Large-scale shifts in water mass boundaries also influence local plankton community composition (e.g., Keister et al. 2011). The main recurring feature of the phytoplankton dynamics on the SS and in the GoM is the spring bloom, which generally develops under favorable conditions of increased insolation, warming water temperatures, and water column stratification and stability. However, Ross et al. (2017) observed spring blooms on the SS when stratification was at its lowest, water temperature at its coldest, and when the surface mixed layer was still much deeper than the euphotic depth, in apparent contradiction with Sverdrup's (1953) critical-depth hypothesis. Similar observations of phytoplankton spring bloom initiation in the absence of vertical stratification have also been reported in the GoM (Townsend et al. 1992) and on the Newfoundland and Labrador shelf (Cyr et al. 2023).

Chlorophyll-*a* concentrations derived from satellite remote sensing were consistently below normal across the region in 2025, indicating a widespread reduction in surface phytoplankton biomass. While the spring bloom intensity appeared to be close to normal, the low annual chlorophyll-*a* concentration seemed to be driven by low concentrations in winter and summer. This regional decline may reflect the combined influence of stratification, although it was weaker in 2025 compared to previous years, and near-normal subsurface nitrate concentrations, conditions that together could limit the vertical flux of nutrients to the euphotic zone. In addition, elevated grazing pressure associated with above-normal abundances of *Pseudocalanus* spp. and Appendicularia could have further contributed to the reduced chlorophyll-*a* levels observed throughout the region.

With the exception of Cabot Strait where the spring bloom typically occurs in mid-April, the timing of the spring phytoplankton bloom in 2025 generally followed the characteristic westward progression described by Song et al. 2010, with peak chlorophyll-*a* concentrations observed in late-March on the eastern and central SS, to mid- to late-April in the western part of the region (Figure 19a and 19b). For the ESS, the earlier-than-normal timing of the spring bloom appears associated with warmer-than-normal surface conditions as observed in winter and spring in area 4Vs (Figure 12 in Layton et al. 2026). However, Friedland et al. (2024) suggested that warm winter conditions should have limited effects on spring bloom phenology and would instead result in a decreased bloom magnitude and intensity, and hence negatively affecting the overall bloom productivity. While phytoplankton growth increases with temperature (Eppley 1972), temperature effects are not solely responsible for controlling the seasonal evolution of phytoplankton populations since nutrient supply, light history, and other ecosystem-linked processes (e.g., grazing) also play prominent roles (Moisan et al. 2002).

At HL2, the development of bloom conditions in 2025 was consistent with a transient water column stratification, indicated by shoaling of the surface mixed layer in mid-March (Figure 12 in Layton et al. 2026) with subsequent peak conditions occurring in the final days of March. Transient early-season increases in phytoplankton biomass can be linked to intermittent events of mixed layer restratification (Lacour et al. 2017) or intermittency in vertical stability (Keerthi et al. 2021), typically associated with sufficiently long periods of reduced surface wind and cooling, at timescales of days, which is necessary for phytoplankton population growth before the vernal restratification. Chlorophyll-*a* dynamics at HL2 also indicated a relatively weak subsurface chlorophyll-*a* maximum that persisted from mid-June to early October in 2025. Although summertime chlorophyll-*a* is a poor proxy of the phytoplankton biomass (Craig et al., 2015), the presence of chlorophyll-*a* subsurface maxima is nevertheless indicative of phytoplankton production in the subsurface layer, which can represent a significant portion of the annual primary production on the SS (Ross et al. 2017).

In recent years, the fall phytoplankton bloom on the SS has occurred later than normal. This pattern continued in some areas in 2025, also accompanied by lower-than-normal fall bloom intensity. For example, fall bloom initiation in the western SS in 2025 was delayed by 20 days and its intensity was the lowest observed since the early 2000s. Coinciding with these observations, sea surface temperatures in early fall on the SS were anomalously warm in 2025, reaching +2.8 °C in October in area 4XSS (Figure 12 in Layton et al. 2026). Warmer sea surface temperatures during fall prolong stratification, suppressing the upward flux of nutrients required to support the development of the fall bloom. The fall bloom is ecologically significant as it provides a critical food source for overwintering zooplankton and hence is an important preconditioner for the subsequent spring population development.

The period from 2011 to 2022 was characterized by a persistent change in the zooplankton assemblage on the SS, marked most notably by the decline in the abundance of *C. finmarchicus*, the biomass-dominant member of the zooplankton assemblage, and an associated decline in mesozooplankton biomass. The year 2011 marked a regime shift to lower biomass of *Calanus* spp. on the SS, which coincided with a shift to warmer temperatures (Sorochan et al. 2019). Since 2023, however, *C. finmarchicus* abundance has returned to near- or slightly above-normal levels across much of the region, whereas the mesozooplankton biomass remained below normal, except in the BoF (P5). Although *C. finmarchicus* is a major contributor to the mesozooplankton biomass, annual-scale increases in its abundance have been weighted toward early copepodite stages, CI to CIII (Figure B3). These stages contribute less to the total biomass, and their prevalence may partly explain the counterintuitive pattern of higher *C. finmarchicus* abundance coinciding with persistently low mesozooplankton biomass in most areas, with the exception of P5.

The winter abundance level of *C. finmarchicus* is an indicator of initial conditions for production, while the late-fall abundance level is an indicator of the overwintering stock for production in the following year. Although total abundance was normal to above normal from December 2024 (Figure 21 in Casault et al. 2025) through February 2025, the population was characterized by below-normal abundance of the overwintering CV stage and elevated abundance of the younger CIII and CIV stages. The persistence of abundant CIII and CIV during December and January, followed by an increase in adults by February, suggests continued development during a period typically dominated by diapausing CVs. This pattern is consistent with delayed seasonal development or an extension of production into late autumn and early winter, suggesting a potential shift in *C. finmarchicus* phenology. Match/mismatch between phytoplankton and zooplankton resulting from shifts in their respective phenologies can have important consequences throughout the entire food web (e.g., Suchy et al. 2022).

The abundance and population dynamics of *C. finmarchicus* is particularly significant because *Calanus* spp. are an important food source for the endangered North Atlantic right whale and other ecologically important planktivores (Pershing and Stamieszkin 2020). The decline in *C. finmarchicus* abundance observed during the last decade has been linked to changes in the foraging environment and habitat use of right whales (Meyer-Gutbrod et al. 2021). During the same period, AZMP observations from nets and the Continuous Plankton Recorder (Casault et al. 2024) both suggest changes in the phytoplankton community characterized by a higher abundance of smaller taxa and lower abundance of larger diatoms, with possible effects on the zooplankton assemblage. It remains unclear whether the return of *C. finmarchicus* abundance to near- or slightly above-normal levels observed since 2023 signals a return to more normal conditions for this species or, alternatively, a change in its seasonal dynamics as seen at HL2 and P5.

Warmer temperatures are often associated with a shift to a smaller-sized taxa in the copepod community (Campbell et al. 2021), as was observed on the SS during about 2011 to 2021. Although deep water temperatures have cooled in recent years and *C. finmarchicus* abundances have returned to normal levels, surface conditions continue to be warmer than normal (Layton et al. 2026). This could favour smaller species, as seen in the near- or above-normal abundances of small taxa (e.g., *O. similis*, *Pseudocalanus* spp., *Microcalanus* sp., and *Paracalanus* sp.) at HL2 in recent years. In particular, *Pseudocalanus* spp., an important food source for larval and juvenile fish, reached record high levels in parts of the SS in 2025. The higher relative abundance of smaller taxa also contributes in part to the disconnect between total copepod abundance and mesozooplankton biomass. The cooler deep water conditions since 2022 are associated with stronger LC flow along the Scotian slope (Galbraith et al. 2026), and there is uncertainty around how long these conditions will persist.

The relationships among environmental and plankton conditions are complex, and their interpretation from a deterministic perspective requires a comprehensive analysis beyond the scope of this report. However, observations in recent years provide increasing evidence for changes in deep-nutrient availability, coupled with a shift in both phytoplankton and zooplankton communities away from the dominance of large phytoplankton cells and large, energy-rich copepods like *C. finmarchicus* toward smaller phytoplankton and copepod species. Since “classical” food webs, dominated by diatoms and *C. finmarchicus,* are associated with more efficient transfer of energy to higher trophic level pelagic animals than food webs dominated by small phytoplankton zooplankton taxa, this shift may contribute to less-productive conditions for planktivorous fish, marine mammals, and planktivorous or piscivorous seabirds in the Maritimes Region.

5. SUMMARY

- Surface nitrate inventories in 2025 were mainly slightly below or below normal in the region for a second consecutive year. One exception was P5 where the surface nitrate inventory was normal, ending a 10-year sequence of mainly below-normal conditions.
- Subsurface nitrate inventories were normal across the region in 2025. The normal subsurface nitrate inventory at P5 in 2025 also marks the end of a 10-year sequence of mainly below-normal conditions. With the exception of 2021 and 2022, subsurface nitrate inventories have remained mainly near or below normal across the region since 2016.
- Bottom dissolved oxygen saturation was mainly near to above normal levels across the region in 2025, with a record-high anomaly observed for CSL. Bottom dissolved oxygen saturation has remained mainly near to above normal across the region in the last three years.
- The inventory of *in situ* chlorophyll-*a* over the 0–100 m layer was mainly near or slightly above normal in the eastern (CSL, LL, and HL) and slightly below or below normal in the western (HL2, BBL, and P5) parts of the region in 2025. Positive anomalies observed for CSL and HL appeared linked to sampling on those sections having occurred near the peak of the spring phytoplankton bloom. On the other hand, the mean annual surface chlorophyll-*a* measured by remote sensing was mainly below normal across the region in 2025, with record-low conditions observed for HL2, WSS, and GB.
- Remote sensing observations of surface chlorophyll-*a* indicated that the peak spring phytoplankton bloom in 2025 was slightly earlier or earlier than normal in the eastern (CS and ESS) part of the region but normal elsewhere. The intensity of the spring phytoplankton bloom was variable with normal conditions for CSS and WSS, slightly above normal for CS and LS, and slightly below to below normal for ESS and GB. On the other hand, the onset of the fall phytoplankton bloom in 2025 was mainly near or later than normal, with an intensity mainly near to lower than normal. A record-low fall bloom intensity was recorded for GB in 2025.

- The abundance of both copepods and non-copepods ranged from near to above normal across the region in 2025. Non-copepod abundance has remained mainly near or above normal since 2014, while copepod abundance exhibits moderately high regional and interannual variability throughout the timeseries.
- The abundance of *C. finmarchicus* in 2025 was slightly above normal for LL but normal elsewhere. *C. finmarchicus* abundance has remained mainly near to slightly above normal across the region in the last three years after a period of mainly below normal abundance from 2011 to 2022. The abundance of *Pseudocalanus* spp. was near to above normal across the region in 2025, with record-high abundances observed for HL2 and HL. *Pseudocalanus* spp. abundance has remained mainly near to above normal across the region since 2021.
- Mesozooplankton biomass was mainly near to slightly below normal across the region in 2025, continuing the general regional pattern observed since 2011.
- Abundance anomalies of copepod indicator species (i.e., Arctic *Calanus* species, warm-water offshore species, and warm-water shelf species) were variable across the region in 2025. Arctic *Calanus* species were more abundant than normal at P5, while the abundance of warm offshore and warm shelf species was above normal for HL. On the other hand, abundances of warm offshore species were below normal at CSL and P5.

6. ACKNOWLEDGEMENTS

The authors thank the personnel at the Bedford Institute of Oceanography and St. Andrews Biological Station who contributed to sample collection, sample analysis, data analysis, data management, and data sharing. We also thank the officers and crews of the Canadian Coast Guard Ships *Capt. Jacques Cartier,* S*igma-T*, *Viola M. Davidson,* as well as the R/V *Endeavor*, the R/V *L'Atalante*, and the RRS *James Cook,* for their assistance in the collection of oceanographic data during 2025. Reviews by Marjolaine Blais (Maurice Lamontagne Institute, Mont-Joli, QC) and Gary Maillet (Northwest Atlantic Fisheries Centre, St. John's, NL) improved the manuscript.

7. REFERENCES

Beazley, L., Cardoso, D., Gordon, C., and Gjerdrum, C. 2025. Mission Report for the Maritimes Region Atlantic Zone Monitoring Program 2025 Spring Survey (EN728). Can. Tech. Rep. Hydrogr. Ocean Sci. 407: vi + 72 p.

Beazley, L., Lawson, M., Colbourne, N., Cardoso, D., Gjerdrum, C., Moors-Murphy, H., and Upson, P. 2026. Mission Report for the Maritimes Region Atlantic Zone Monitoring Program 2025 Fall Survey (JC28302). Can. Tech. Rep. Hydrogr. Ocean Sci. 422: vii + 105p.

Behrenfeld, M.J., and Boss, E.S. 2014. Resurrecting the Ecological Underpinnings of Ocean Plankton Blooms. Annu. Rev. Mar. Sci. 6: 167–194.

Brennan, C.E., Blanchard, H., and Fennel, K. 2016. Putting Temperature and Oxygen Thresholds of Marine Animals in Context of Environmental Change: A Regional Perspective for the Scotian Shelf and Gulf of St. Lawrence. PLoS ONE 11(12): e0167411.

Brickman, D., Hebert, D., and Wang, Z. 2018. Mechanism for the recent ocean warming events on the Scotian Shelf of eastern Canada. Cont. Shelf Res. 156: 11–22.

Bhuiyan, M.M.U., Rahman, M., Naher, S., Shahed, Z.H., Ali, M.M., and Islam, A.R.M.T. 2024. Oxygen declination in the coastal ocean over the twenty-first century: Driving forces, trends, and impacts. Case Studies in Chemical and Environmental Engineering. 9. 100621.

Campbell, M. D. et al. 2021. Testing Bergmann's rule in marine copepods. Ecography. 44: 1283–1295.

Casault, B., Beazley, L., Johnson, C., Devred, E., and Head, E. 2024. Chemical and Biological Oceanographic Conditions on the Scotian Shelf and in the Eastern Gulf of Maine during 2022. Can. Tech. Rep. Fish. Aquat. Sci. 3589 : vi + 72 p.

Casault, B., Johnson, C.L., Devred, E., Clay, S., and Beazley, L. 2025. Chemical and Biological Oceanographic Conditions on the Scotian Shelf and in the Eastern Gulf of Maine during 2024. Can. Tech. Rep. Fish. Aquat. Sci. 3744: vi + 58 p.

Churilova, T., Suslin, V., Krivenko, O., Efimova, T., Moiseeva, N., Mukhanov, V., and Smirnova L. 2017. Light Absorption by Phytoplankton in the Upper Mixed Layer of the Black Sea: Seasonality and Parametrization. Frontiers in Mar. Sci. 4: 90.

Clay, S., Peña, A., DeTracey, B., and Devred, E. 2019. Evaluation of Satellite-Based Algorithms to Retrieve Chlorophyll-a Concentration in the Canadian Atlantic and Pacific Oceans. Remote Sens. 11(22): 2609.

Clay, S., Layton, C., and Devred, E. 2021. BIO-RSG/PhytoFit: First release (Version v1.0.0). Zenodo.

Craig, S.E., Thomas, H., Jones, C.T., Li, W.K., Greenan, B.J., Shadwick, E.H., and Burt, W.J., 2015. The effect of seasonality in phytoplankton community composition on CO2 uptake on the Scotian Shelf. J. Mar. Syst. 147:52–60.

Cyr, F., Lewis, K., Bélanger, D., Regular, P., Clay, S., and Devred, E. 2023. Physical controls and ecological implications of the timing of the spring phytoplankton bloom on the Newfoundland and Labrador shelf. Limn. Ocean. Letters.

Cyr, F., Coyne, J., Snook, S., Bishop, C., Galbraith, P.S., Chen, N., Han, G. 2024. Physical Oceanographic Conditions on the Newfoundland and Labrador Shelf during 2023. Can. Tech. Rep. Hydrogr. Ocean Sci. 382: iv + 54 p.

DFO. 2000. Chemical and Biological Oceanographic Conditions in 1998 and 1999 – Maritimes Region. DFO Sci. Stock Status Rep. G3-03 (2000).

Eppley, R.W. 1972. Temperature and phytoplankton growth in the sea. Fishery Bull. 70(4): 1063–1085.

Friedland, K.D., Nielsen, J.M., Record, N.R, Brady, D.C., and Morrow, C.J. 2024. The phenology of the spring phytoplankton bloom in the North Atlantic does not trend with temperature. Elem. Sci. Anth., 12: 1.

Galbraith, P.S., Blais, M., Lizotte, M., Bélanger, D., Casault, B., Clay, S., Layton, C., Penney, J., Gabriel, C.-E., Ringuette, M., Azetsu-Scott, K., Chassé, J., Coyne, J., Devred, E., Johnson, C.L., Maillet, G., Shaw, J.-L., Starr, M. 2026. Oceanographic conditions in the Atlantic zone in 2025. Can. Tech. Rep. Hydrogr. Ocean. Sci. 420 : v + 49 p.

Garcia, H.E., and Gordon, L.I. 1992. Oxygen solubility in seawater: Better fitting equations. Limnol. Oceanogr. 37(6): 1307-1312.

Gilbert, D., Rabalais, N., Díaz, R., and Zhang, J. 2010. Evidence for greater oxygen decline rates in the coastal ocean than in the open ocean. Biogeosciences. 2010;7:2283–2296.

Gonçalves Neto, A., Langan, J.A., and Palter, J.B. 2021. Changes in the Gulf Stream preceded rapid warming of the Northwest Atlantic Shelf. Commun. Earth Environ. 2(74).

Greenan B.J.W., Petrie B.D., Harrison W.G., Strain P.M. 2008. The onset and evolution of a spring bloom on the Scotian Shelf. Limnol. Oceanogr. 53(5): 1759-1775.

Hannah, C. G., Shore, J. A., Loder, J. W., and Naimie, C. E. (2001). Seasonal circulation on the western and central Scotian Shelf. J. Phys. Oceanogr., 31(2), 591–615.

Harrison, G., Colbourne, E., Gilbert, D., and Petrie, B. 2005. Oceanographic Observations and Data Products Derived from Large-scale Fisheries Resource Assessment and Environmental Surveys in the Atlantic Zone. AZMP/PMZA Bull. 4: 17–23.

Hebert, D., Layton, C., Brickman, D., and Galbraith, P.S. 2024. Physical Oceanographic Conditions on the Scotian Shelf and in the Gulf of Maine during 2023. Can. Tech. Rep. Hydrogr. Ocean Sci. 380: vi + 71 p.

Holmes, R.W. 1970. The Secchi Disk in Turbid Coastal Waters. Limnol. Oceanogr. 15(5): 688–694.

Johnson, C., Harrison, G., Head, E., Casault, B., Spry, J., Porter, C., and Yashayaev, I. 2012. Optical, Chemical, and Biological Oceanographic Conditions in the Maritimes Region in 2011. DFO Can. Sci. Advis. Sec. Res. Doc. 2012/071.

Keerthi, M.G., Lévy, M., and Aumont, O. 2021. Intermittency in phytoplankton bloom triggered by modulations in vertical stability. Sci. Rep. 11, 1285.

Keister, J.E., Di Lorenzo, E., Morgan, C.A., Combes, V., and Peterson, W.T. 2011. Zooplankton species composition is linked to ocean transport in the Northern California Current. Global Change Biol. 17: 2498–2511.

Kelley, D., and Richards, C. 2025. oce: Analysis of Oceanographic Data. R package version 1.8-4.

Lacour, L., Ardyna, M., Stec, K., Claustre, H., Prieur, L., Poteau, A., Ribera D'Alcala, M., and Iudicone, D. 2017. Unexpected winter phytoplankton blooms in the North Atlantic subpolar gyre. Nature Geosci. 10: 836–839.

Layton, C., Brickman, D., Greenan, B., Galbraith, P.S., and Shaw, J.-L. 2026. Physical Oceanographic Conditions on the Scotian Shelf and in the Gulf of Maine during 2025. Can. Tech. Rep. Hydrogr. Ocean Sci. 421: vi + 93 p.

Lehmann, N., Reed, D.C., Buchwald, C., Lavoie, D., Yeats, P.A., Mei, Z.-P., and Johnson, C.L. 2023. Decadal Variability in Subsurface Nutrient Availability on the Scotian Shelf Reflects Changes in the Northwest Atlantic Ocean. J. Geophys. Res.: Oceans. 128: e2023JC019928.

Lenth, R., Piaskowski, J., Balazs, B., Bolker, B., Buerkner, P., Giné-Vázquez, I., Herve, M., Jung, M., Love, J., Miguez, F., Riebl, H., Singmann, H., Derumigny, A., and Schmidt, P. 2026. emmeans: Estimated Marginal Means, aka Least-Squares Means. R package version 2.0.4.

Mackas, D.L., Greve, W., Edwards, M., Chiba, S., Tadokoro, K., Eloire, D., Mazzocchi, M.G., Batten, S., Richardson, A.J., Johnson, C., Head, E., Conversi, A., and Pelosi, T. 2012. Changing zooplankton seasonality in a changing ocean: Comparing time series of zooplankton phenology. Progr. Oceanogr. 97–100: 31–62.

Meyer-Gutbrod, E.L., Greene, C.H., Davies, K.T.A., and Johns, D.G. 2021. Ocean regime shift is driving collapse of the north Atlantic right whale population. Oceanography 34: 22–31.

Mitchell, M., Harrison, G., Pauley, K., Gagné, A., Maillet, G., and Strain, P. 2002. Atlantic zonal monitoring program sampling protocol. Can. Tech. Rep. Hydrogr. Ocean Sci. 223.

Moisan, J.R., Moisan, T.A., and Abbott, M.R. 2002. Modelling the effect of temperature on the maximum growth rates of phytoplankton populations. Ecol. Model. 153: 197–215.

Mojica, K.D.A., Huisman, J., Wilhelm, S.W., and Brussaard, C.P.D. 2016. Latitudinal variation in virus-induced mortality of phytoplankton across the North Atlantic Ocean. ISME J. 10: 500–513.

O'Reilly, J.E., Maritorena, S., Mitchell, B. G., Siegel, D. A., Carder, K. L., Garver, S. A., Kahru, M., and McClain, C. R. 1998. Ocean color chlorophyll algorithms for SeaWiFS. J. Geophys. Res. 103: 24937–24953.

Pepin, P., Maillet, G.L., Lavoie, D., and Johnson, C. 2013. Temporal trends in nutrient concentrations in the Northwest Atlantic basin. Ch. 10 (pp. 127–150) In: Aspects of climate change in the Northwest Atlantic off Canada [Loder, J.W., G. Han, P.S. Galbraith, J. Chassé and A. van der Baaren (Eds.)]. Can. Tech. Rep. Fish. Aquat. Sci. 3045: x + 190 p.

Pershing, A.J. and Stamieszkin, K. 2020. The North Atlantic Ecosystem, from Plankton to Whales. Annu. Rev. Mar. Sci. 12(1): 339–359.

Petrie, B. 2007. Does the North Atlantic oscillation affect hydrographic properties on the Canadian Atlantic continental shelf? Atmos. Ocean 45(3): 141–151.

Petrie, B., and Yeats, P. 2000. Annual and interannual variability of nutrients and their estimated fluxes in the Scotian Shelf - Gulf of Maine region. Can. J. Fish. Aquat. Sci. 57: 2536–2546.

Petrie, B., Yeats, P., and Strain, P. 1999. Nitrate, Silicate and Phosphate Atlas for the Scotian Shelf and the Gulf of Maine. Can. Tech. Rep. Hydrogr. Ocean Sci. 203.

Record, N.R., A.J. Pershing, and Rasher, D.B. 2024. Early warning of a cold wave in the Gulf of Maine. *Oceanography* 37(3):6–9.

Ross, T., Craig, S.E., Comeau, A., Davis, R., Dever, M., and Beck, M. 2017. Blooms and subsurface phytoplankton layers on the Scotian Shelf: Insights from profiling gliders. J Marine Syst. 172: 118–127.

Song, H., Ji, R., Stock, C., et Wang, Z. 2010. Phenology of phytoplankton blooms in the Nova Scotian Shelf–Gulf of Maine region: remote sensing and modeling analysis. *J. Plankton Res.,* 32(11), 1485–1499.

Sorochan, K.A., Plourde, S., Morse, R., Pepin, P., Runge, J., Thompson, C., and Johnson, C.L. 2019. North Atlantic right whale (Eubalaena glacialis) and its food: (II) interannual variations in biomass of Calanus spp. on western North Atlantic shelves. J. Plankton Res. 41(5): 687–708.

Suchy, K.D., Young, K., Galbraith, M., Perry, R.I., and Costa, M. 2022. Match/Mismatch Between Phytoplankton and Crustacean Zooplankton Phenology in the Strait of Georgia, Canada. Front. Mar. Sci. 9.

Sverdrup, H.U. 1953. On Conditions for the Vernal Blooming of Phytoplankton. J. Cons. Perm. Int. Explor. Mer. 18: 287–295.

Therriault, J.-C., Petrie, B., Pepin, P., Gagnon, J., Gregory, D., Helbig, J., Herman, A., Lefaivre, D., Mitchell, M., Pelchat, B., Runge, J., and Sameoto, D. 1998. Proposal for a Northwest Atlantic Zonal Monitoring Program. Can. Tech. Rep. Hydrogr. Ocean Sci. 194.

Townsend, D.W., Keller, M.D., Sieracki, M.E., and Ackleson, S.G. 1992. Spring phytoplankton blooms in the absence of vertical water column stratification. Nature. 360: 59–62.

Utermöhl, von H. 1931. Neue Wege in der quantitativen Erfassung des Plankton.(Mit besonderer Berücksichtigung des Ultraplanktons.). Verh. Int. Verein. Theor. Angew. Limnol. 5**:** 567–595.

Vaquer-Sunyer, R, and Duarte, C. 2008. Thresholds of hypoxia for marine biodiversity. Proc Natl Acad Sci USA. 105:15452–15457.

Wiebe, P.H., Baumgartner, M.F., Copley, N.J., Lawson, G.L., Davis, C., Ji, R., and Greene, C.H. 2022. Does predation control the diapausing stock of Calanus finmarchicus in the Gulf of Maine?. Progr. Oceanogr., 206.

Wilson, K., Hilborn, A., Clay, S. and Devred, E. 2024. Improving Satellite Chlorophyll-a Retrieval in the Turbid Waters of the Bay of Fundy, Canada. Estuaries and Coasts, 47: 1012-1031.

8. TABLES

Table 1. Atlantic Zone Monitoring Program sampling surveys in the Maritimes Region in 2025.

Group	Location	Survey ID	Dates	# Hydro Stations	# Net Stations
Ecosystem Trawl Survey - Winter	Western Scotian Shelf/Georges Bank/Bay of Fundy	CAR2025-002	Mar 1–Mar 30	120	19
Ecosystem Trawl Survey - Summer	Scotian Shelf/ Bay of Fundy	CAR2025-010	Jun 30–Aug 5	180	39
Seasonal Sections - Spring	Scotian Shelf	EN728	Mar 29–Apr 18	96	92
Seasonal Sections - Fall	Scotian Shelf	JC28302	Sep 28–Oct 21	91	83
High-frequency Stations	Halifax-2	BCD2025-666	Jan 13–Nov 20	22(7)[1]	19(7)[1]
High-frequency Stations	Prince 5	BCD2025-669	Mar 4–Nov 21	10	10
			Total:	504	250

[1]For Halifax-2, the first number indicates the total number of occupations (including occupations during the ecosystem trawl surveys and the seasonal sections), and the number in parentheses indicates the number of dedicated occupations with station-specific survey ID.

9. FIGURES

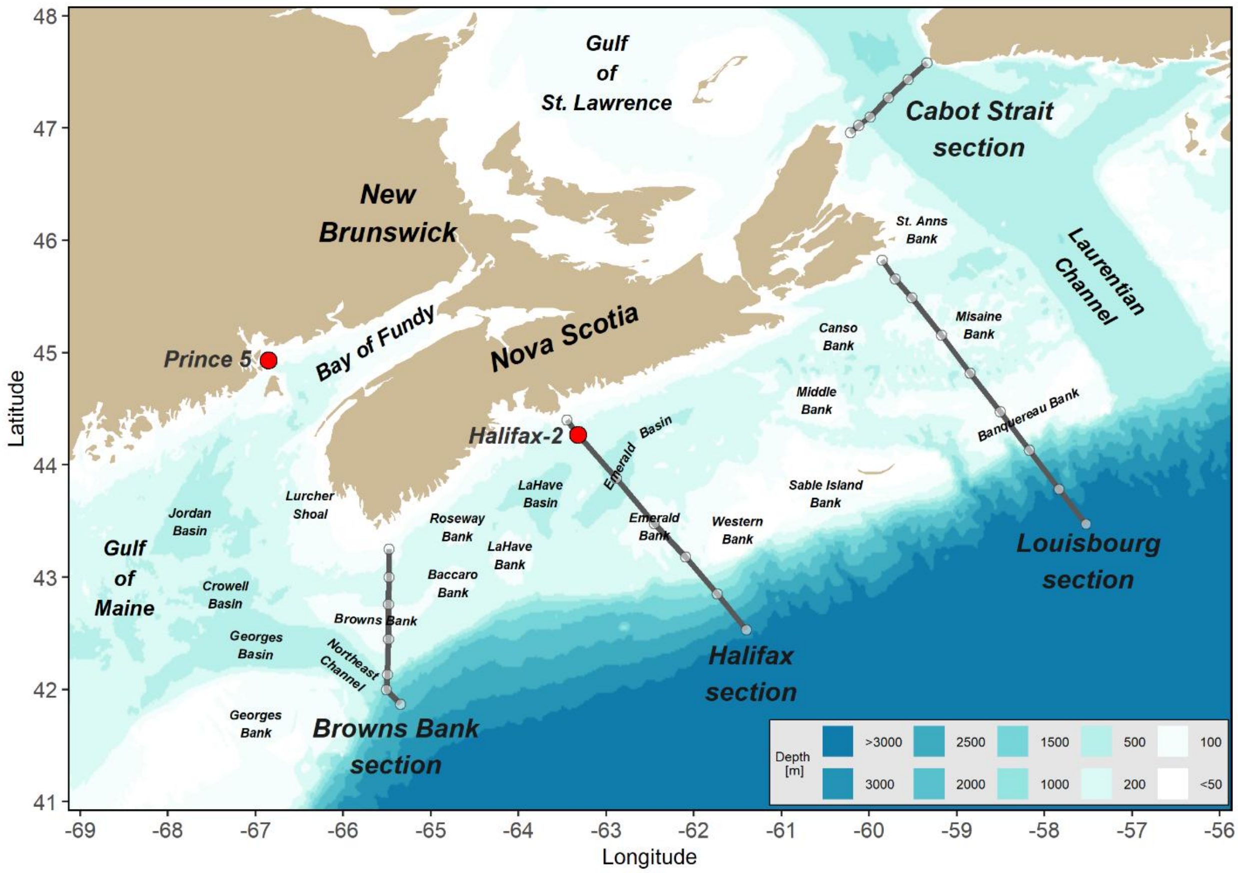

Figure 1. Map of core sections (Cabot Strait [CSL]; Louisbourg [LL]; Halifax [HL]; Browns Bank [BBL]) and high-frequency sampling stations (Halifax-2 [HL2]; Prince 5 [P5]) sampled in the DFO Maritimes Region. Gray open circles indicate the location of core sampling stations on each section.

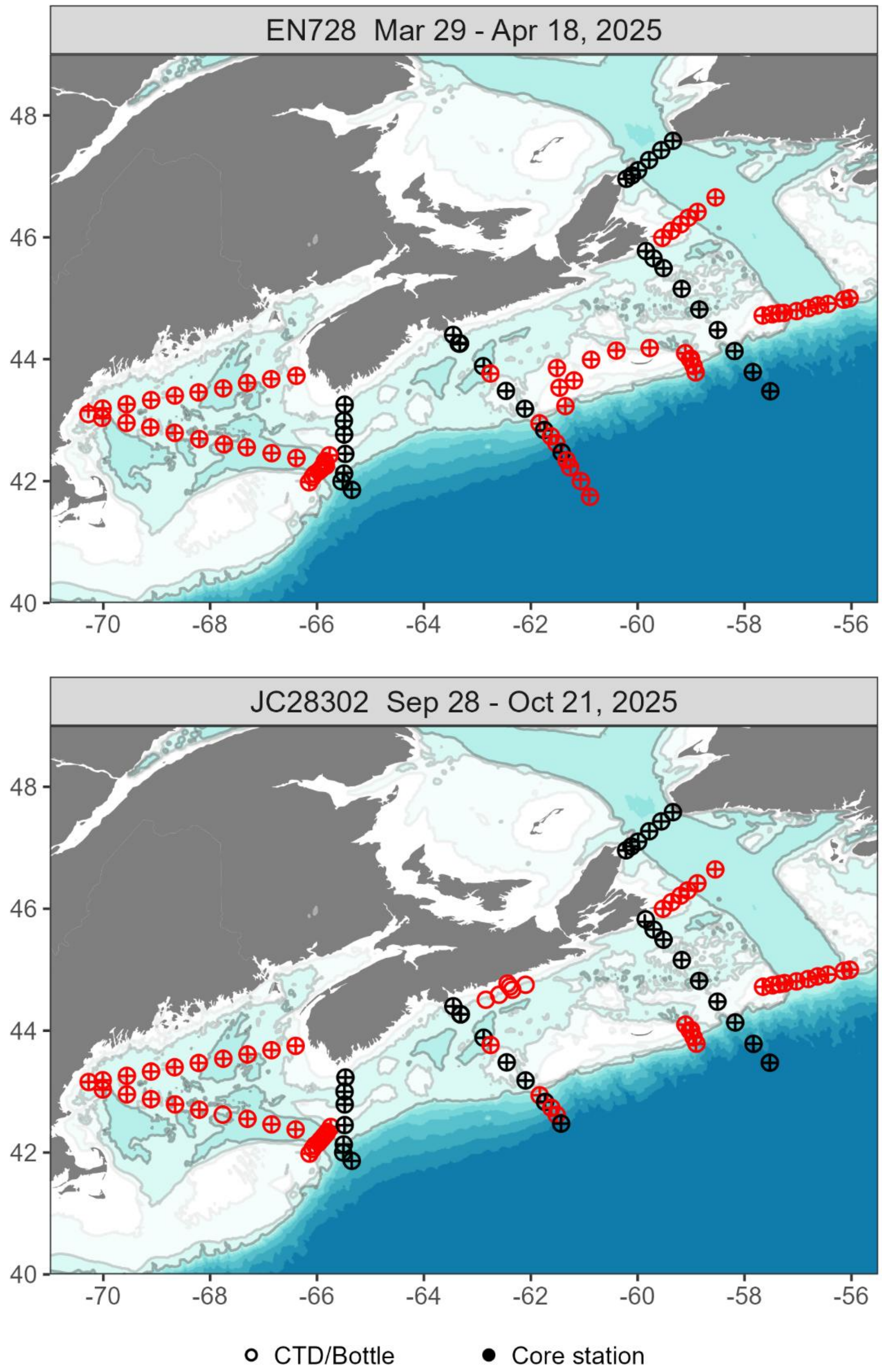

Figure 2. Stations sampled during the 2025 spring (top panel) and fall (bottom panel) surveys. Black markers indicate core stations and red markers indicate stations sampled for ancillary programs; **o** *markers indicate CTD/Bottle casts and* **+** *markers indicate ring net tows.*

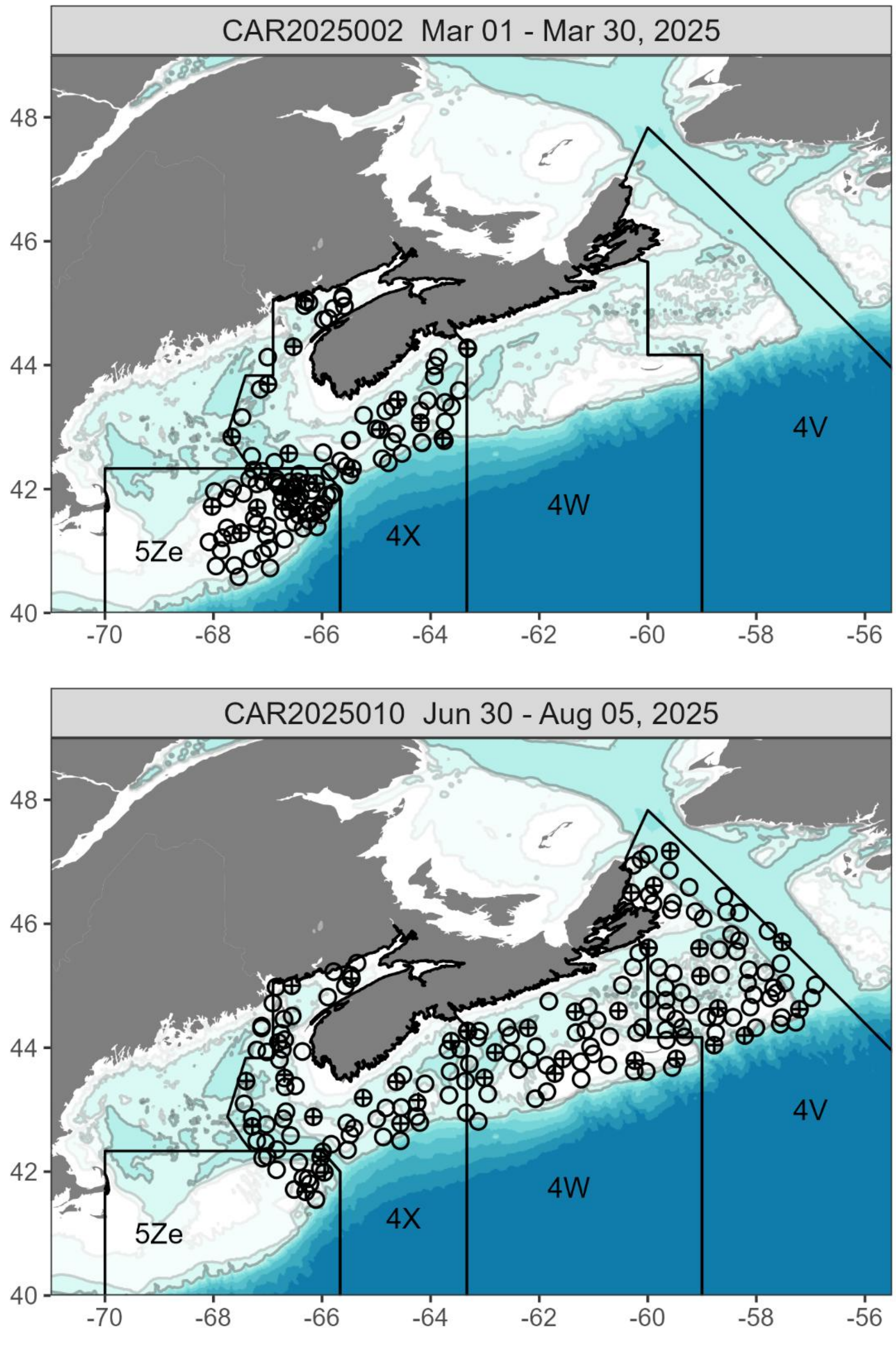

Figure 3. Stations sampled during the 2025 winter (top panel) and summer (bottom panel) ecosystem trawl surveys. Station locations are superimposed on NAFO areas. ***o*** *markers indicate CTD/Bottle casts and* ***+*** *markers indicate ring net tows.*

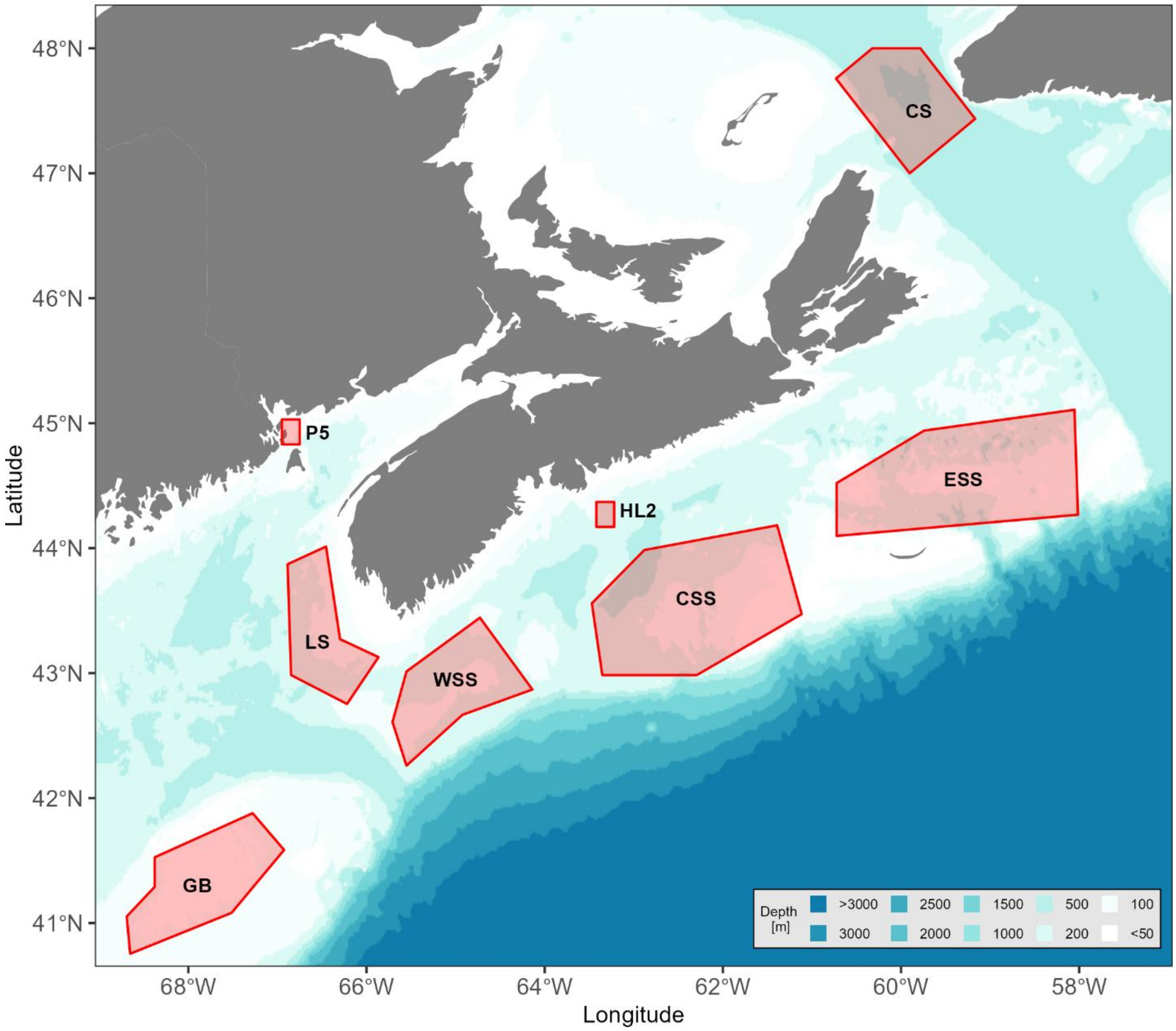

Figure 4. Sub-regions in the Maritimes Region identified for spatial/temporal analysis of satellite ocean color data. Halifax-2 [HL2]; Prince-5 [P5]; Cabot Strait [CS]; Eastern Scotian Shelf [ESS]; Central Scotian Shelf [CSS]; Western Scotian Shelf [WSS]; Lurcher Shoal [LS]; Georges Bank [GB].

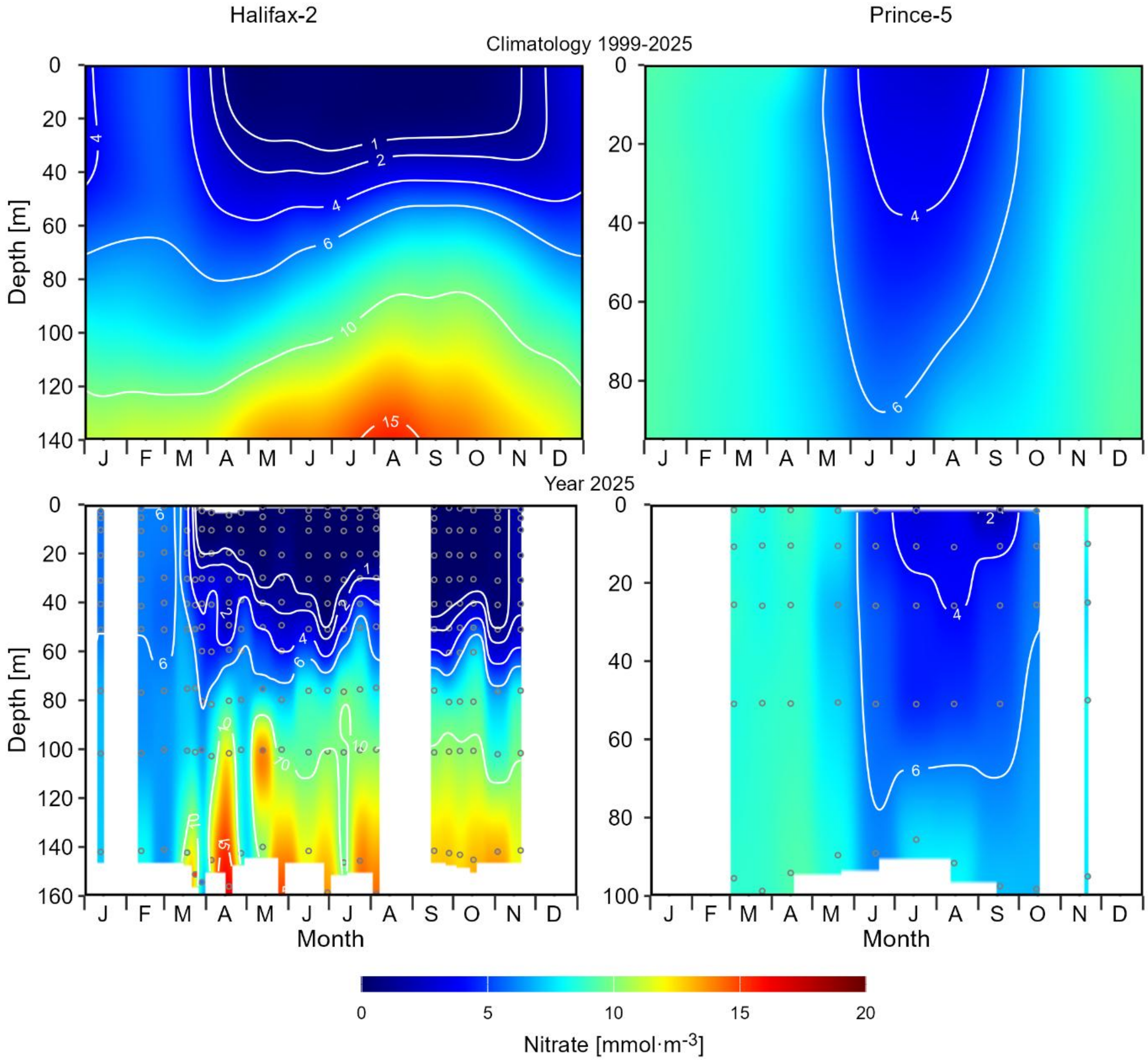

Figure 5. Nitrate concentrations at the Maritimes high-frequency sampling stations. Top panels: Climatological mean vertical structure of nitrate concentrations for the reference period 1999-2025. Bottom panels: Vertical structure of nitrate concentrations in 2025. Colored circles in the bottom panels indicate discrete samples. Blanked areas indicate no data.

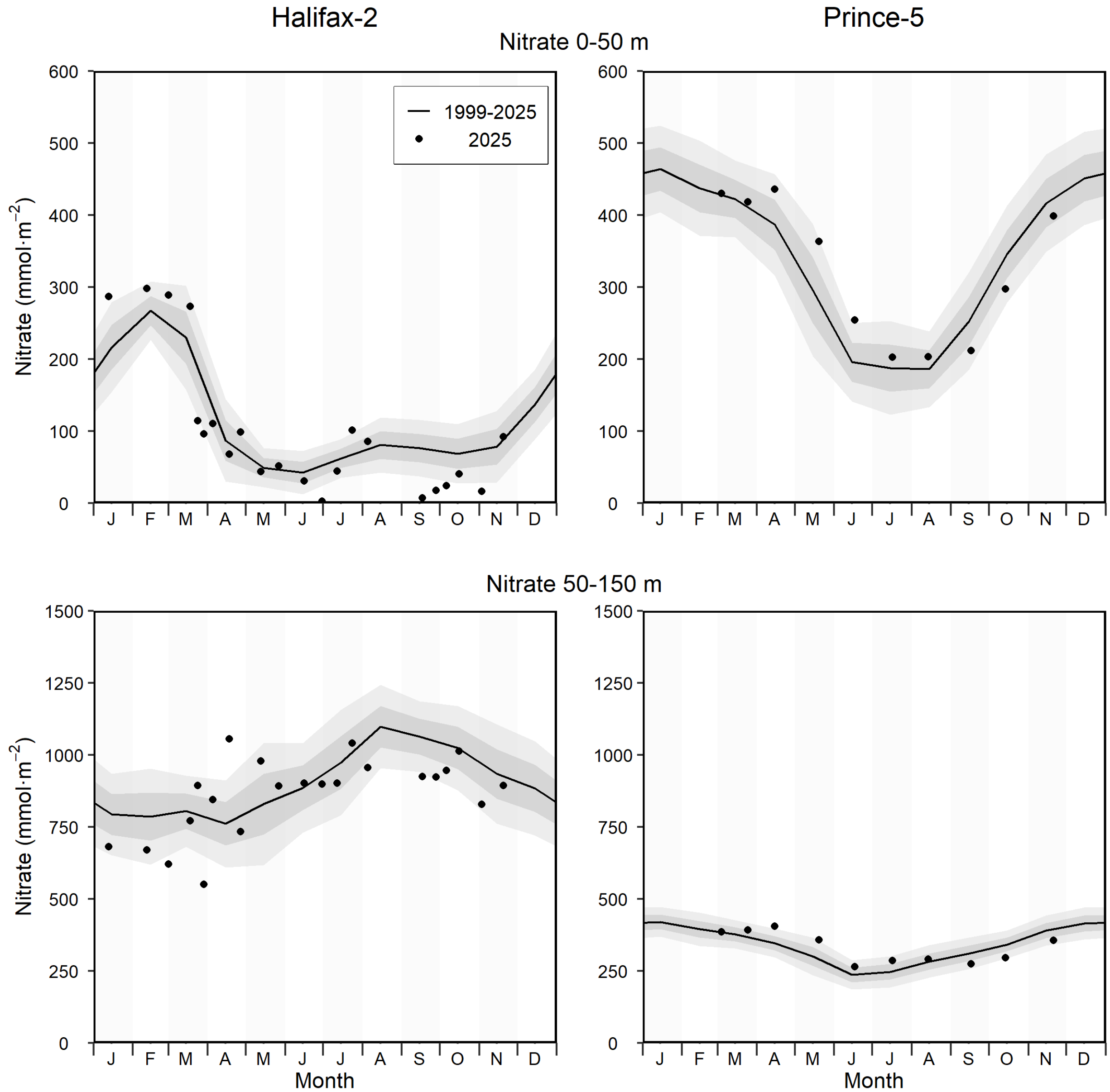

Figure 6. Nitrate inventories at the Maritimes high-frequency sampling stations. Top panels: Surface (0–50 m) nitrate inventory. Bottom panels: Subsurface (50–150 m for Halifax-2 and 50–95 m for Prince 5) nitrate inventory. The solid circles represent the 2025 data; the solid line represents the monthly climatological means for the reference period 1999-2025; the gray shaded ribbons represent the standard deviation (±0.5 and ±1 sd) of the monthly means.

	1999	2000	2001	2002	2003	2004	2005	2006	2007	2008	2009	2010	2011	2012	2013	2014	2015	2016	2017	2018	2019	2020	2021	2022	2023	2024	2025	
Surface Nitrate [0-50 m]																												
CSL	1.02	0.20	-0.25		-1.02	-0.60	0.14	-0.42	0.71	0.98	-0.14	-1.67	1.11	0.64	1.77	0.51	-0.33	-0.93	0.37	-0.72	-0.87	0.41	1.51	1.14	0.14	-1.86	-1.84	106.0 ± 27.5
LL	0.98	0.83	-0.89	-1.59	0.18	-0.65	-0.37	0.14	0.26	0.91	-0.17	0.09	-0.18	-0.23	0.54	0.87	0.90	-1.05	1.25	-1.48	0.35	-1.58	0.39	2.74	-0.02	-1.09	-1.10	75.5 ± 20.7
HL	1.73	-0.05	0.15	-0.80	-1.06	-1.17	-0.51	-0.24	-0.85	1.45	-0.44	0.11	0.70	1.12	1.53	1.68	-0.65	-0.54	-0.14	0.54	-1.91	-0.31	0.84	0.26	0.94	-0.81	-1.60	77.8 ± 24.1
HL2	-1.54	1.79	-1.42	-0.67	1.27	0.16	0.19	0.52	0.59	1.75	0.22	1.47	-0.22	-2.27	1.25	-0.19	0.23	-1.07	-0.13	-0.68	-0.36	0.04	0.73	0.07	-0.17	-0.84	-0.72	118.7 ± 22.3
BBL	-0.11	1.38	-0.03	-0.15	0.26	-0.34	0.07	-0.01	-1.45	1.50	0.27	-0.21	0.70	-0.36	0.52	2.54	0.13	0.07	-0.15	0.56	-0.80	-1.81	1.48	-1.75	-0.21	-1.45	-0.65	140.4 ± 39.1
P5	-0.70	0.17	-0.18	1.40	1.35	0.56	0.34	1.78	0.30	0.92	1.77	-0.56	0.87	0.94	0.14	0.41	-1.07	-0.80	-1.21	-1.12	-0.83	-0.57	-0.53	-0.90	-2.17	-0.65	0.35	334.3 ± 36.8
Surface Silicate [0-50 m]																												
CSL	1.05	0.26	-0.14		-0.29	-0.32	0.11	-0.33	1.22	1.25	-0.06	-1.31	1.18	-0.27	1.98	0.61	-0.44	-1.20	0.51	-0.99	-0.98	-0.51	1.71	0.71	-0.61	-1.84	-1.30	130.1 ± 35.8
LL	2.22	1.28	-0.54	-1.05	-0.09	0.57	-0.11	0.28	1.53	0.63	-0.15	0.14	-0.04	-0.78	-0.00	0.60	0.53	-0.54	0.34	-2.24	-0.87	-1.25	-0.14	1.97	-0.95	-0.96	-0.37	86.0 ± 25.5
HL	1.33	0.21	-0.17	-0.95	-1.10	-0.70	-0.11	-0.07	-0.17	1.47	0.56	-0.10	1.12	2.21	2.12	-0.44	-0.70	-0.64	-0.34	-1.15	-1.97	-0.06	0.74	0.01	0.24	-0.19	-1.16	84.7 ± 26.8
HL2	-0.58	1.60	-0.76	-1.36	-0.49	-1.06	0.18	0.78	1.09	1.79	0.45	2.29	0.30	-1.76	0.55	-0.68	0.02	-1.20	-0.18	-0.86	-0.12	0.41	1.04	-0.52	0.48	-0.68	-0.72	147.4 ± 25.6
BBL	-0.42	1.50	-0.08	-0.27	-0.38	-0.24	0.75	0.12	-0.65	1.95	0.87	-0.34	1.36	-0.60	1.62	0.69	0.22	-0.90	-0.71	-0.72	-1.46	-0.65	1.49	-1.99	0.27	-1.26	-0.16	135.3 ± 31.0
P5	-0.86	-1.17	-0.18	0.28	0.80	0.43	0.16	1.27	0.61	1.62	1.78	1.03	1.34	0.48	-1.21	-1.09	-1.14	-1.67	-0.27	-1.45	-0.94	0.17	-1.01	-0.41	0.46	0.08	0.88	324.1 ± 34.3
Surface Phosphate [0-50 m]																												
CSL	-0.80	1.58	2.81		0.10	-0.38	0.16	-0.31	0.96	0.31	0.92	0.10	0.53	0.58	0.59	0.42	0.14	-0.32	-0.10	-0.75	-0.19	-0.74	0.19	-0.71	-1.42	-1.97	-1.72	26.8 ± 5.2
LL	-0.47	1.55	2.76	0.05	0.64	-0.03	0.39	0.11	0.38	0.69	0.38	1.45	0.24	-1.04	0.54	0.15	-0.33	-0.65	-0.24	-1.57	-0.30	-1.65	0.00	0.47	-0.53	-1.33	-1.65	21.7 ± 3.8
HL	-0.11	0.46	2.75	-0.26	-0.90	-0.04	0.55	-0.19	0.17	1.66	0.53	0.60	1.55	0.16	0.96	0.33	-0.64	-0.58	-0.29	-1.16	-1.16	-0.47	0.21	-0.48	-0.21	-1.32	-2.09	19.9 ± 3.6
HL2	-0.14	1.37	-1.17	1.48	0.85	-0.26	0.71	0.48	0.90	1.49	-0.03	0.67	0.84	-1.20	2.08	-0.21	-0.19	-0.07	-0.27	-1.24	-0.38	-0.68	-0.24	-0.36	-1.46	-1.38	-1.59	26.0 ± 3.7
BBL	-1.15	1.39	2.52	-0.10	-0.14	0.06	0.56	-0.31	-0.20	1.62	1.06	0.35	1.28	0.01	0.26	0.69	-0.10	-0.40	-0.22	-0.73	-0.54	-1.65	0.34	-1.15	-0.51	-1.41	-1.55	24.4 ± 5.2
P5	-0.27	0.53	1.16	0.90		0.58	0.33	0.73	1.76	0.54	0.85	1.36	1.40	0.74	-0.29	-0.12	-0.65	0.21	-0.55	-1.38	-0.96	-1.42	-0.71	-0.95	-2.13	-0.71	-0.97	38.7 ± 4.1
Sub-surface Nitrate [50-150 m]																												
CSL	0.03	1.26	-0.97		-0.56	-0.45	-0.48	1.19	-0.93	-0.25	0.88	-1.41	-0.55	1.19	0.47	0.09	1.28	-1.51	-1.84	-0.23	0.77	0.09	1.14	2.17	-0.32	-0.73	-0.33	761.6 ± 114.7
LL	1.11	1.75	-0.77	-0.96	0.08	0.32	0.05	2.11	-0.37	0.55	0.64	0.86	-0.40	0.57	-0.35	0.14	1.23	-1.00	-1.88	-1.78	-1.46	-0.41	0.96	0.35	-0.82	-0.39	-0.15	613.6 ± 70.8
HL	0.91	1.34	-0.04	-0.56	0.30	-0.42	-1.84	0.96	-0.99	0.95	0.78	-0.72	-0.78	-0.03	0.02	0.47	1.20	-0.04	-2.19	-0.77	-0.31	0.63	1.90	-0.30	0.83	-1.68	0.35	685.7 ± 61.3
HL2	0.05	1.36	-1.16	0.72	1.43	1.12	-1.89	0.73	-0.69	0.04	0.40	1.28	-0.71	1.55	-0.11	0.18	0.56	-0.34	-1.10	-1.60	-0.42	-0.41	0.77	1.10	-1.19	-1.32	-0.37	910.6 ± 102.7
BBL	-0.49	0.47	0.25	-0.38	1.45	1.31	-0.11	0.46	-0.73	0.46	0.52	0.89	0.52	1.36	0.55	1.84	0.26	-1.13	-1.77	-0.56	-0.67	-2.46	-0.49	0.41	-1.04	-0.95	0.02	656.6 ± 65.2
P5	-0.46	0.17	-0.30	1.48	1.52	0.25	0.22	1.53	0.24	0.88	1.99	-0.51	0.09	1.18	0.02	0.33	-0.60	-0.76	-1.89	-0.81	-0.74	-0.64	-0.29	-0.49	-2.33	-0.43	0.34	337.2 ± 32.3
Sub-surface Silicate [50-150 m]																												
CSL	0.59	1.16	-0.93		-0.26	-0.61	-0.88	0.75	-0.58	-0.07	1.04	-1.67	-0.17	0.68	0.85	-0.31	1.05	-1.41	-1.70	-0.19	0.72	-0.14	1.68	2.16	-0.40	-0.75	-0.62	748.4 ± 126.1
LL	1.93	1.29	0.02	-0.70	0.48	0.49	0.18	1.08	0.16	1.03	0.29	0.40	-0.46	1.11	-0.22	0.15	-0.00	-0.35	-1.22	-1.94	-2.39	-0.99	1.44	-0.11	-0.99	-0.68	-0.00	515.9 ± 80.1
HL	2.08	0.80	0.84	-0.60	-0.67	-0.38	-0.96	1.01	0.15	1.34	1.15	-0.99	0.52	1.23	0.34	-1.36	-0.07	-0.05	-1.28	-1.83	-1.30	-0.24	1.42	-0.36	-0.52	-0.53	0.27	485.3 ± 61.6
HL2	1.51	1.44	-0.23	0.14	0.72	1.29	-1.62	0.82	0.10	0.35	0.37	0.57	-0.31	1.39	-0.49	-0.35	0.38	-0.54	-1.19	-1.82	-0.67	-0.32	0.85	1.21	-1.26	-1.83	-0.51	887.7 ± 95.1
BBL	-0.59	0.49	-0.19	0.66	0.73	1.76	0.06	0.24	0.98	1.00	0.50	0.39	1.55	0.54	0.50	0.11	0.44	-1.74	-1.45	-1.99	-1.52	-1.94	-0.36	-0.07	0.42	-0.49	-0.02	427.8 ± 42.1
P5	-0.58	-1.28	-0.03	0.81	0.78	0.25	0.65	0.97	0.80	1.28	2.15	1.05	0.96	0.55	-1.25	-1.53	-0.79	-1.55	-1.01	-0.95	-1.35	-0.09	-0.91	-0.16	0.43	0.41	0.41	307.7 ± 28.9
Sub-surface Phosphate [50-150 m]																												
CSL	-2.19	1.90	1.81		0.59	-0.58	0.07	0.34	-0.17	-0.12	2.03	-0.22	0.07	1.20	0.25	-0.23	0.49	-0.96	-0.91	-0.72	0.40	-0.90	0.47	0.36	-0.97	-0.93	-1.07	86.3 ± 11.2
LL	-1.28	1.62	2.18	-0.40	0.92	0.32	0.50	0.79	-0.16	0.84	1.70	0.87	0.26	0.64	-0.38	-0.44	-0.04	-0.11	-1.05	-1.50	-1.26	-1.34	0.57	-0.73	-0.90	-0.64	-0.99	66.5 ± 8.5
HL	-0.87	0.87	2.76	-0.33	-0.24	0.58	0.02	0.48	0.63	1.32	0.31	0.99	1.71	-0.21	-0.13	-0.30	0.48	-0.34	-0.95	-1.76	-0.76	-0.72	0.32	-0.86	-0.68	-1.59	-0.75	62.6 ± 6.9
HL2	-0.19	0.56	-0.29	1.01	0.95	0.84	-0.49	0.27	0.11	0.36	-0.07	0.69	0.82	0.45	3.35	-0.19	0.08	-0.32	-0.70	-1.50	-0.71	-0.52	-0.28	-0.17	-1.92	-1.33	-0.81	98.3 ± 13.7
BBL	-2.11	0.57	1.93	-0.20	0.17	1.02	0.40	-0.24	0.80	0.87	0.70	0.45	1.84	1.33	-0.08	0.20	0.36	-1.13	-0.81	-1.23	-0.31	-1.74	-0.83	0.05	-0.43	-0.81	-0.79	57.3 ± 7.8
P5	-0.33	0.70	0.95	0.80		0.54	0.21	0.59	1.81	0.55	1.18	1.50	1.13	0.55	-0.62	-0.17	-0.36	0.62	-0.75	-1.25	-0.95	-1.58	-0.50	-0.88	-2.08	-0.52	-1.14	36.9 ± 3.8

Figure 7. Annual anomaly scorecards for surface (0–50 m) and subsurface (50–150 m) nitrate, silicate, and phosphate inventories. Values in each cell are anomalies from the mean for the reference period 1999–2025, in standard deviation (sd) units (mean and sd listed at right in units of mmol·m^{-2}). Red (blue) cells indicate higher- (lower-) than-normal nutrient inventories, with shading intensity reflecting the magnitude of the anomaly. Gray cells indicate missing data. CSL: Cabot Strait section; LL: Louisbourg section; HL: Halifax section; HL2: Halifax-2; BBL: Browns Bank section; P5: Prince 5.

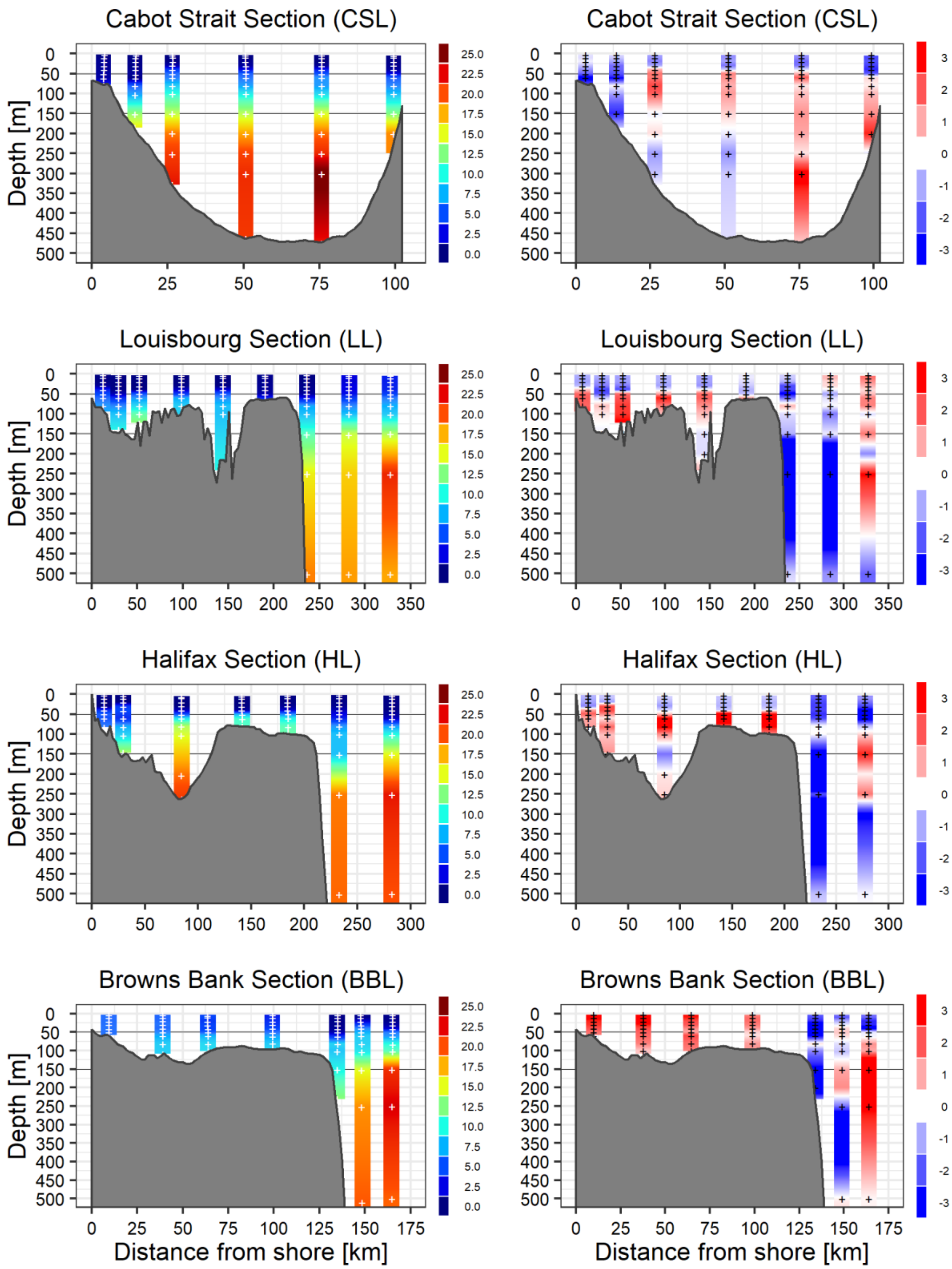

Figure 8a. Nitrate concentrations on the core sections in spring 2025. Left panels: Nitrate concentration profiles (mmol·m^{-3}) measured in spring 2025. Right panels: Nitrate concentration anomalies (mmol·m^{-3}) from the climatological means for the reference period 1999–2025. White markers on the left panels indicate the actual sampling depths. Black markers on the right panels indicate the depths at which station-specific climatological values were calculated.

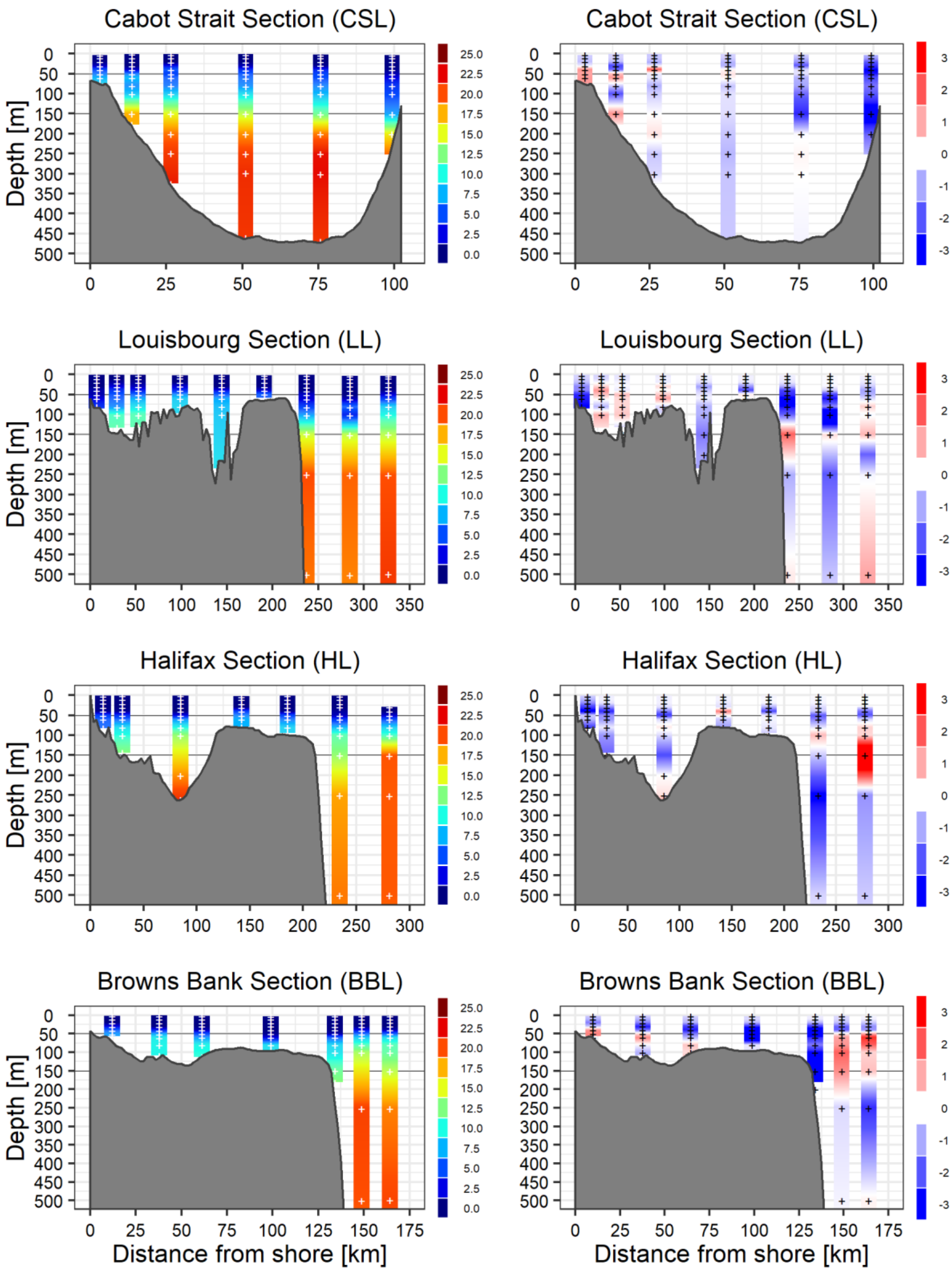

Figure 8b. Nitrate concentrations on the core sections in fall 2025. Left panels: Nitrate concentration profiles (mmol·m^{-3}) measured in fall 2025. Right panels: Nitrate concentration anomalies (mmol·m^{-3}) from the climatological means for the reference period 1999–2025. White markers on the left panels indicate the actual sampling depths. Black markers on the right panels indicate the depths at which station-specific climatological values were calculated.

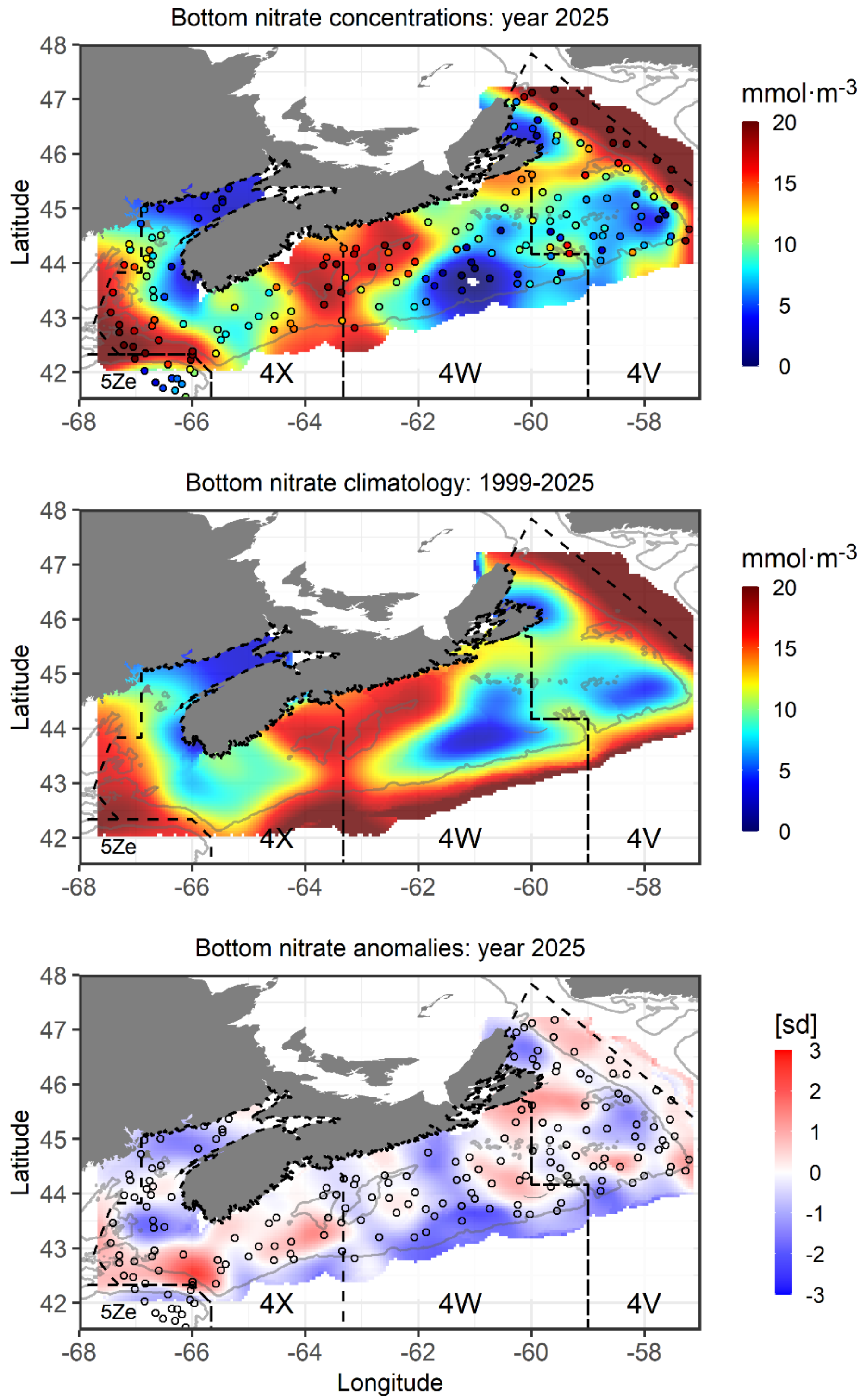

Figure 9. Bottom nitrate concentrations during the summer ecosystem trawl survey. Top panel: Nitrate concentrations during 2025. Middle panel: Climatological mean spatial structure of nitrate concentrations for the reference period 1999-2025. Bottom panel: Normalized anomalies (in units of standard deviations, sd) of bottom nitrate concentrations. Colored circles in the top and bottom panels represent the 2025 sampling locations. The light gray line is the 200 m isobath.

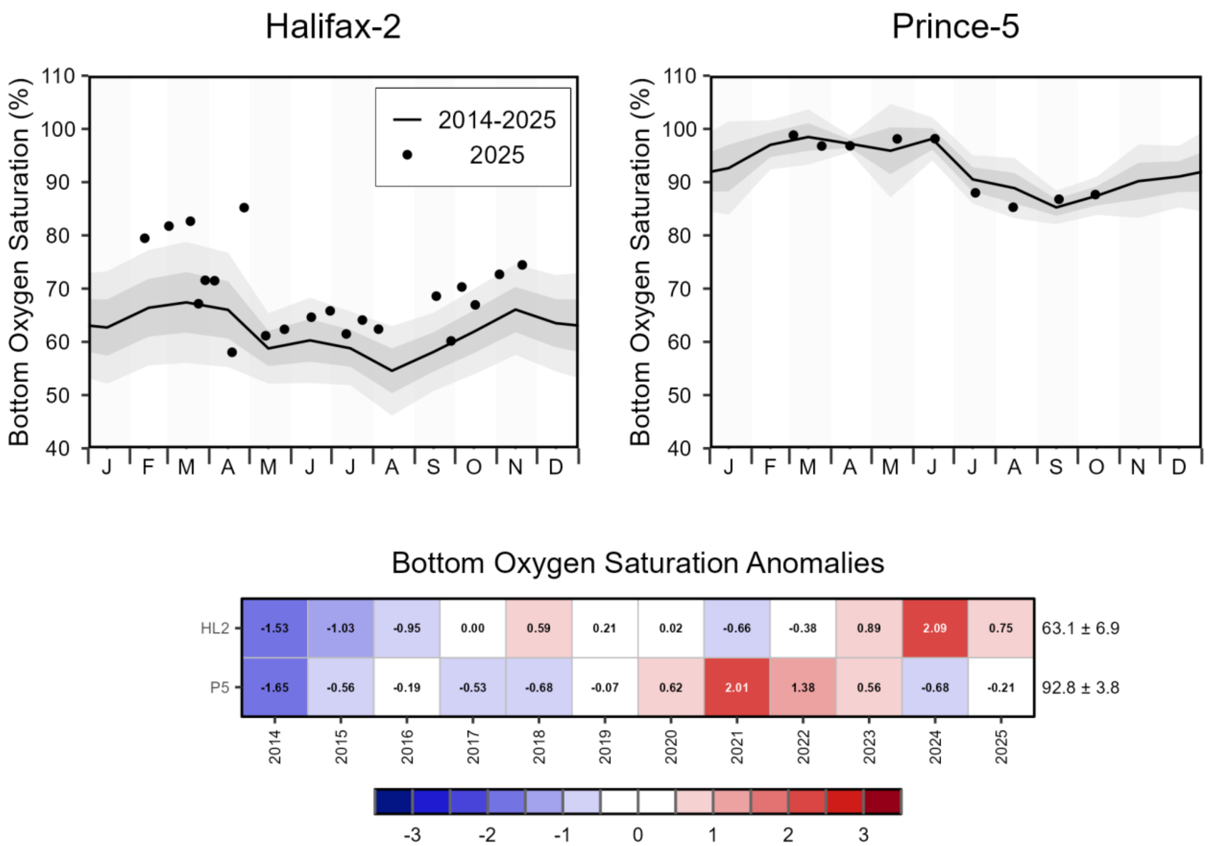

Figure 10. Bottom oxygen saturation at the Maritimes high-frequency sampling stations. Top panels: Annual variability in bottom oxygen saturation. The solid circles represent the 2025 data; the solid line represents the monthly climatological means for the reference period 2014-2025; the gray shaded ribbons represent the standard deviation (±0.5 and ±1 sd) of the monthly means. Bottom panel: Annual anomaly scorecard for bottom oxygen saturation; values in each cell are anomalies from the mean for the reference period 2014–2025, in standard deviation (sd) units (mean and sd listed at right in % saturation); red (blue) cells indicate above- (below-) normal saturation levels, with shading intensity reflecting the magnitude of the anomaly.

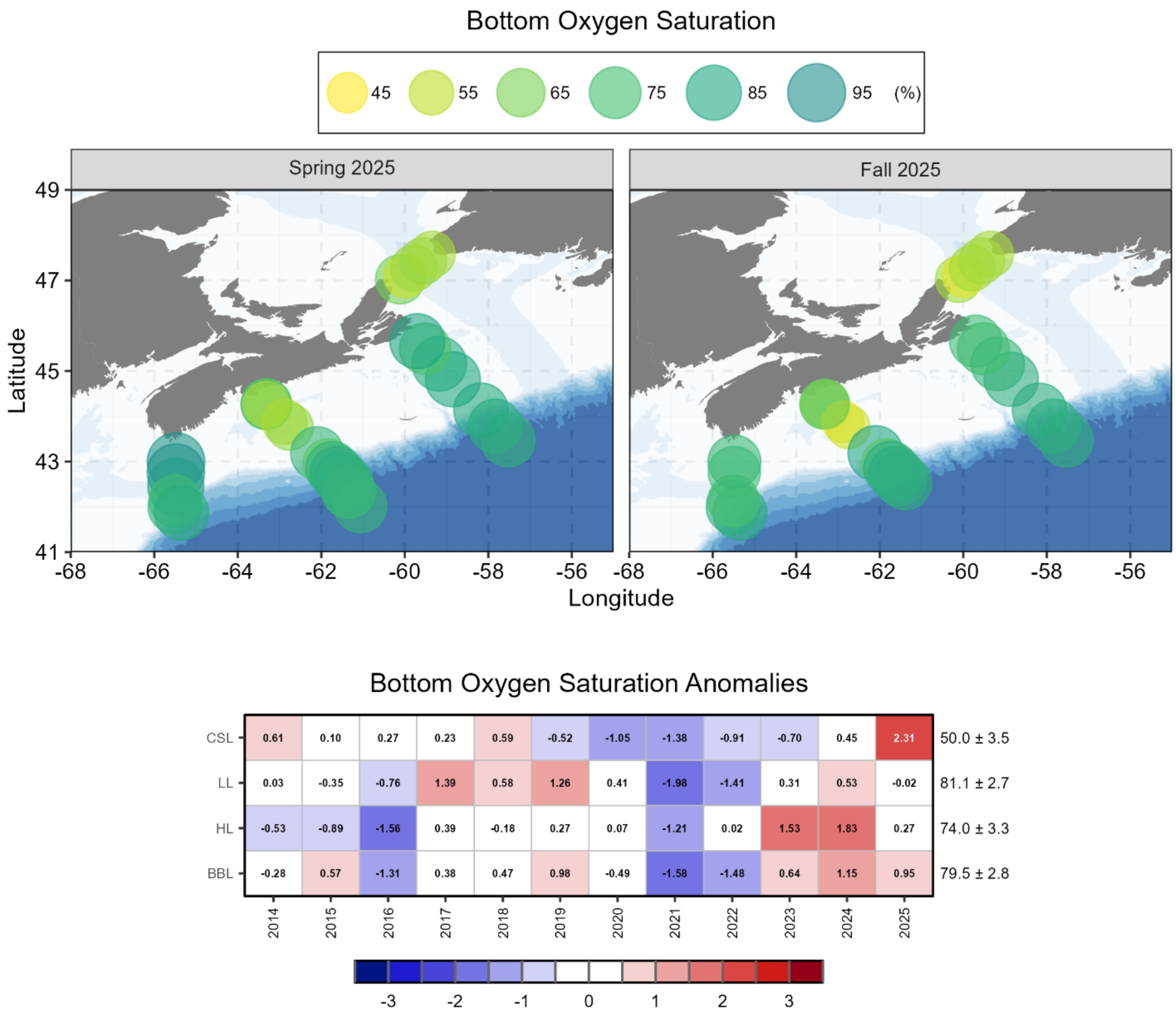

Figure 11. Bottom oxygen saturation during the seasonal surveys on the core sections. Top panels: Bottom oxygen saturation in spring (left) and fall (right) 2025. Bottom panel: Annual anomaly scorecard for bottom oxygen saturation; values in each cell are anomalies from the mean for the reference period 2014–2025, in standard deviation (sd) units (mean and sd listed at right in % saturation); red (blue) cells indicate above- (below-) normal saturation levels, with shading intensity reflecting the magnitude of the anomaly. CSL: Cabot Strait section; LL: Louisbourg section; HL: Halifax section; BBL: Browns Bank section.

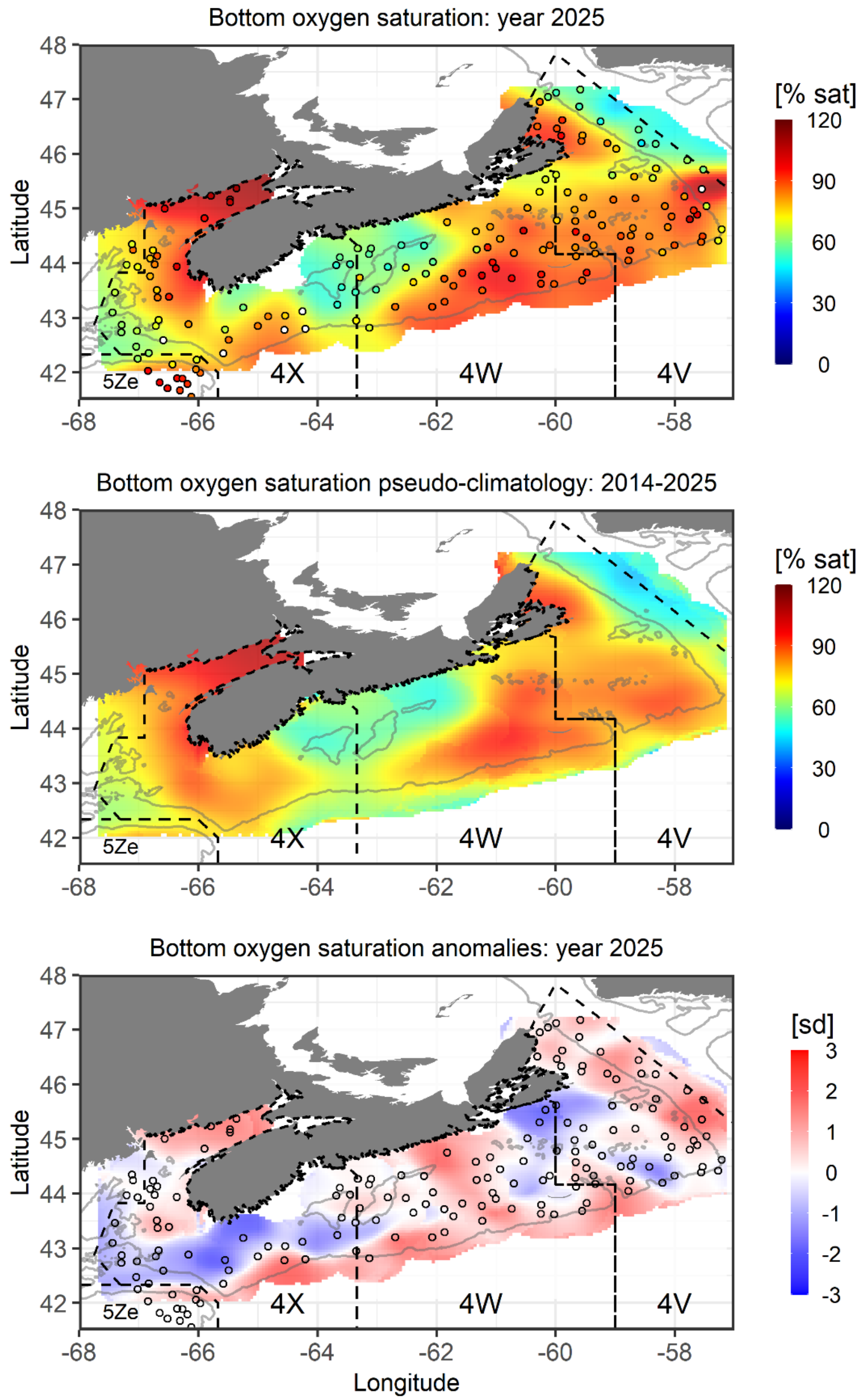

Figure 12. Bottom oxygen saturation during the summer ecosystem trawl survey. Top panel: Bottom oxygen saturation during 2025. Middle panel: Pseudo-climatological mean spatial structure of bottom oxygen saturation for the reference period 2014-2025. Bottom panel: Normalized anomalies (in units of standard deviations, sd) of bottom oxygen saturation. Colored circles in the top and bottom panels represent the 2025 sampling locations. The light gray line is the 200 m isobath.

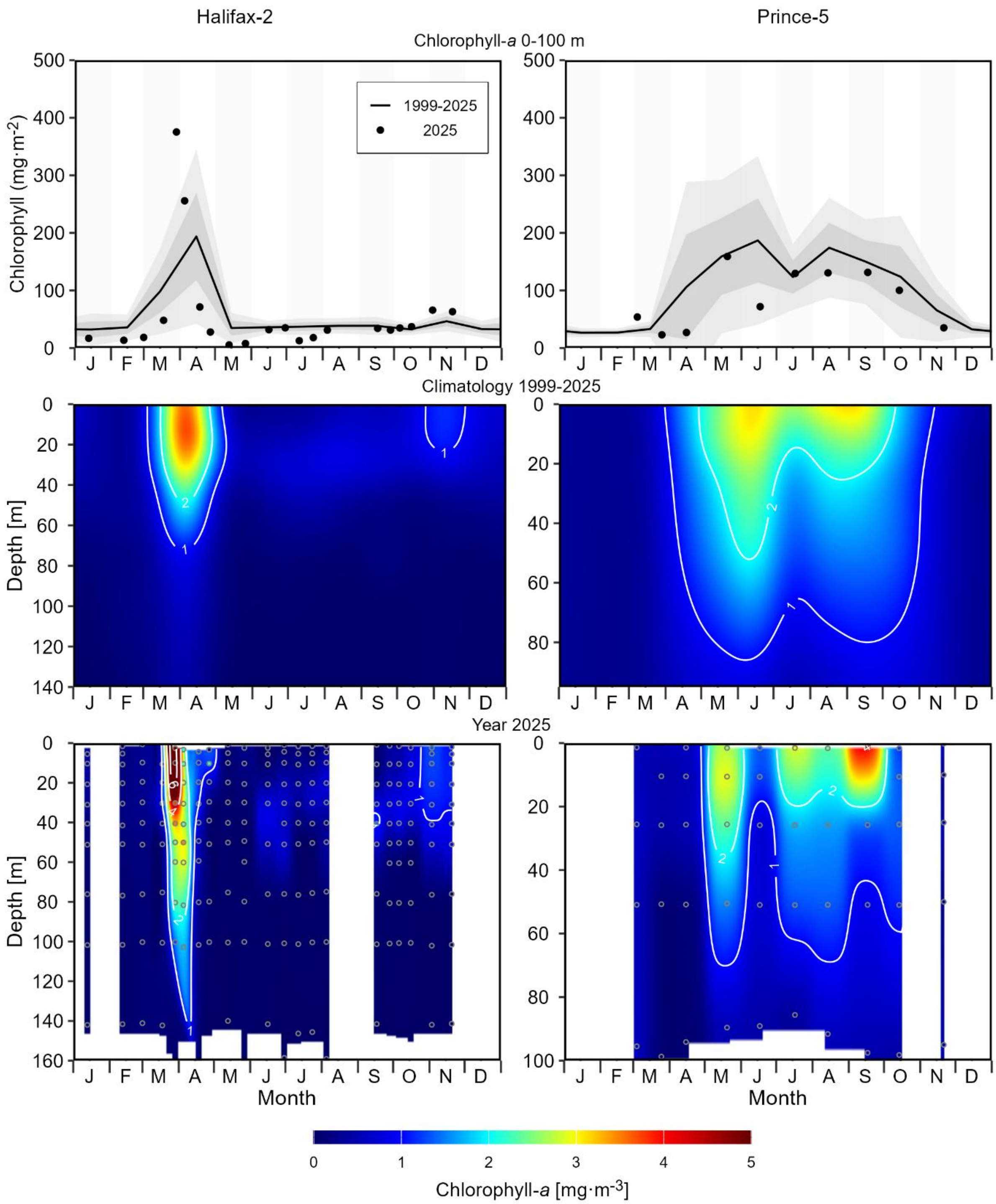

Figure 13. Chlorophyll-a inventory and concentrations at the Maritimes high-frequency sampling stations. Top panels: Chlorophyll-a inventory (0–100 m for Halifax-2 and 0–95 m for Prince 5); the solid circles represent the 2025 data; the solid line represents the monthly climatological means for the reference period 1999-2025; the gray shaded ribbons represent the standard deviation (±0.5 and ±1 sd) of the monthly means. Middle panels: Monthly climatological mean vertical structure of chlorophyll-a concentrations for the reference period 1999-2025. Bottom panels: Vertical structure of chlorophyll-a concentrations in 2025. Colored circles in the bottom panels indicate discrete samples. Blanked areas indicate no data.

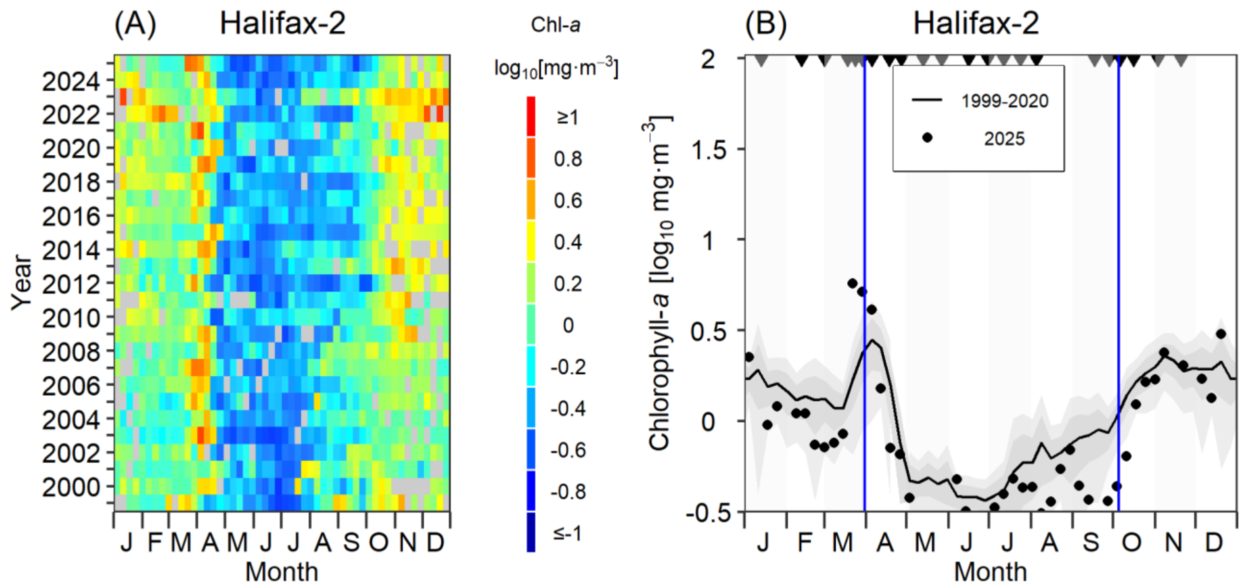

(C) Bloom Metrics Anomalies

Halifax-2

	1999	2000	2001	2002	2003	2004	2005	2006	2007	2008	2009	2010	2011	2012	2013	2014	2015	2016	2017	2018	2019	2020	2021	2022	2023	2024	2025	
Spring maximum	-2.85	0.36	1.62	-0.56	0.13	0.25	-0.78	-0.56	-0.44	0.47	0.47	-1.01	0.93	-1.01	0.59	0.02	1.51	-0.78	-0.21	-0.67	0.36	1.39	-0.44	1.51	1.05	-0.56	-0.78	97±9
Spring intensity	-0.83	0.30	-1.23	-0.37	3.12	-0.47	-0.57	0.36	2.01	-0.68	0.43	-1.45	-1.34	-0.43	-0.96	1.14	-0.13	-0.86	0.10	-0.24	0.80	0.41	0.40	0.47	-0.25	-0.05	0.31	1.95±0.64
Fall initiation	-2.46	1.83	-1.03	-0.55	0.88	0.09	0.09	-0.31	1.20	-0.63	-1.90	-0.39	0.64	-0.95	-1.11	0.48	0.24	0.16	0.88	0.16	-0.07	1.20	-1.19	0.40	0.40	0.72	1.20	263±13
Fall intensity	0.65	-0.37	-0.26	-0.13	-1.56	-0.93	-0.77	-0.83	-0.50	0.73	-0.24	-0.42	0.12	-0.80	1.07	0.29	-0.07	0.24	-0.13	-0.36	0.59	-0.41	0.31	1.87	3.48	-0.46	-1.13	1.47±0.36

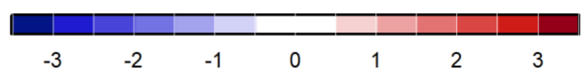

Figure 14. Surface chlorophyll-a concentrations and phytoplankton bloom metrics derived from remote sensing ocean color data for Halifax-2 sub-region. Top left panel (A): Time series of weekly mean surface chlorophyll-a concentrations; gray pixels indicate missing data. Top right panel (B): Weekly mean surface chlorophyll-a concentrations; the solid circles represent the 2025 data; the solid line represents the weekly climatological means for the reference period 1999-2025; the gray shaded ribbons represent the standard deviation (±0.5 and ±1 sd) of the weekly means; the vertical blue lines indicate the timing of the spring bloom maximum intensity (left) and the timing of the fall bloom initiation (right) in 2025; black triangles indicate in situ chlorophyll-a sampling dates. Bottom panel (C): Annual anomaly scorecard for the spring and fall phytoplankton bloom metrics; values in each cell are anomalies from the mean for the reference period 1999–2025, in standard deviation (sd) units (mean and sd listed at right in units of Day-of-Year for spring maximum and fall initiation, $mg_{chl} \cdot m^{-3}$ for spring and fall intensity); red (blue) cells indicate later (earlier) timing, or higher- (lower-) than-normal intensity of the bloom, with shading intensity reflecting the magnitude of the anomaly.

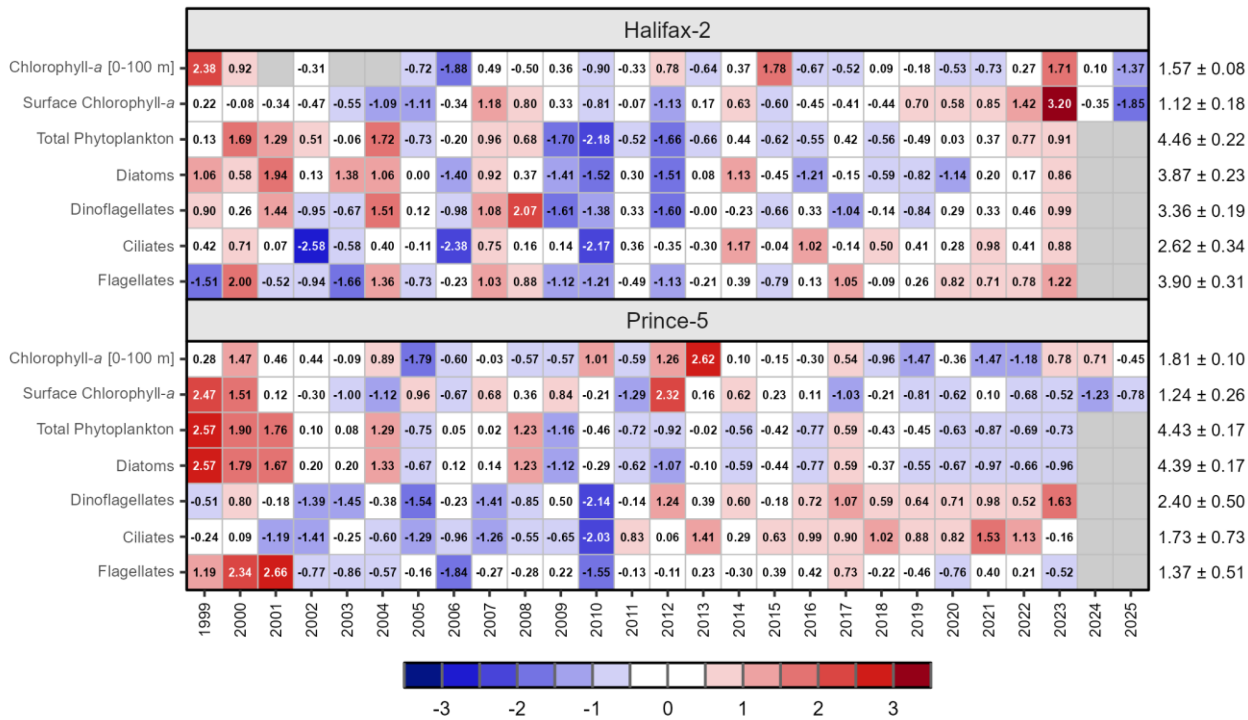

Figure 15. Annual anomaly scorecards for in situ chlorophyll-a inventory, remote sensing surface chlorophyll-a concentration, and phytoplankton abundance at the Maritimes high-frequency sampling stations. Values in each cell are anomalies from the mean for the reference period 1999–2025 in standard deviation (sd) units (mean and sd listed at right in units of $log_{10}(mg \cdot m^{-2})$ for chlorophyll-a inventory, $log_{10}(mg \cdot m^{-3})$ for chlorophyll-a concentration, and $log_{10}(cells \cdot L^{-1}+1)$ for phytoplankton abundance). Red (blue) cells indicate higher- (lower-) than-normal chlorophyll-a inventories/concentrations or phytoplankton abundances, with shading intensity reflecting the magnitude of the anomaly. Gray cells indicate missing data.

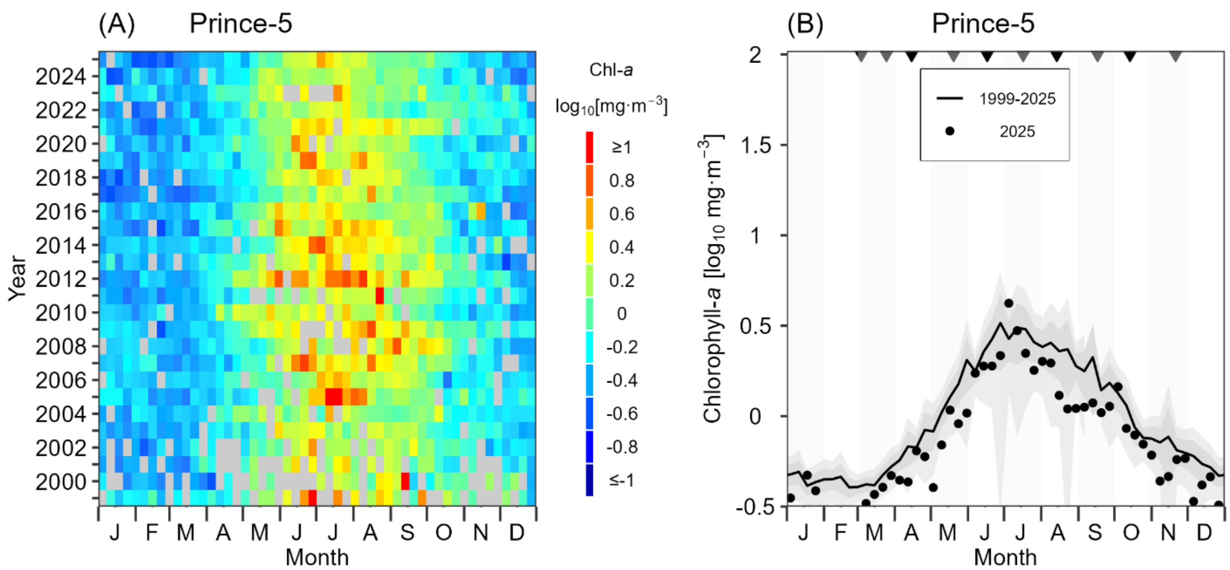

Figure 16. Surface chlorophyll-a concentrations derived from remote sensing ocean color data for Prince-5 sub-region. Top left panel (A): Time series of weekly mean surface chlorophyll-a concentrations; gray pixels indicate missing data. Top right panel (B): Weekly mean surface chlorophyll-a concentrations; the solid circles represent the 2025 data; the solid line represents the weekly climatological means for the reference period 1999-2025; the gray shaded ribbons represent the standard deviation (±0.5 and ±1 sd) of the weekly means; black triangles indicate in situ chlorophyll-a sampling dates.

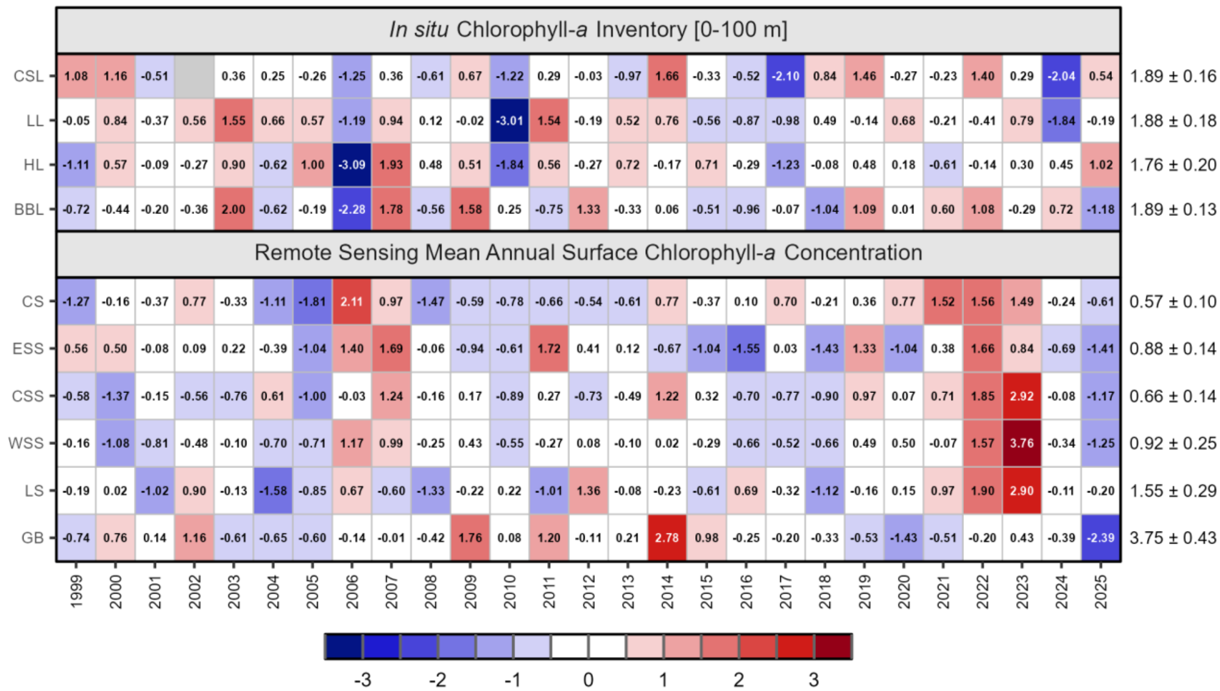

Figure 17. Annual anomaly scorecards for in situ chlorophyll-a inventory (0–100 m) on the Cabot Strait [CSL], Louisbourg [LL], Halifax [HL] and Browns Bank [BBL] sections (top panel) and for remote sensing surface chlorophyll-a concentrations on the Cabot Strait [CS], Eastern Scotian Shelf [ESS], Central Scotian Shelf [CSS], Western Scotian Shelf [WSS], Lurcher Shoal [LS], and Georges Bank [GB] sub-regions (bottom panel). Values in each cell are anomalies from the mean for the reference period 1999–2025, in standard deviation (sd) units (mean and sd listed at right in units of $log_{10}(mg \cdot m^{-2})$ for chlorophyll-a inventory and $log_{10}(mg \cdot m^{-3})$ for chlorophyll-a concentration). Red (blue) cells indicate higher- (lower-) than-normal chlorophyll-a inventories or surface chlorophyll-a concentrations, with shading intensity reflecting the magnitude of the anomaly. Gray cells indicate missing data.

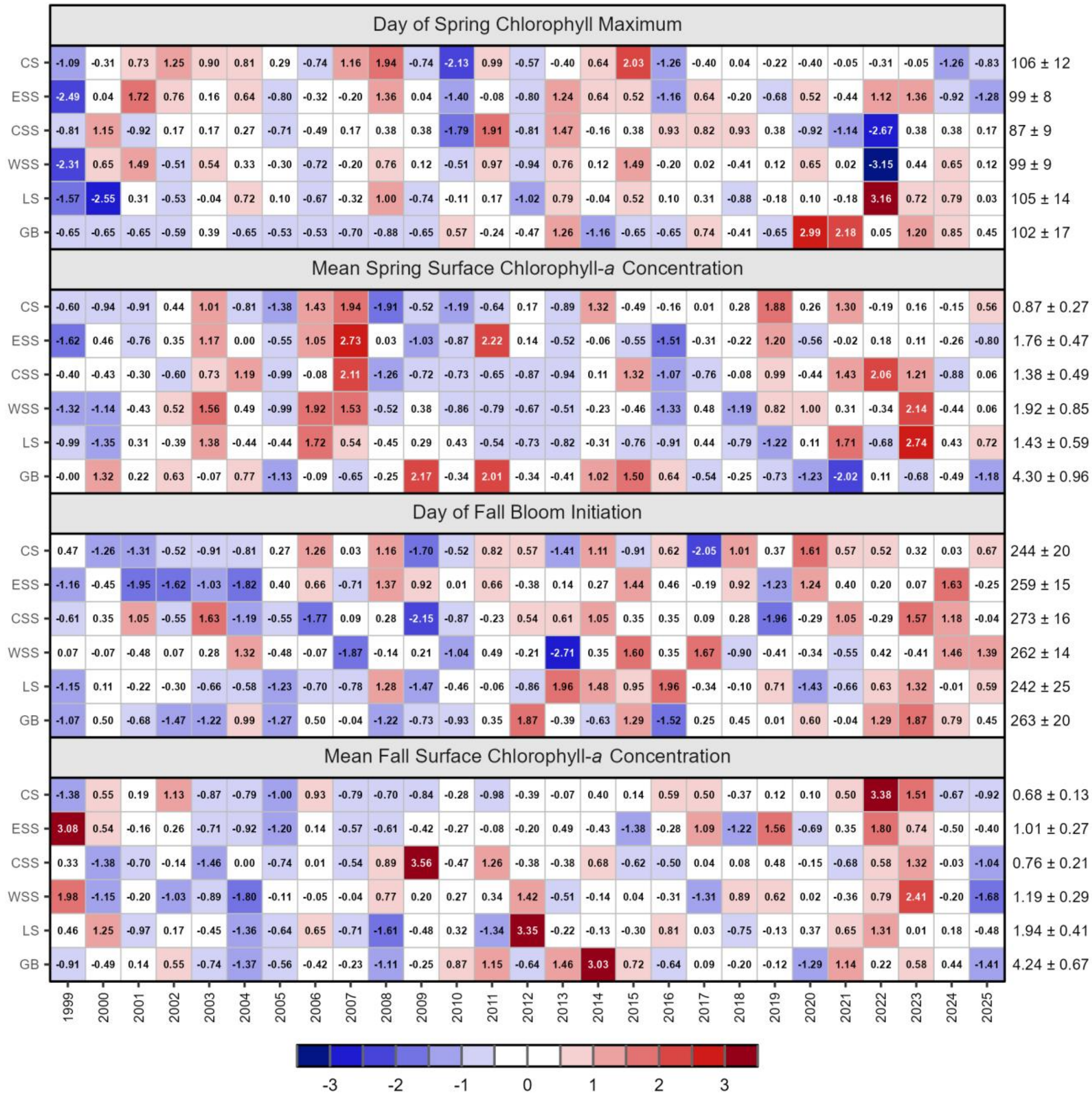

Figure 18. Annual anomaly scorecards for spring and fall phytoplankton bloom metrics. Values in each cell are anomalies from the mean for the reference period 1999–2025, in standard deviation (sd) units (mean and sd listed at right in units of Day-of-Year for spring maximum and fall initiation, $mg_{chl}\cdot m^{-3}$ for spring and fall intensity); red (blue) cells indicate later (earlier) timing, or higher- (lower-) than-normal intensity of the bloom, with shading intensity reflecting the magnitude of the anomaly.

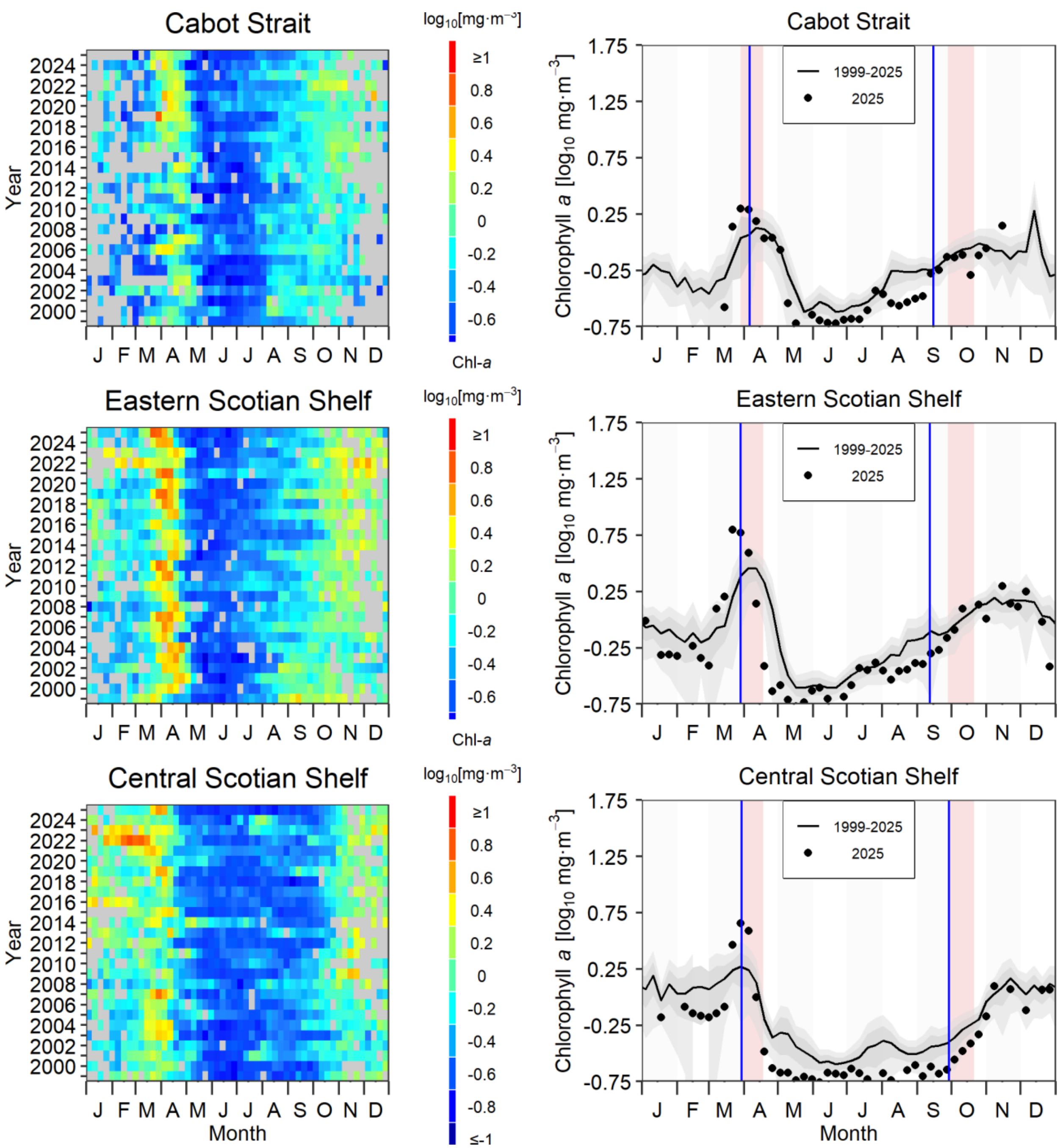

Figure 19a. Surface chlorophyll-a concentrations from remote sensing ocean color data in the Maritimes sub-regions. Left panels: Time series of weekly mean surface chlorophyll-a concentrations; gray pixels indicate missing data. Right panels: Weekly mean surface chlorophyll-a concentrations; the solid circles represent the 2025 data; the solid line represents the weekly climatological means for the reference period 1999-2025; the gray shaded ribbons represent the standard deviation (±0.5 and ±1 sd) of the weekly means; the vertical blue lines indicate the day of year of the spring bloom maximum intensity (left) and the day of year of the fall bloom initiation (right); the pink vertical stripes indicate the timing of the spring and fall surveys.

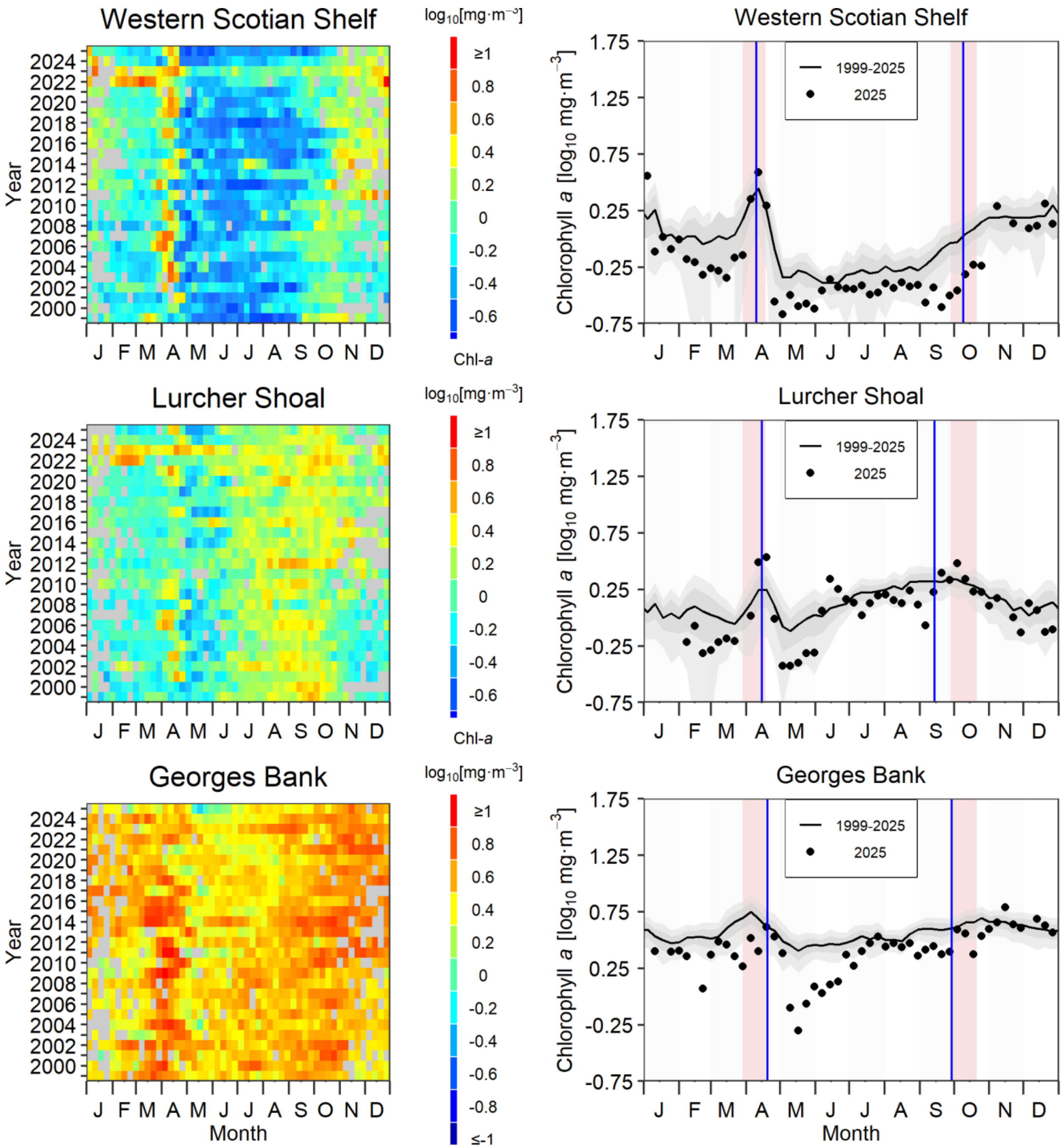

Figure 19b. Surface chlorophyll-a concentrations from remote sensing ocean color data in the Maritimes sub-regions. Left panels: Time series of weekly mean surface chlorophyll-a concentrations; gray pixels indicate missing data. Right panels: Weekly mean surface chlorophyll-a concentrations; the solid circles represent the 2025 data; the solid line represents the weekly climatological means for the reference period 1999-2025; the gray shaded ribbons represent the standard deviation (±0.5 and ±1 sd) of the weekly means; the vertical blue lines indicate the day of year of the spring bloom maximum intensity (left) and the day of year of the fall bloom initiation (right); the pink vertical stripes indicate the timing of the spring and fall surveys.

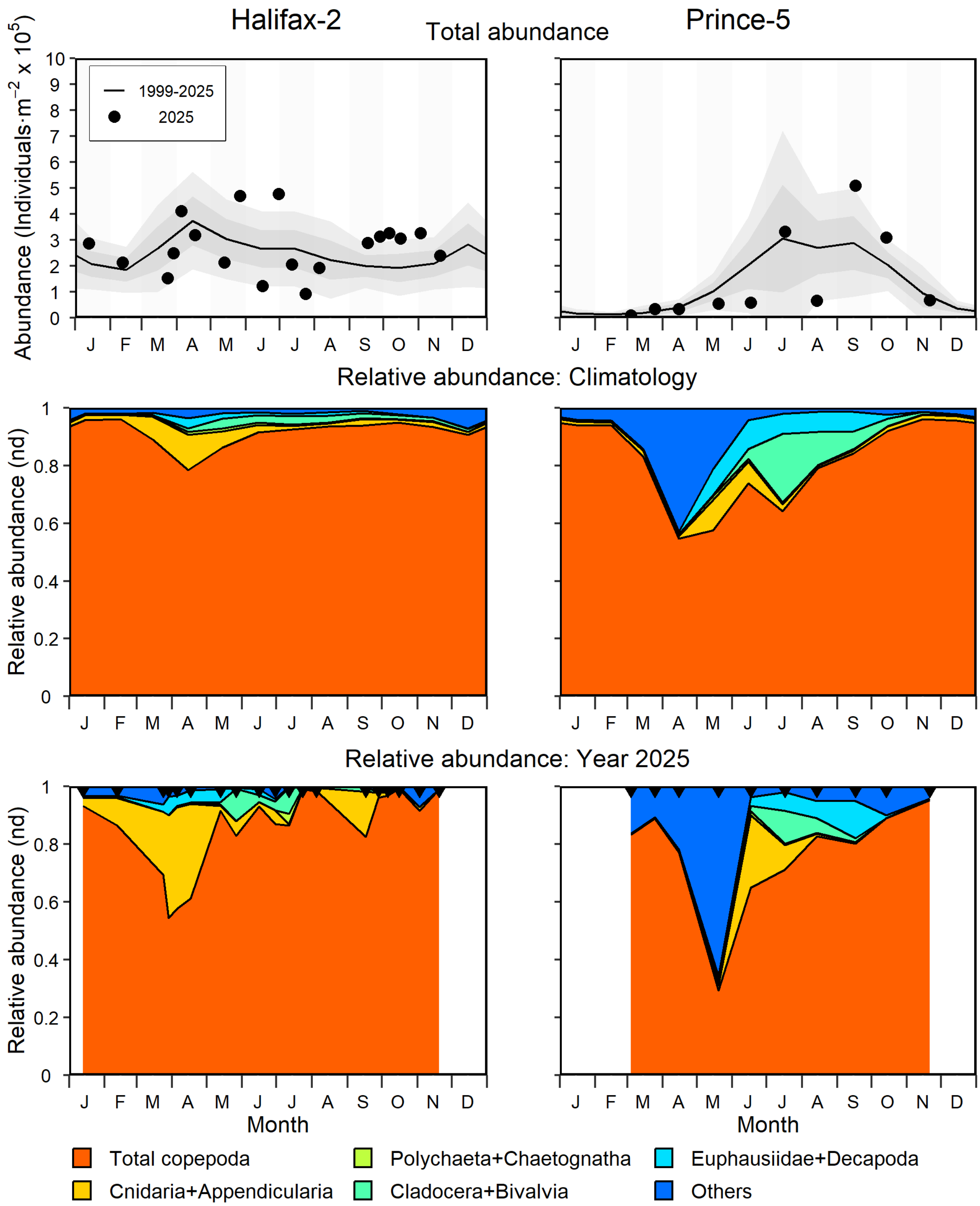

Figure 20. Zooplankton (> 200 µm) abundance and community composition at the Maritimes high-frequency sampling stations. Top panels: Zooplankton abundance; the solid circles represent the 2025 data; the solid line represents the monthly climatological means for the reference period 1999-2025; the gray shaded ribbons represent the standard deviation (±0.5 and ±1 sd) of the monthly means. Middle panels: Climatological mean zooplankton relative abundance for the reference period 1999-2025. Bottom panels: Zooplankton relative abundance in 2025. Black triangles in the bottom panels indicate sampling dates. Blanked areas indicate no data.

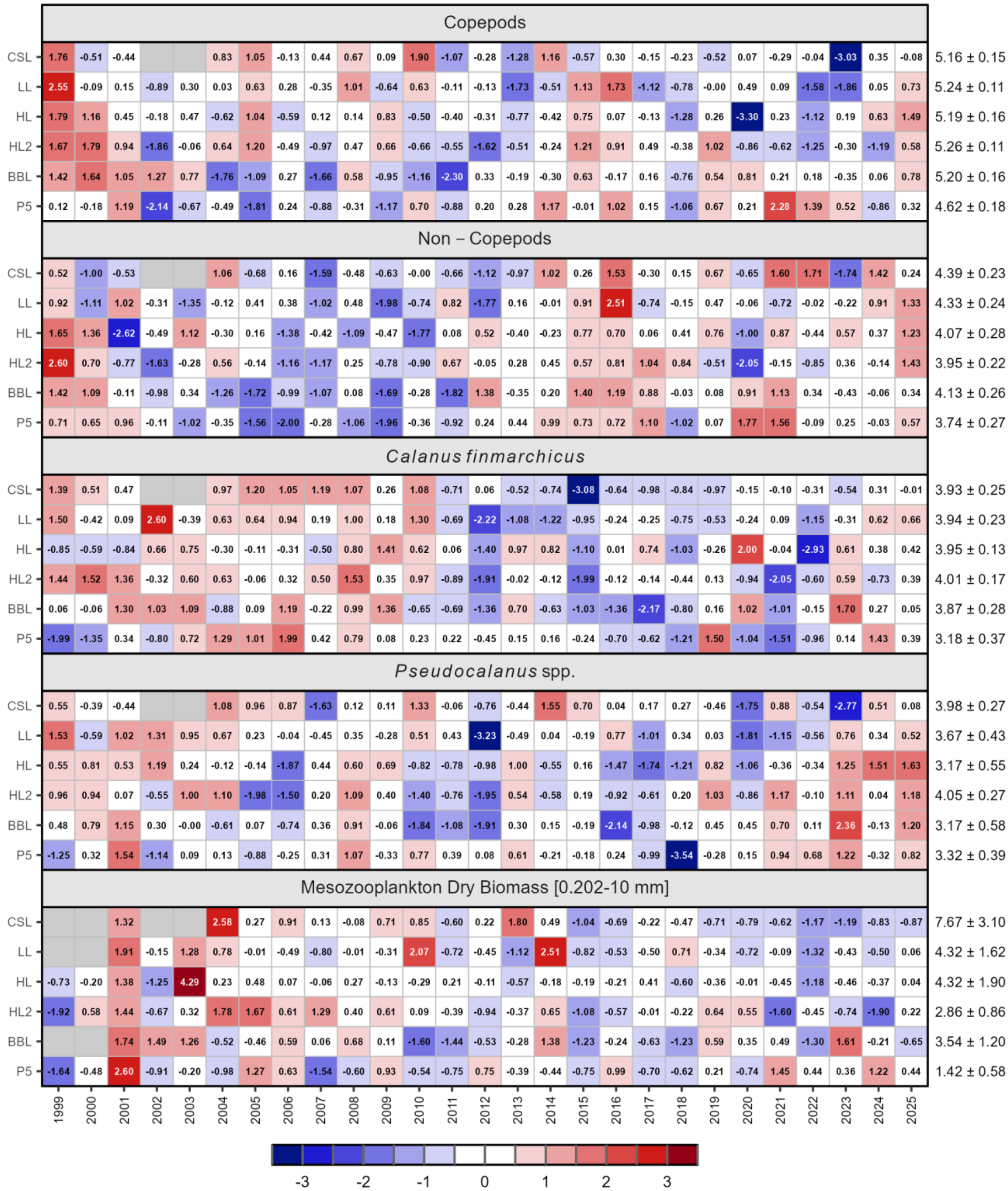

Figure 21. Annual anomaly scorecards for zooplankton abundance and biomass. Values in each cell are anomalies from the mean for the reference period 1999–2020, in standard deviation (sd) units (mean and sd listed at right in units of $\log_{10}$(individuals·m^{-2}+1) for abundance and g·m^{-2} for biomass). Red (blue) cells indicate higher- (lower-) than-normal abundances or biomass, with shading intensity reflecting the magnitude of the anomaly. Gray cells indicate missing data. CSL: Cabot Strait section; LL: Louisbourg section; HL: Halifax section; HL2: Halifax-2; BBL: Browns Bank section; P5: Prince 5.

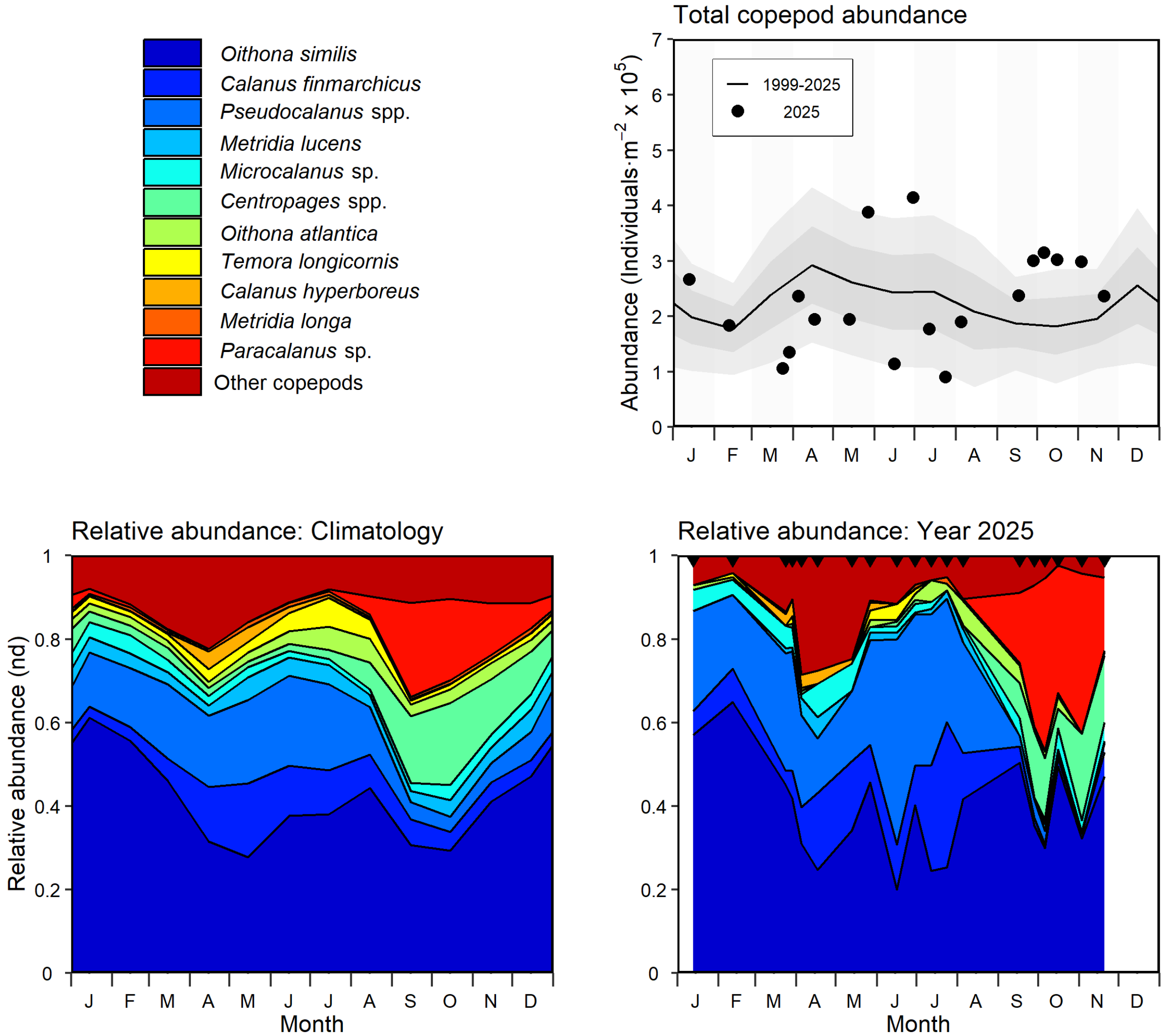

Figure 22. Copepod abundance and composition at Halifax-2; the top 95% copepod taxa by abundance (ordered from most to least abundant) are shown individually; unidentified copepods (mostly nauplii) are grouped as “others”. Top right panel: Copepod abundance; the solid circles represent the 2025 data; the solid line represents the monthly climatological means for the reference period 1999-2025; the gray shaded ribbons represent the standard deviation (±0.5 and ±1 sd) of the monthly means. Bottom left panel: Climatological mean copepod relative abundance for the reference period 1999-2025. Bottom right panel: Copepod relative abundance in 2025. Black triangles in the bottom right panel indicate sampling dates. Blanked areas indicate no data.

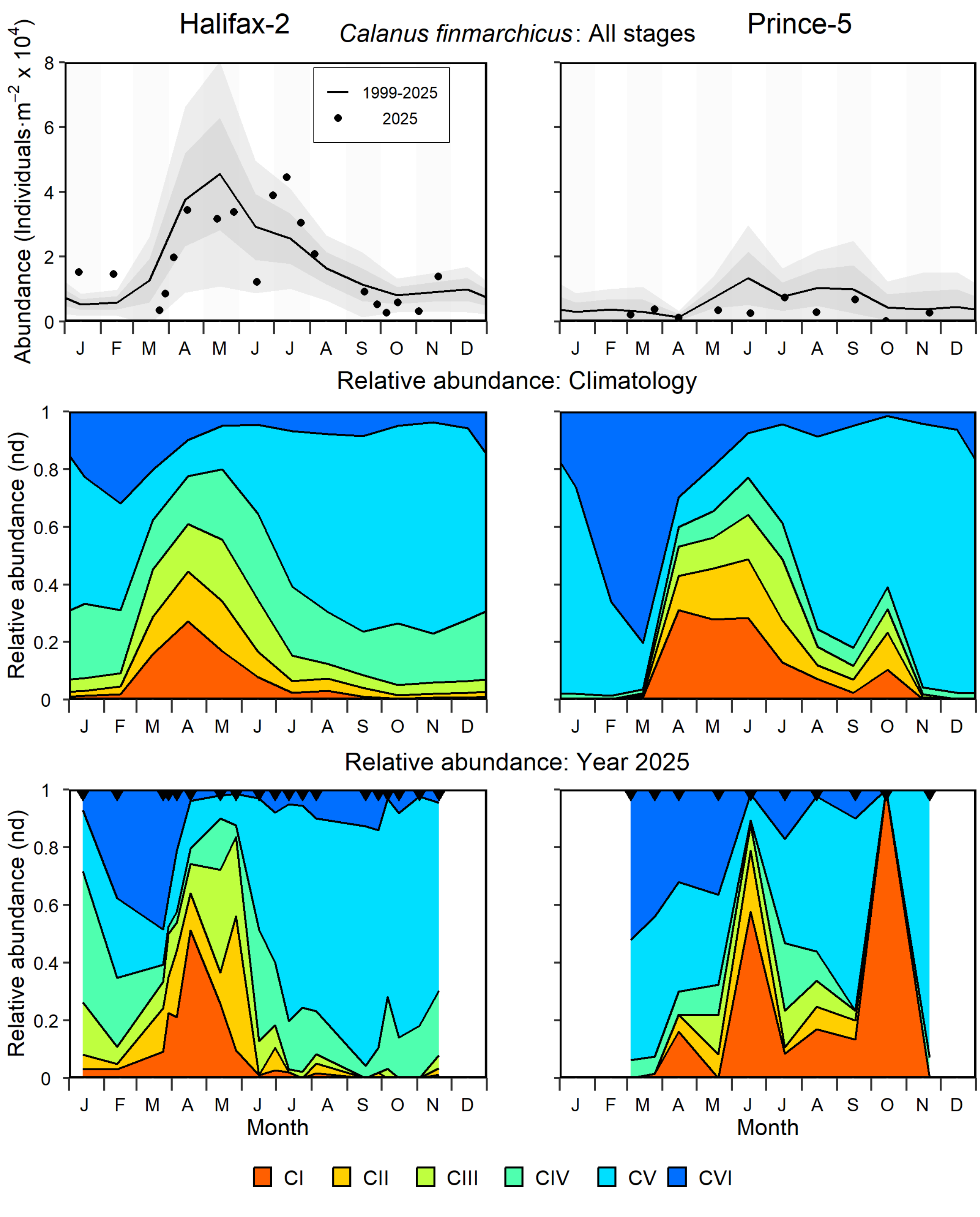

Figure 23. Calanus finmarchicus abundance and developmental stage distribution at the Maritimes high-frequency sampling stations. Top panels: C. finmarchicus abundance; the solid circles represent the 2025 data; the solid line represents the monthly climatological means for the reference period 1999-2025; the gray shaded ribbons represent the standard deviation (±0.5 and ±1 sd) of the monthly means. Middle panels: Climatological mean C. finmarchicus stage relative abundance for the reference period 1999-2025. Bottom panels: C. finmarchicus stage relative abundance in 2025. Black triangles in the bottom panels indicate sampling dates. Blanked areas indicate no data.

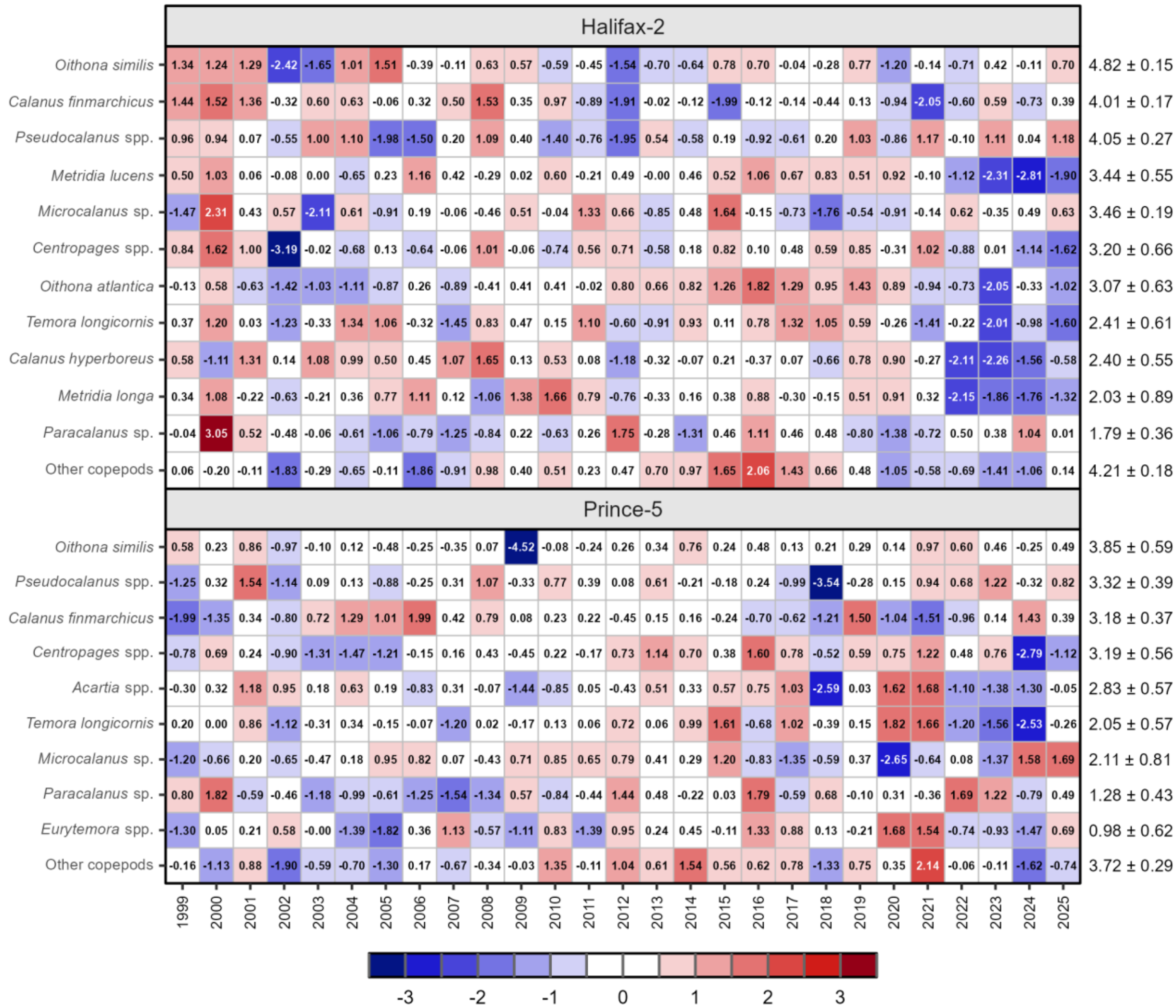

Figure 24. Annual anomaly scorecards for the top 95% of copepod taxa by abundance (ordered from most to least abundant) at the Maritimes high-frequency sampling stations. Values in each cell are anomalies from the mean for the reference period 1999–2025, in standard deviation (sd) units (mean and sd listed at right in units of log_{10}(individuals·m^{-2}+1)). Red (blue) cells indicate higher- (lower-) than-normal abundances, with shading intensity reflecting the magnitude of the anomaly.

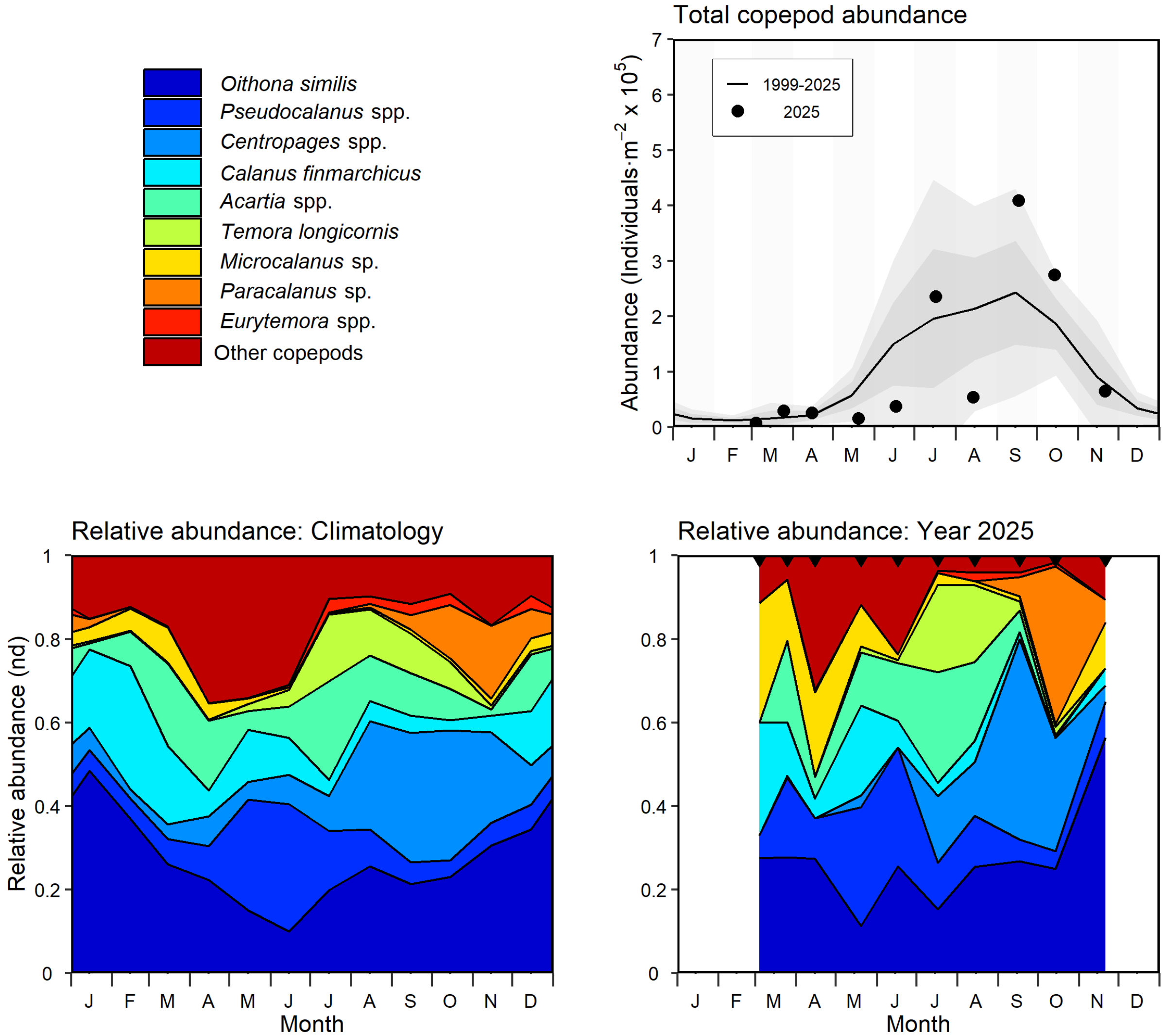

Figure 25. Copepod abundance and composition at Prince 5; the top 95% copepod taxa by abundance (ordered from most to least abundant) are shown individually; unidentified copepods (mostly nauplii) are grouped as "others". Top right panel: Copepod abundance; the solid circles represent the 2025 data; the solid line represents the monthly climatological means for the reference period 1999-2025; the gray shaded ribbons represent the standard deviation (±0.5 and ±1 sd) of the monthly means. Bottom left panel: Climatological mean copepod relative abundance for the reference period 1999-2025. Bottom right panel: Copepod relative abundance in 2025. Black triangles in the bottom right panel indicate sampling dates. Blanked areas indicate no data.

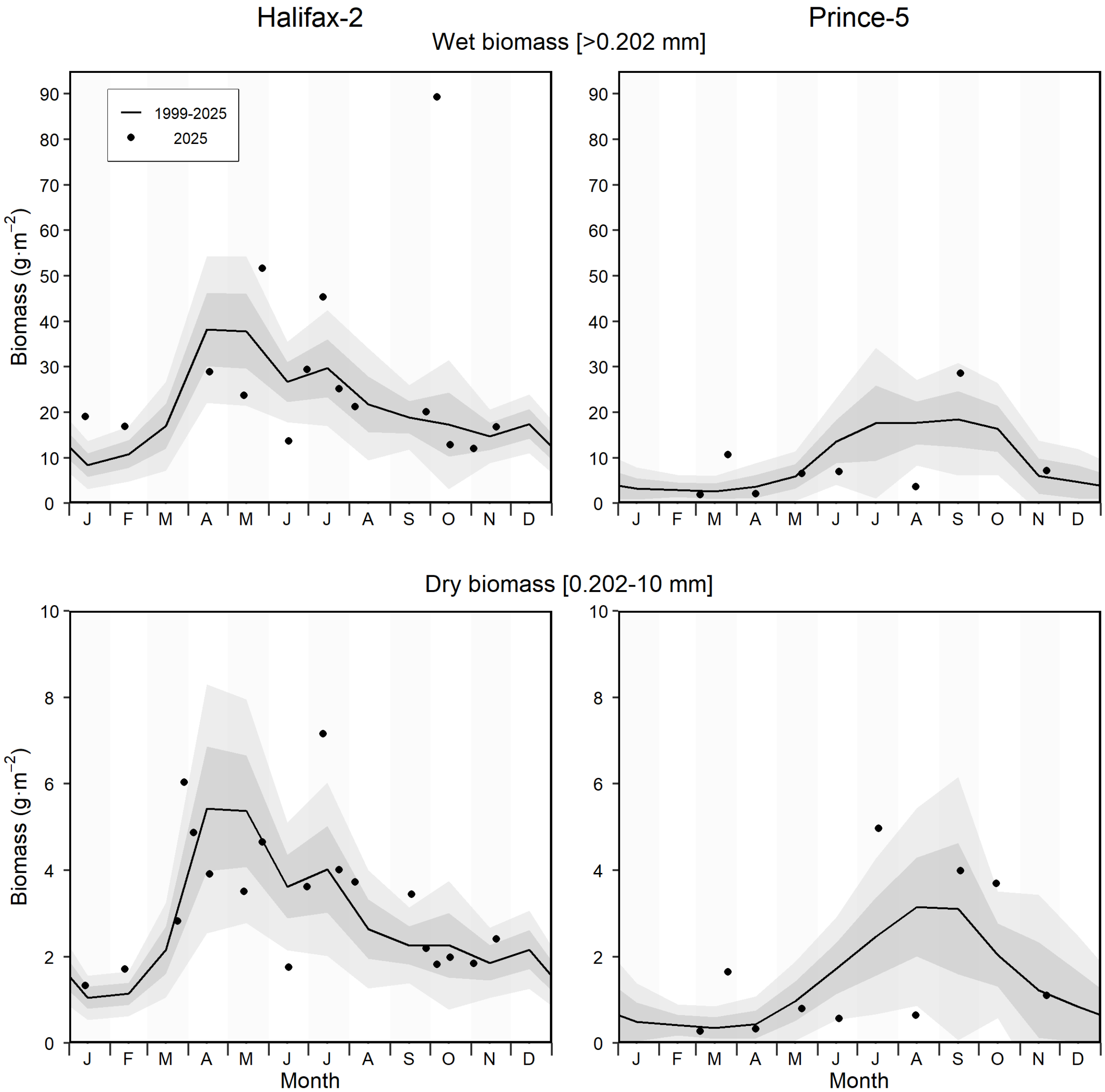

Figure 26. Zooplankton biomass at the Maritimes high-frequency sampling stations. Top panels: Total zooplankton wet biomass. Bottom panels: Mesozooplankton dry biomass. The solid circles represent the 2025 data; the solid line represents the monthly climatological means for the reference period 1999-2025; the gray shaded ribbons represent the standard deviation (±0.5 and ±1 sd) of the monthly means.

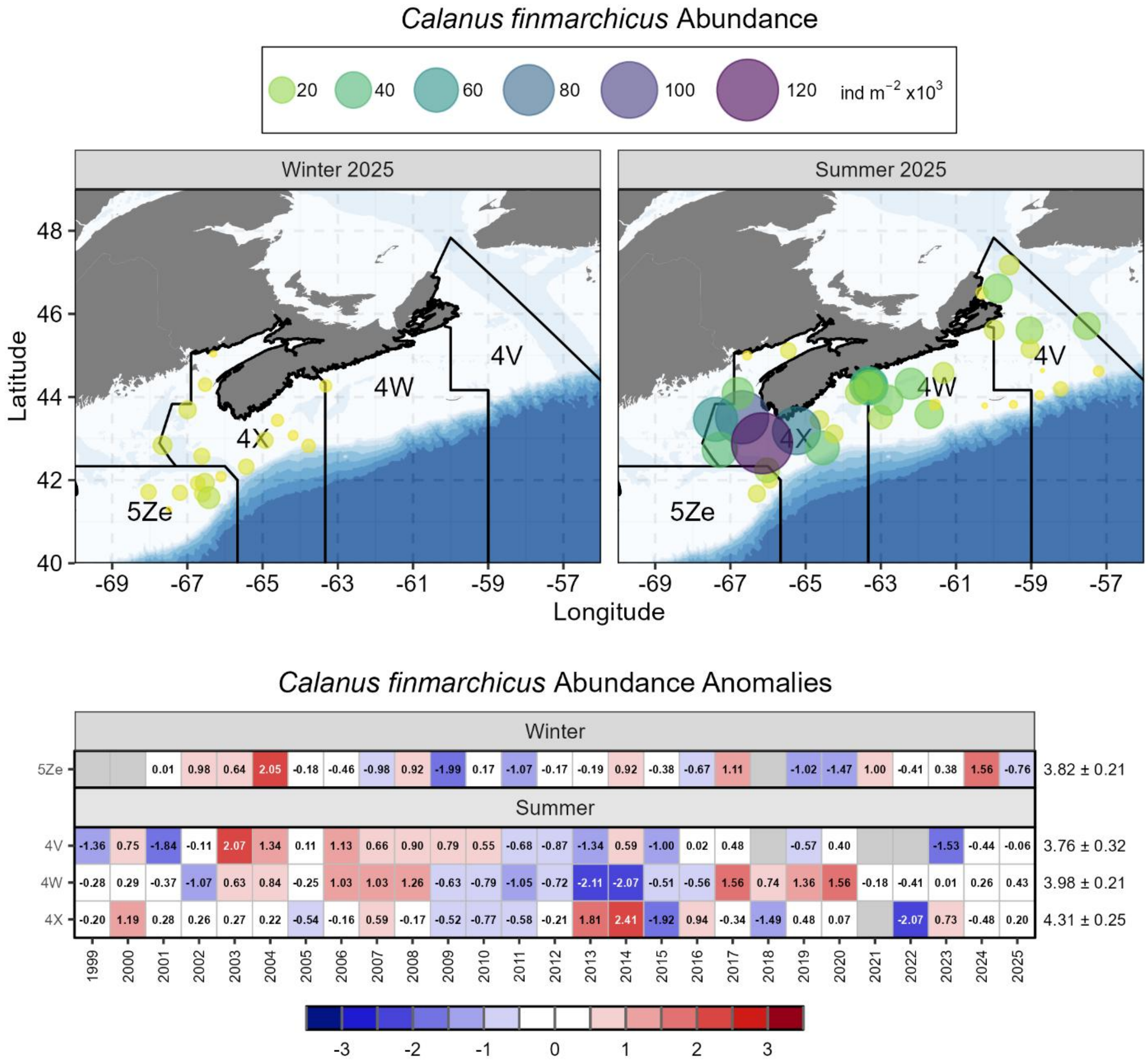

Figure 27. Calanus finmarchicus abundance during the ecosystem trawl surveys. Top panels: Spatial distribution of C. finmarchicus in winter (left) and summer (right) 2025. Bottom panels: Seasonal anomaly scorecards for C. finmarchicus abundance on Georges Bank (5Ze in winter) and the Scotian Shelf and eastern Gulf of Maine (4X, 4W, and 4V in summer); values in each cell are anomalies from the mean for the reference period 1999–2020, in standard deviation (sd) units (mean and sd listed at right in units of log_{10}(individuals·m^{-2}+1)). Red (blue) cells indicate higher- (lower-) than-normal abundances, with shading intensity reflecting the magnitude of the anomaly. Gray cells indicate missing data.

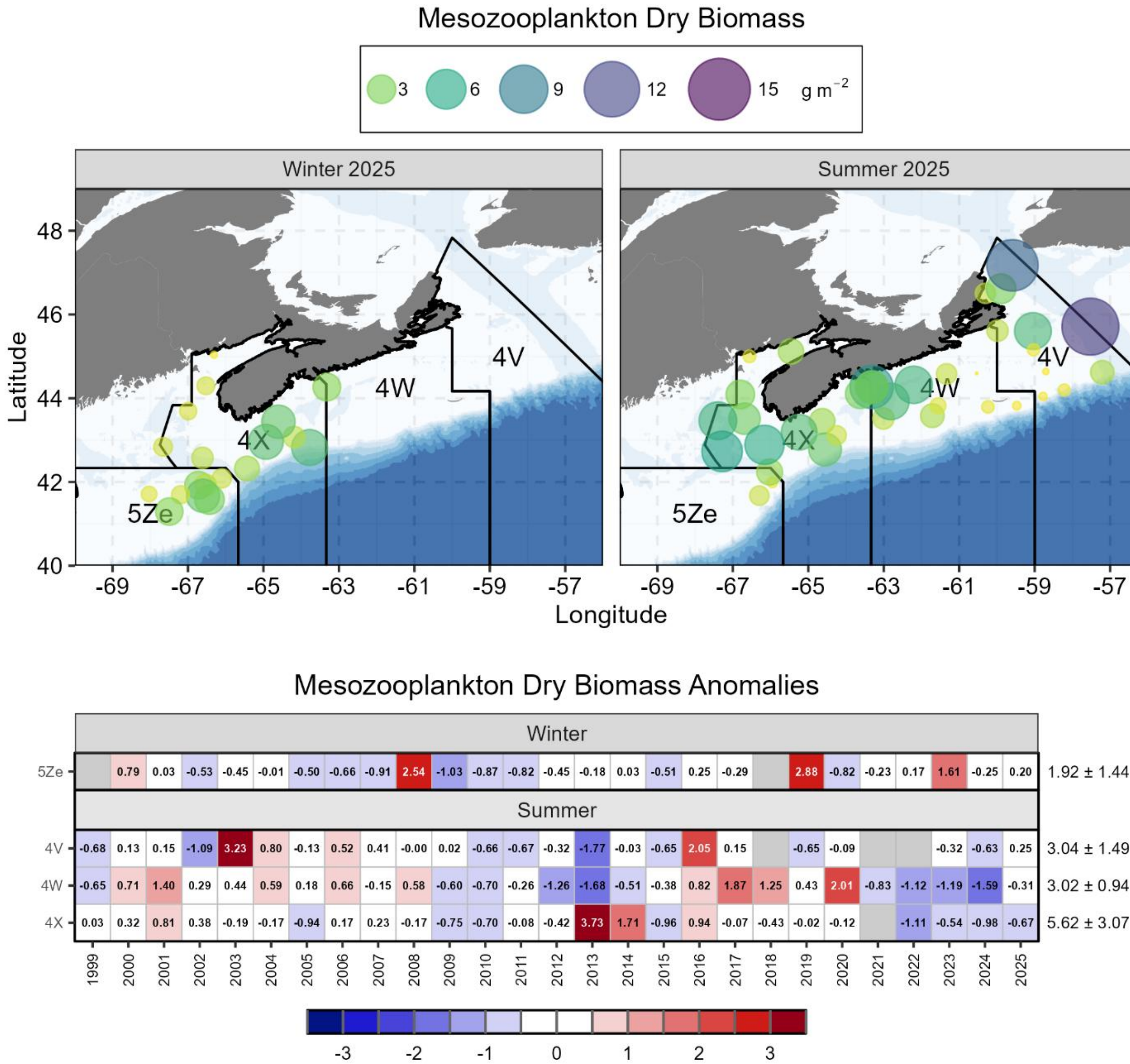

Figure 28. Mesozooplankton dry biomass during the ecosystem trawl surveys. Top panels: Spatial distribution of mesozooplankton dry biomass in winter (left) and summer (right) 2025. Bottom panels: Seasonal anomaly scorecards for mesozooplankton dry biomass on Georges Bank (5Ze in winter) and the Scotian Shelf and eastern Gulf of Maine (4X, 4W, and 4V in summer); values in each cell are anomalies from the mean for the reference period 1999–2025, in standard deviation (sd) units (mean and sd listed at right in units of g·m^{-2}). Red (blue) cells indicate higher- (lower-) than-normal abundances, with shading intensity reflecting the magnitude of the anomaly. Gray cells indicate missing data.

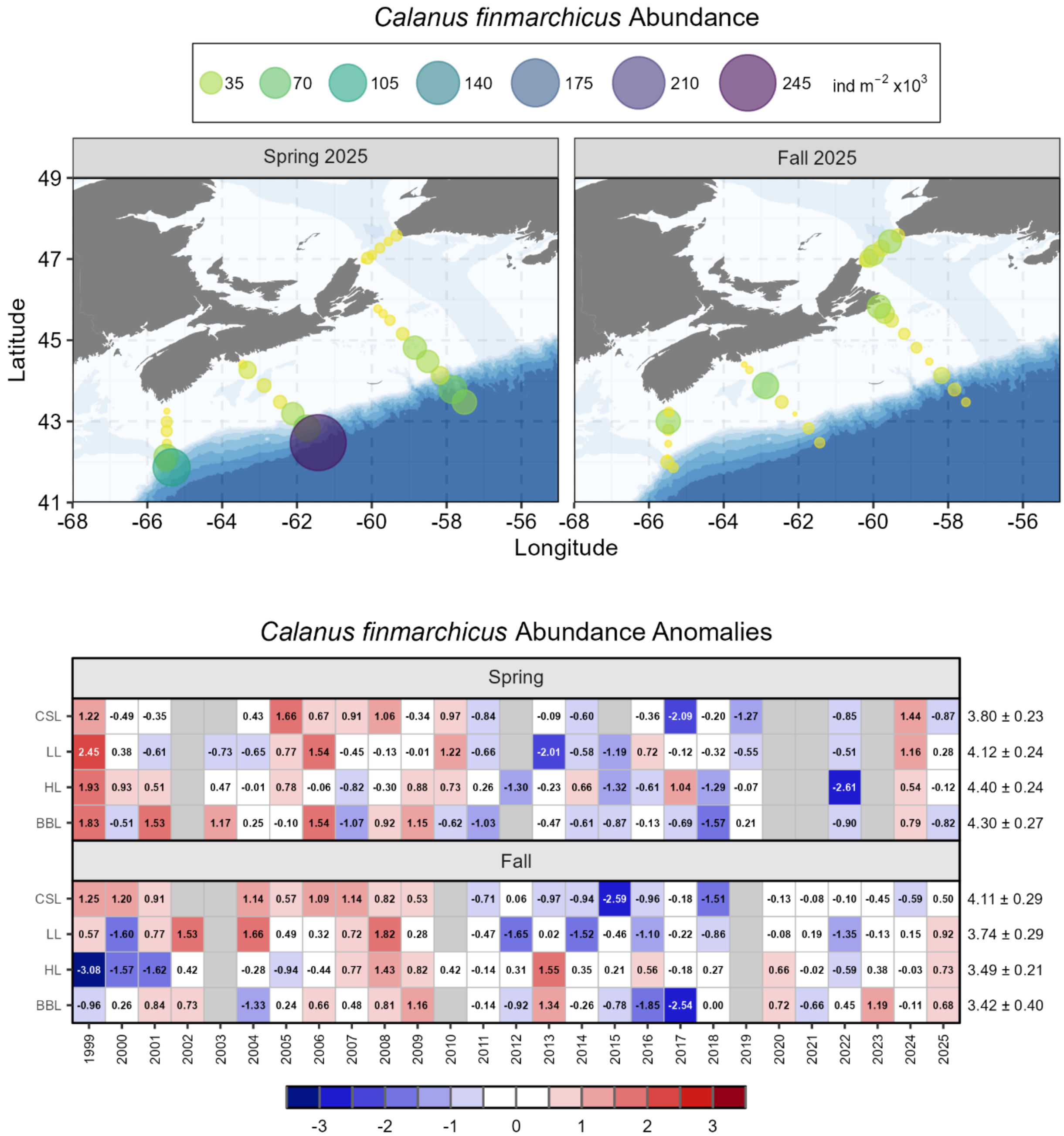

Figure 29. Calanus finmarchicus abundance during the seasonal surveys on the core sections. Top panels: Spatial distribution of C. finmarchicus in spring (left) and fall (right) 2025. Bottom panels: Seasonal anomaly scorecards for C. finmarchicus abundance during spring and fall surveys; values in each cell are anomalies from the mean for the reference period 1999–2025, in standard deviation (sd) units (mean and sd listed at right in units of log_{10}(individuals·m^{-2}+1)). Red (blue) cells indicate higher- (lower-) than-normal abundances, with shading intensity reflecting the magnitude of the anomaly. Gray cells indicate missing data. CSL: Cabot Strait section; LL: Louisbourg section; HL: Halifax section; BBL: Browns Bank section.

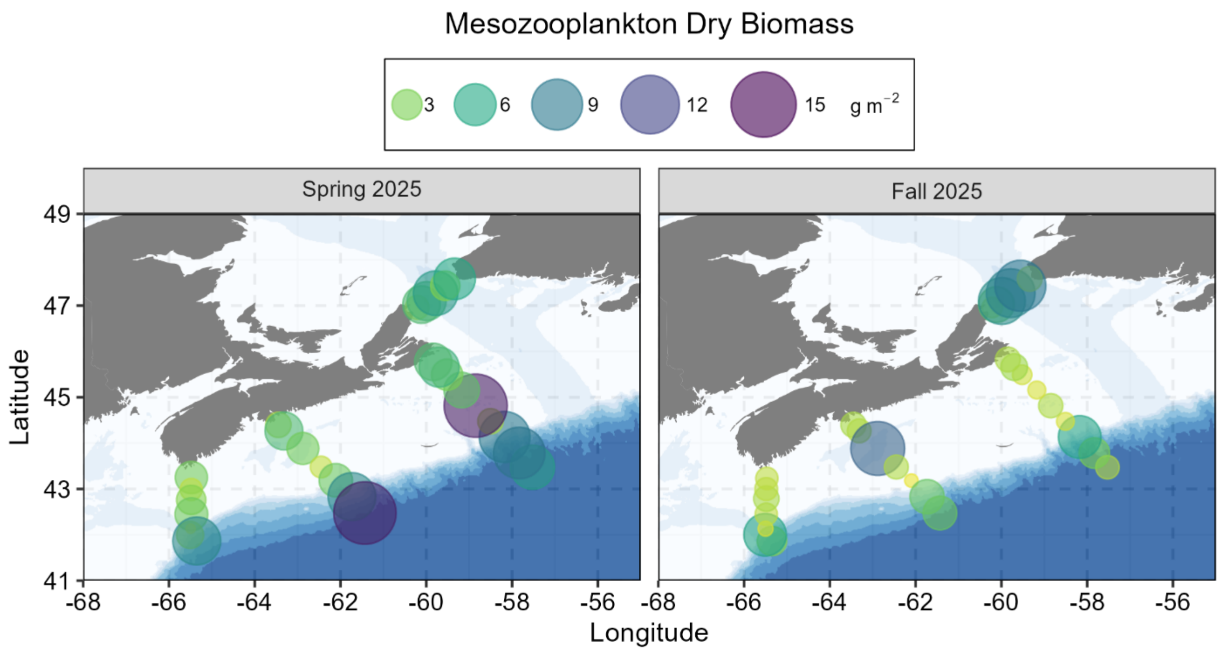

Mesozooplankton Dry Biomass Anomalies

Spring

	1999	2000	2001	2002	2003	2004	2005	2006	2007	2008	2009	2010	2011	2012	2013	2014	2015	2016	2017	2018	2019	2020	2021	2022	2023	2024	2025	
CSL			1.18			2.87	0.64	0.46	-0.61	-0.19	-0.13	0.59	-0.54		0.10	0.24		-0.40	-0.25	-0.24	-0.80			-1.99		-0.04	-0.87	7.59 ± 3.47
LL			2.29		0.99	1.00	0.24	-0.41	-0.75	-0.13	-0.05	1.57	-1.00		-1.08	1.29	-0.89	-0.56	-0.52	0.03	-0.34			-1.68		-0.41	0.41	5.71 ± 2.04
HL	-0.57	-0.18	2.34	-2.20	2.86	0.57	0.57	-0.05	-0.33	0.31	-0.33	0.08	0.40	-0.26	-0.65	-0.09	-0.28	-0.35	0.38	-0.71	-0.26			-1.26		0.02	-0.00	5.35 ± 2.83
BBL			2.98		0.91	-0.29	-0.02	0.49	0.37	0.89	0.36	-0.98	-1.08		-1.14	0.78	-0.67	-0.51	-0.20	-0.98	0.47			-1.25		0.37	-0.51	4.08 ± 1.82

Fall

	1999	2000	2001	2002	2003	2004	2005	2006	2007	2008	2009	2010	2011	2012	2013	2014	2015	2016	2017	2018	2019	2020	2021	2022	2023	2024	2025	
CSL			0.90			1.46	-0.29	0.92	0.63	-0.11	1.15		-0.63	0.19	2.73	0.45	-0.85	-0.91	-0.29	-0.68		-0.65	-0.51	-0.44	-0.98	-1.32	-0.77	8.30 ± 3.75
LL			1.08	-0.24		0.24	-0.30	-0.44	-0.67	0.20	-0.61		-0.13	-0.19	-0.87	3.75	-0.49	-0.22	-0.30	1.47		-0.60	0.06	-0.49	-0.30	-0.58	-0.36	2.84 ± 1.58
HL		0.10	-0.60	-1.28		-0.85	0.64	0.73	1.46	1.68	1.02	-1.34	-0.23	0.99	-0.10	-0.32	0.49	0.50	1.07	-0.13		0.81	-0.97	-1.11	-1.00	-2.13	0.58	3.09 ± 0.63
BBL			0.22	1.58		-0.53	-0.84	0.70	-0.36	0.13	-0.23		-1.25	-0.57	1.36	1.98	-1.41	0.48	-1.05	-0.93		0.36	0.65	-0.64	1.71	-0.92	-0.44	2.87 ± 1.13

Figure 30. Mesozooplankton dry biomass during the seasonal surveys on the core sections. Top panels: Mesozooplankton dry biomass in spring (left) and fall (right) 2025. Bottom panels: Seasonal anomaly scorecards for mesozooplankton dry biomass during spring and fall surveys; values in each cell are anomalies from the mean for the reference period 1999–2025, in standard deviation (sd) units (mean and sd listed at right in units of g·m^{-2}). Red (blue) cells indicate higher- (lower-) than-normal abundances, with shading intensity reflecting the magnitude of the anomaly. Gray cells indicate missing data. CSL: Cabot Strait section; LL: Louisbourg section; HL: Halifax section; BBL: Browns Bank section.

Non-Copepods

	1999	2000	2001	2002	2003	2004	2005	2006	2007	2008	2009	2010	2011	2012
Appendicularia	-0.23	-0.90	1.18	0.95	0.68	-0.11	0.26	-0.97	-1.04	0.44	-0.66	-0.71	0.34	-0.99
Euphausiacea	-0.71	0.02	-0.42	-1.67	1.42	0.28	-0.46	0.29	0.84	0.81	-0.80	0.23	1.10	-0.06
Gastropoda	1.88	0.52	0.41	-1.82	0.55	0.36	-1.08	-1.44	-1.19	-1.39	-0.67	-1.35	0.70	1.10
Chaetognatha	0.92	-0.01	-1.03	-2.31	-0.04	0.80	-1.05	0.34	0.01	0.58	0.42	-0.24	-0.63	0.85
Polychaeta	1.27	-1.09	0.98	-1.06	-1.28	1.19	0.92	1.34	-0.31	0.70	-0.37	-0.34	0.35	-0.59
Ostracoda	1.11	0.45	1.31	1.31	1.00	0.29	0.18	1.14	0.72	0.67	0.37	0.11	0.50	0.26
Bivalvia	1.84	0.33	1.25	-0.39	-0.91	-0.36	-0.97	-0.30	-1.39	0.11	-0.27	-0.32	0.50	-0.42
Echinodermata	0.14	-0.29	0.51	-1.01	-1.95	0.27	-0.49	0.50	-1.00	-0.13	-1.25	-0.12	0.42	0.97
Cirripedia	-3.00	-1.02	-1.12	0.05	0.66	-0.61	-0.58	0.21	-0.29	-0.15	-0.45	0.59	0.20	-0.99
Amphipoda	-0.44	-1.47	1.40	-1.45	0.36	-0.39	-1.67	-1.14	-0.19	0.35	0.33	0.05	-0.71	-0.06

	2013	2014	2015	2016	2017	2018	2019	2020	2021	2022	2023	2024	2025	
Appendicularia	-0.49	0.21	0.25	0.40	0.24	-0.22	0.84	-2.85	-1.42	0.49	1.15	1.36	1.79	2.88 ± 0.43
Euphausiacea	-1.37	-0.78	0.08	0.64	-0.72	-0.56	0.60	-1.95	2.59	-0.90	1.15	0.29	0.08	2.59 ± 0.27
Gastropoda	0.37	1.43	0.95	1.22	-0.91	0.70	-0.33	-0.82	0.80	0.19	-0.09	0.39	-0.48	2.48 ± 0.44
Chaetognatha	1.04	-0.86	-0.56	1.73	0.30	-0.07	-1.15	0.48	-2.38	0.25	0.40	0.92	1.29	1.69 ± 0.27
Polychaeta	-0.75	-0.73	-0.18	1.22	1.54	1.09	-1.36	1.17	0.19	-0.40	-0.68	-1.29	-1.53	1.45 ± 0.37
Ostracoda	0.38	0.75	0.21	0.03	-1.56	-1.76	-2.01	-1.20	-1.56	-1.33	0.24	-0.79	-0.81	1.14 ± 0.36
Bivalvia	0.53	0.43	0.60	1.66	0.89	-0.07	-1.12	-0.36	2.32	-0.09	-1.71	-0.35	-1.43	1.08 ± 0.45
Echinodermata	0.54	0.32	0.78	2.92	-0.53	0.46	-1.65	1.37	0.49	0.55	-0.21	-0.59	-1.01	1.08 ± 0.47
Cirripedia	-0.48	0.81	0.63	-0.07	1.26	0.62	1.72	-0.69	2.00	-0.34	-0.28	0.77	0.56	0.99 ± 0.31
Amphipoda	-0.03	-0.02	0.67	1.36	-0.81	2.07	0.60	1.03	-0.48	-0.80	2.12	-0.04	-0.65	0.83 ± 0.26

-3 -2 -1 0 1 2 3

Figure 31. Annual anomaly scorecard for non-copepod groups abundance on the Scotian Shelf sections, ordered from higher to lower abundance. Anomalies are based on annual abundances estimated using a general linear model fitted with data from all stations of the four core sections. Values in each cell are anomalies from the mean for the reference period 1999–2025, in standard deviation (sd) units (mean and sd listed at right in units of $\log_{10}$(individuals·m^{-2}+1)). Red (blue) cells indicate higher- (lower-) than-normal abundances, with shading intensity reflecting the magnitude of the anomaly.

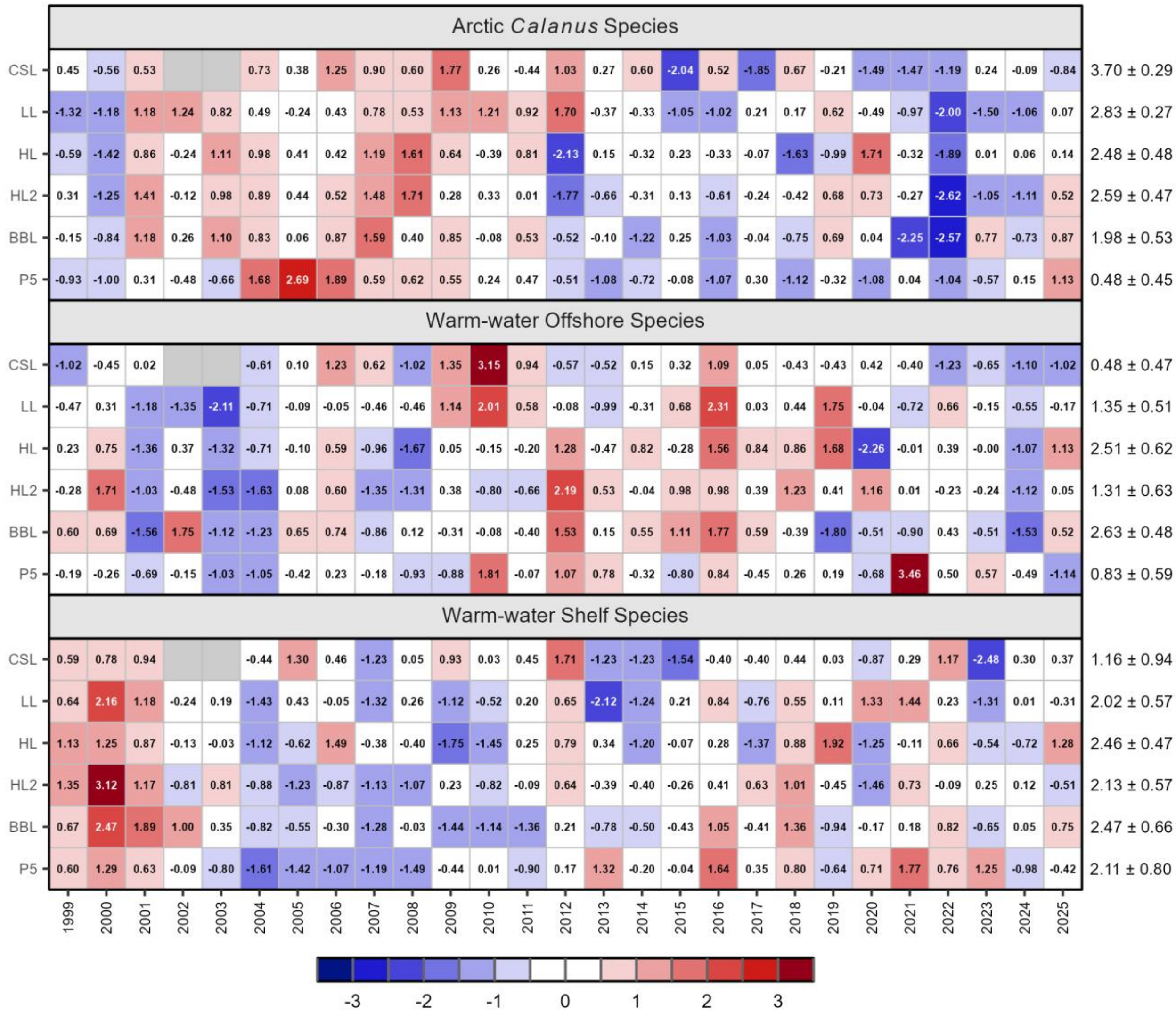

Figure 32. Annual anomaly scorecards for copepod indicator species grouped abundance. Values in each cell are anomalies from the mean for the reference period 1999–2025, in standard deviation (sd) units (mean and sd listed at right in units of log_{10}[individuals·m^{-2}+1]). Red (blue) cells indicate higher- (lower-) than-normal abundances, with shading intensity reflecting the magnitude of the anomaly. Gray cells indicate missing data. CSL: Cabot Strait section; LL: Louisbourg section; HL: Halifax section; HL2: Halifax-2; BBL: Browns Bank section; P5: Prince 5.

APPENDIX A: OPTICAL PROPERTIES AT THE HIGH-FREQUENCY SAMPLING STATIONS

The optical properties of seawater (attenuation coefficient [K_d], euphotic depth [Z_{eu}]) are derived from *in situ* light attenuation measurements using a rosette-mounted PAR radiometer and Secchi disk, according to the following procedures:

1. The downward vertical attenuation coefficient for PAR ($K_{d\text{-}PAR}$) is estimated as the slope of the linear regression of $\ln(E_d(z))$ as a function of depth z (where $E_d(z)$ is the value of downward irradiance at depth z) in the depth interval from minimum depth to around 50 m. The minimum depth is typically around 2 m although the calculation is sometimes forced below that target when near-surface PAR measurements appear unreliable.
2. The value of the light attenuation coefficient $K_{d\text{-}Secchi}$ from Secchi disc observations is found using:

$$K_{d\_secchi}\ (m^{-1}) = 1.44 / Z_{sd}$$

where Z_{sd} is the depth (in m) at which the Secchi disc disappears from view (Holmes 1970).

Estimates of the euphotic depth (Z_{eu}), defined as the depth where PAR is 1% of the surface value, are obtained using the following expression (Churilova et al. 2017):

$$Z_{eu}\ (m) = 4.6 / K_d$$

Estimates of the euphotic depth (Z_{eu}) at the high-frequency sampling stations are summarised in Figure A1.

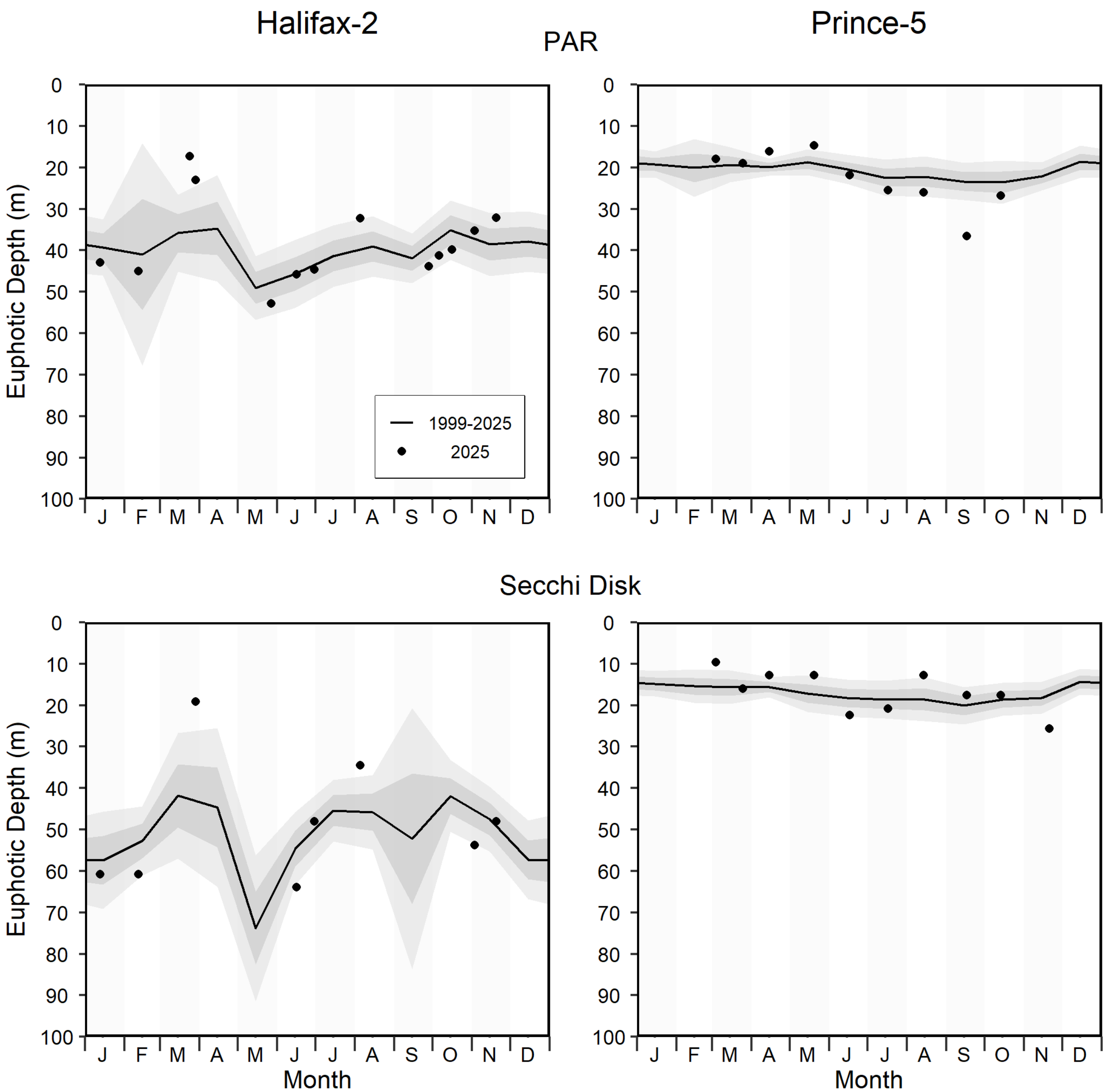

Figure A1. Euphotic depth at the Maritimes high-frequency sampling stations. Top panels: Euphotic depth calculated from PAR irradiance meter. Bottom panels: Euphotic depth calculated from Secchi disc measurements. The solid circles represent the 2025 data; the solid line represents the monthly climatological means for the reference period 1999-2025 (except 2001–2025 for euphotic depth from PAR at Prince 5); the gray shaded ribbons represent the standard deviation (±0.5 and ±1 sd) of the monthly means.

APPENDIX B: SUPPLEMENTARY FIGURES

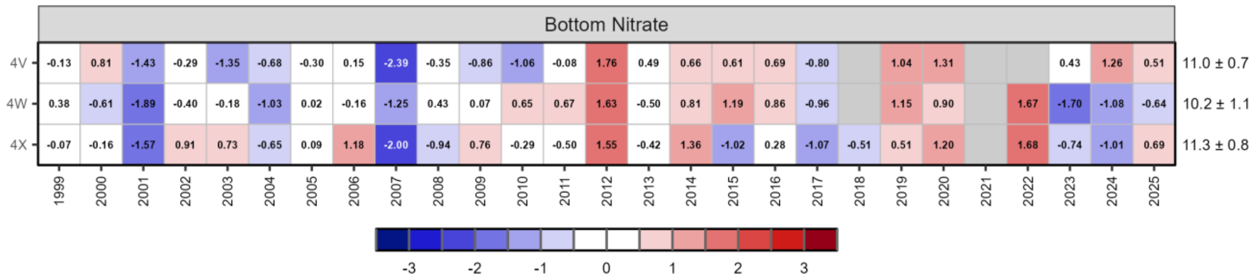

Figure B1. Seasonal anomaly scorecard for bottom nitrate concentrations during the summer ecosystem trawl surveys; values in each cell are anomalies from the mean for the reference period 1999–2025, in standard deviation (sd) units (mean and sd listed at right in units of mmol·m^{-3}). Red (blue) cells indicate higher- (lower-) than-normal concentrations, with shading intensity reflecting the magnitude of the anomaly. Gray cells indicate missing data.

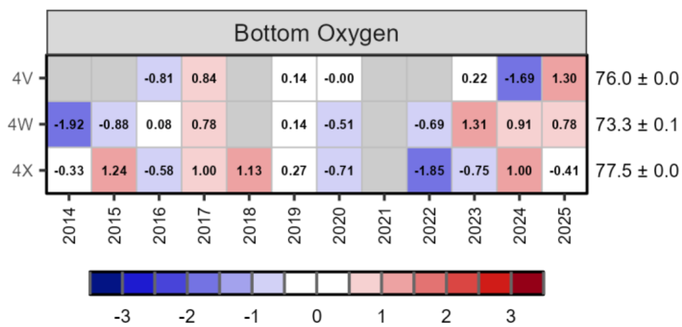

Figure B2. Seasonal anomaly scorecard for bottom oxygen saturation during the summer ecosystem trawl surveys; values in each cell are anomalies from the mean for the reference period 2014–2025, in standard deviation (sd) units (mean and sd listed at right in units of % saturation). Red (blue) cells indicate higher- (lower-) than-normal saturation levels, with shading intensity reflecting the magnitude of the anomaly. Gray cells indicate missing data.

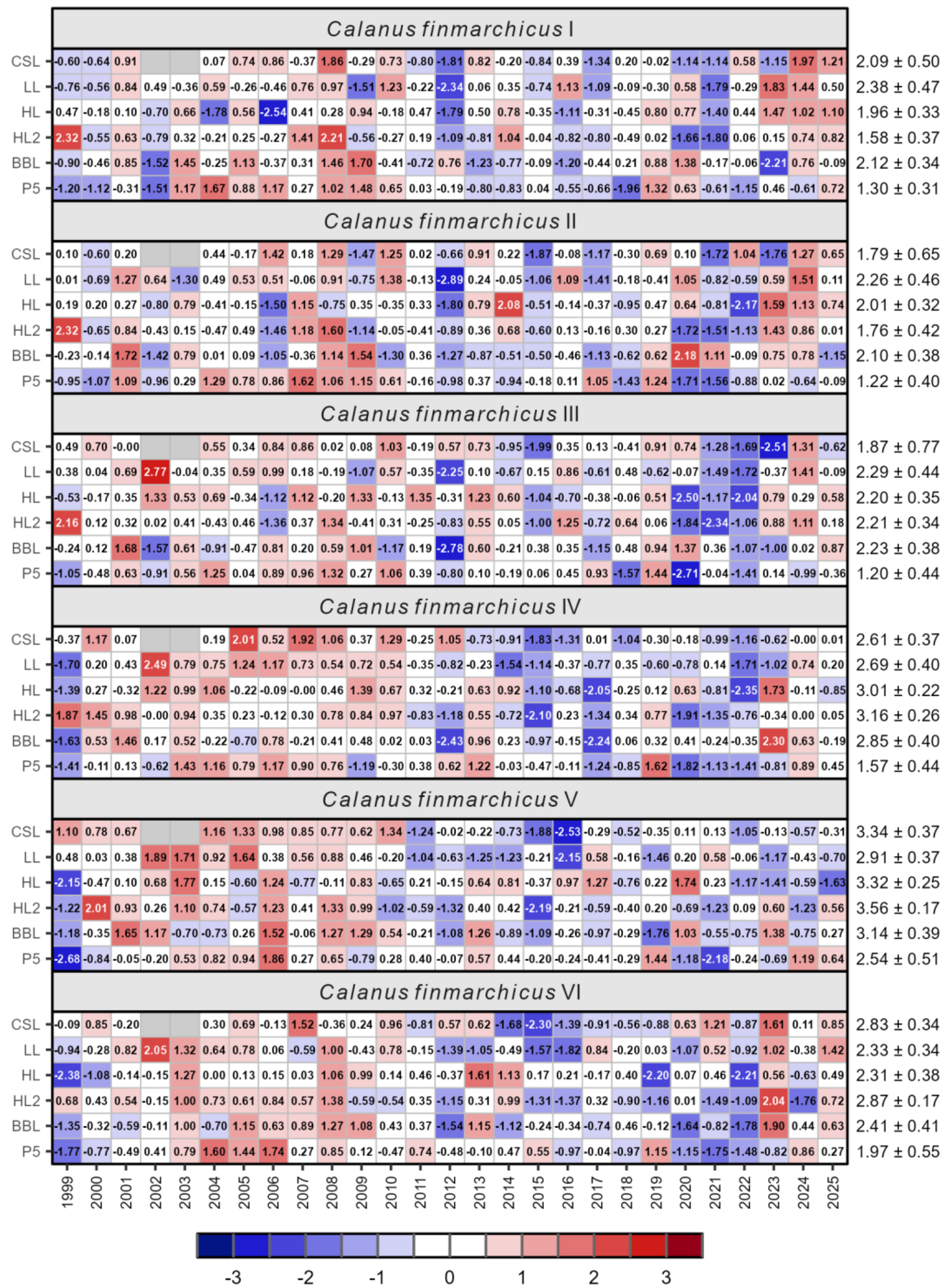

Figure B3. Annual anomaly scorecards for stage-specific Calanus finmarchicus abundance. Values in each cell are anomalies from the mean for the reference period 1999–2025, in standard deviation (sd) units (mean and sd listed at right in units of $\log_{10}$(individuals·m^{-2}+1)). Red (blue) cells indicate higher- (lower-) than-normal abundances, with shading intensity reflecting the magnitude of the anomaly. Gray cells indicate missing data. CSL: Cabot Strait section; LL: Louisbourg section; HL: Halifax section; HL2: Halifax-2; BBL: Browns Bank section; P5: Prince 5.